# Detecting Clathrate Concentrations Through High Resolution Seismic Velocity Analysis of Shallow Sediments

WARREN T. WOOD[1], PAUL L. STOFFA[1] AND THOMAS H. SHIPLEY[2]

[1]*Institute for Geophysics and Department of Geological Sciences, The University of Texas at Austin, 8701 Mopac Blvd., Austin, TX 78759*

[2]*Institute for Geophysics, The University of Texas at Austin, 8701 Mopac Blvd., Austin, TX 78759*

January 1991

University of Texas Institute for Geophyiscs Technical Report No. 229

## ABSTRACT

For marine sediments in water deeper than a few hundred meters pressure and temperature conditions are frequently optimal for the formation of ice like crystalline gas/water clathrates, also called gas hydrates. The existence of clathrates has been verified by coring and has been inferred from seismic data in many parts of the world. The sharp acoustic impedance contrast between a high velocity clathrate and either low velocity, gas charged sediments or just normal non-hydrated sediment below, make the bottom of the clathrate zone detectable as a bottom simulating reflector (BSR) in seismic data. Also, the presence of clathrate tends to increase the velocity of the surrounding sediment creating velocity anomalies which can be detected in seismic data. Examples of these phenomena are seen in 6 km aperture seismic data collected by UTIG near the Blake Ridge, offshore U.S. A high resolution velocity analysis performed in the domain of intercept time and ray parameter is used to quantitatively assess the thickness and velocity of the anomalies on one seismic line in this area. Local regions of anomalously high velocity were seen above the BSR and at the same sub-bottom depth in other areas where no BSR is seen. Where the BSR is present an anomalously low velocity region just below the BSR is also seen. Results show no correlation of velocity with seismic transparency in the sediments above the BSR. Results also show no individual interval velocities approaching the velocity of clathrate, ~3.8 km/sec. The general velocity profile is normal at the water bottom gradually increasing to ~0.3 km/sec faster than normal just above the BSR, decreasing to slightly below normal just below the BSR, and returning to normal by ~0.8 km sub-bottom. Using the derived interval velocities and laboratory measurements of the velocity and density of solid and interstitial clathrate, we test two models of clathrate distribution in the sediment: 1) clathrate displaces the pore fluids within the matrix but displaces no grains; and 2) the clathrate displaces the matrix and the pore fluids to form pockets of solid clathrate. Results indicate that in this area clathrates make up about 25% of the volume of the anomalously fast layers.

# INTRODUCTION

*The Nature of Clathrates*

For marine sediments in water deeper than a few hundred meters pressure and temperature conditions are frequently optimal for the formation of ice like crystalline gas/water clathrates, also called gas hydrates. The clathrates are found in the upper few hundred meters of the sedimentary section and have been sampled directly off the Pacific coast of southern Mexico, (Shipley and Didyk, 1982) off the southern Atlantic coast of the United States, (Kvenvolden and Barnard, 1983) and elsewhere. The sharp acoustic impedance contrast between a high velocity clathrate and either low velocity, gas charged sediments or just normal non-hydrated sediment below, make the bottom of the clathrate zone detectable as a bottom simulating reflector (BSR) in seismic data. BSRs are found in many places in the worlds oceans (Shipley et al., 1979; Field and Kvenvolden, 1985; Tucholke et al., 1977; and others) and the amount of gas stored worldwide in these clathrates is probably quite large. The chief component gas of the clathrates is methane, present in excess of 98% (Claypool and Kaplan, 1974; Kvenvolden, 1984).

A key to quantifying the amount of methane in the form of clathrates is understanding the means by which it is generated. Isotopic analyses (Kvenvolden and Barnard, 1983; Shipley and Didyk, 1982) have shown methane from gas hydrates to be primarily biogenic in origin possibly with some contributions from diagenic processes. Claypool and Kaplan (1974) proposed that the biogenic production of methane is a consequence of an ecological succession characterized by three distinct environmental zones in the sediment column, an aerobic zone, an anerobic sulfate reducing zone, and an anerobic carbonate reducing zone (Figure 1). At the water bottom sediments are deposited in an aerobic environment. As these sediments are buried the environment becomes anoxic and over time the sulfate dissolved in the sea water is reduced. When all dissolved sulfate is reduced the environment becomes suitable for the biogenic production of methane. The bottom of the sulfate reducing zone therefore acts as an upper boundary on the location of the biogenic methane source. As deposition continues each of these zones moves upward through the section maintaining roughly the same sub-bottom

depth. The exact sub-bottom depth to the top of the methane producing zone is variable due to the variable biogeochemistry of the sedimentary environment, but samples taken in the Blake Ridge area on DSDP Leg 11 indicate that at depths greater than 25 meters all sulfate ($SO_4$) has been reduced (Lancelot and Ewing, 1973). Analysis of other samples from the Blake Ridge area at DSDP site 533 on leg 76 show that methane production begins in the interval between 14 m and 40 m sub-bottom (Kvenvolden and Barnard, 1983).

Whether the methane exists as a free gas or in a solid form combined with water as a gas hydrate is dictated by the surrounding pressure and temperature (PT) conditions. Figure 2 shows a temperature and pressure profile for a typical deep water environment. Note that increasing depth (pressure) drives the methane further into the region of stability as a hydrate. However, the increasing temperature with depth more than compensates for the pressure effect and drives the material across the phase boundary into the region of stability as a gas. The depth at which this occurs marks the lower limit of the existence of methane as a hydrate. The depth of this phase transition depends on the depth to the water bottom and the geothermal gradient of the sediments, (Shipley et al., 1979; Yamano et al., 1982). For a roughly horizontal water bottom the discontinuity remains at the same sub-bottom depth, for a shallowing water bottom depth the pressure decreases while the sub bottom temperature profile remains roughly the same so the sub-bottom depth to the bottom of the hydrate stability zone decreases.

As is expected, the physical properties of the sediments on either side of the transition are quite different. This discontinuity may be manifest as an acoustic impedance anomaly, acoustic impedance being defined as the product of acoustic velocity and material density, and hence a reflection in seismic data. The velocity of pure methane hydrate has been measured in the laboratory at 3.8 km/sec (Whally, 1980) and the most accurate measurement of *in situ* material came when workers on DSDP leg 84 offshore Guatemala were fortunate enough to drill through a zone of almost pure hydrate several meters thick and record log responses of the *in situ* material (Mathews and von Huene, 1985). The velocity of the pure *in situ* hydrate was measured at 3.3 to 3.8 km/sec and density was measured at 1.024 to 1.045 $Mg/m^3$ for the

hydrate. It is interesting to note that the typical velocity and density of terrigenous clastics at this depth are 1.8 to 2.0 km/sec and 1.6 to 1.7 $Mg/m^3$ respectively (Hamilton, 1976, 1980). The sharp increase in velocity from a hydrate free sediment to a pure hydrate is associated with a sharp decrease in density, so there is no large change in acoustic impedance and a modest reflection coefficient of 0.02 is produced. This is typical of reflections coefficients in sedimentary sequences at this depth. (In a constant density medium a velocity change from 1.8 to 1.9 km/sec yields a reflection coefficient of 0.03)

Perhaps most important is the effect of clathrate in the matrix pore spaces. Most core samples have shown only sparsely disseminated hydrate within the sediment combined with pockets on the order of centimeters in size where it appears sediment has been excluded, (Shipley and Didyk, 1982; Kvenvolden and McDonald, 1985). The presence of methane hydrate in sediment has been shown to substantially increase the acoustic wave velocity through the sediment. Stoll et al. (1971) measured Ottawa sand containing hydrate at 2.7 km/sec and Pearson et al. (1986) measured the velocity of tetrahydrofuran hydrates (structurally similar to methane hydrates) in sandstone and limestone at 4.7 and 5.9 km/sec respectively. Factors affecting the velocity increase are salinity of the surrounding pore water and porosity of the matrix rock.

It is unlikely that deep marine sediments containing methane hydrate would have a higher velocity than pure hydrate so we assume in this study that material at the approximate depth of the phase transition will range in velocity from ~1.7 km/sec (for sediments containing no hydrate) to ~3.8 km/sec for pure *in situ* hydrate. Similarly we expect densities to vary between ~1.6 $Mg/m^3$ and ~1.025 $Mg/m^3$.

The result of the changing physical properties at the depth of the hydrate phase transition is a moderate decrease in acoustic impedance from the sediment containing hydrate to the sediment below resulting in a reversed polarity reflection. This decrease may be augmented by the effect of free methane gas trapped at the phase boundary, which tends to decrease both velocity and bulk density and would increase the amplitude of the reflection (Kvenvolden and McDonald, 1985). For a roughly parallel ocean bottom the discontinuity and resulting

reflection maintains the same sub-bottom depth mimicking small features on the water bottom, hence the name "bottom simulating reflector."

Although clathrates are frequently associated with a BSR, a BSR can be caused by another common process, the diagenisis of biogenic silica, opal-A, to opal-CT (Hein et al., 1978, Hammond et al., 1983). This process is also related to pressure and temperature conditions in the surrounding sediments and occurs in a similar PT regime. In this process the acoustic impedance change responsible for the BSR is positive and created by silica cemented mudstones and porcelanite beds between 600 and 700 m below the water bottom and at a temperature of 35° to 51°C, a higher temperature and pressure regime than needed for the presence of clathrate. Although these BSRs are slightly deeper, the most definitive way to distinguish between the top of opal-CT reflection and the base of hydrate reflection is that opal-CT has a higher acoustic velocity than the sediments above, producing a strong *normal* polarity reflection, whereas the base of hydrate is a *reversed* polarity reflection.

Even if no BSR is present gas hydrates may still be detectable by their effect on acoustic velocity if they are areally extensive. A lateral velocity change of 10%, (e.g., 2.0 to 2.2 km/sec) would create a change in travel time through the section of ~10%, or about 0.1 km/sec for a time thickness of 1 sec. Abrupt changes of this magnitude are not seen in the seismic data, indicating that either the changes are much smaller than 10% or that they occur so gradually that the image below is not significantly distorted. Usually, a velocity estimate better than that done in conventional processing is needed to resolve the small vertical and horizontal variations in velocity the clathrates would be likely to induce. To observe these small or gradual changes a closely spaced, laterally extensive high resolution velocity analysis was performed. We use a seismic line (seaward portion of line BA-6) in this study from the Blake Outer Ridge area offshore eastern U.S. (Figures 3 and 4). The seismic data had an aperture of 6.0 km where the depth to the BSR is only ~3.0 km.

*Importance of Clathrates as a Methane source or sink*

Since the chief component of gas hydrate is methane, a hydrocarbon and "greenhouse" gas, it is of significant economic and environmental interest to determine the amount of clathrate in the oceans and the processes by which it may be released. Estimates by Kvenvolden (1988) suggest that the amount of organic carbon in methane hydrates world wide ($10^4$ gigatons) may exceed that in all fossil fuel deposits (5000 gigatons). One mechanism by which the methane in hydrates could be released into the atmosphere is by slumping. Slumping in marine sediments with very small slope (< 5°) may actually be triggered by decomposition of clathrates (Carpenter, 1981). Slumping suddenly and drastically changes the PT conditions of the shallow sediments so the amount of methane and the proximity to areas prone to slump failure are important to any economic recovery attempts as well as to the atmospheric impact resulting from a large release of methane. The objectives of this study include quantitatively analyzing the effect of clathrate on sediment physical properties (primarily acoustic velocity, but also density indirectly through acoustic impedance), so that the amount of methane, and its lateral and vertical distribution in the sediment column may be determined. Since seismic data are much easier to acquire than actual sediment samples, determining the amount of *in situ* hydrate from surface seismic data would be an ideal way to examine large areas of ocean sediments which contain methane hydrates.

## PREVIOUS EVIDENCE OF CLATHRATES IN THE BLAKE PLATEAU AREA

*Seismic Expressions of Clathrates*

The most prominent seismic expression of clathrates is the strong, reversed polarity BSR present in the Blake Ridge area which has been extensively mapped using single and multichannel seismic data by Paull and Dillon (1981) (stippled area, Figure 3). The occurrence of the BSR is usually between 2.0 and 4.0 km water depth, in most areas tending to mimic the bathymetry. Another expression of clathrates was observed by Paull and Dillon (1981). They pointed out that the reflectivity of the sediments above the BSR is frequently quite dim compared to that of the sediments below the BSR (Figure 5) suggesting that this transparency,

or "blanking" is an effect of sediments being cemented so completely by clathrate that impedance contrasts are significantly reduced. The objectives of this study include determining if the relative transparency of the sediments can be related to the amount of clathrate cement in the sediment and whether the transparency can then be used as a method of quantitatively determining the amount of hydrate in the sediment.

Also interesting is that the BSR is not of uniform strength throughout a section. It tends to appear stronger beneath anticlines and in areas of stratigraphic and structural closure (Dillon and Paull, 1983). This implies that PT conditions are appropriate for free methane gas as opposed to gas entirely in solution. The free gas would be less dense than surrounding water and would tend to migrate upward and substantially reduce the velocity of the sediments where it collects.

*Seismic Velocity Characteristics of Clathrates*

In the Blake Ridge area conventional stacking velocity analyses on multichannel seismic data frequently show the BSR to be the upper interface of an anomalously low velocity zone. This velocity inversion is typically from ~2.1 km/sec above the BSR to ~1.5 km/sec or lower below the BSR (Dillon and Paull, 1983). The presence of a velocity inversion indicates that the BSR is a clathrate and not a diagenic opal transformation process. The velocities of the sediments above the BSR appear to have a slightly higher velocity than sediments containing no clathrate but not, however, as high as would be expected in sediments where clathrates are abundant. Laboratory measurements have shown that clathrate cemented sediments have a velocity of ~2.7 km/sec (Stoll et al., 1971) and pure methane hydrate has a velocity of ~3.8 km/sec (Whally, 1980; Mathews and von Huene, 1985). The slightly elevated velocity of the sediments just above the BSR may be used to quantify the amount of hydrate in the sediment (Pearson et al., 1986).

*Evidence of Clathrates from DSDP Drill Sites*

DSDP sites 102, 103, 104, and 533 are located in areas of the Blake Ridge where a BSR has either been mapped or is suspected, but a typical vertical distribution of clathrates in sediment has yet to be found. Part of the difficulty results from possible decomposition of the hydrate during the coring process, making it difficult to distinguish between free gas in the sediments and small amounts of hydrate which may be decomposing during coring. This may account for the results in DSDP site 533 where gassy sediments were encountered from 15 m sub-bottom to the bottom of the hole even in the zone of hydrate stability where only small intervals of clathrate cemented sediments were found (Kvenvolden and Barnard, 1983). Researchers on the earlier DSDP Leg 11, report abundant methane in the sediment cores some of which were degassing for one or two hours (Lancelot and Ewing, 1973). Although no hydrates were observed directly, semi-quantitative estimates of the amount of gas (more than could be held in solution at that pressure and temperature), and estimates of the acoustic velocity (somewhat higher than expected), lead to the conclusion that at least some the methane had been bound in a hydrate. So although drill cores have been collected at several sites in this area, the vertical distribution of the hydrate is still not well known. The evidence so far is not consistent with the simple model in which clathrates are distributed evenly within the zone of hydrate stability.

## VELOCITY ANALYSIS PROCEDURE

*Travel Time equations in $\tau$-p*

The high resolution velocity analysis was performed in the domain of intercept or vertical delay time, $\tau$, and the ray parameter or horizontal slowness, p. The vertical delay time, $\tau$, can be constructed geometrically as the time intercept at zero offset of a tangent to a seismic travel time trajectory in the source-receiver offset domain. Diebold and Stoffa (1981) and more recently Diebold (1987) developed the vertical delay time equations for planar dipping layers in 2-D and 3-D respectively. For a fixed source (or receiver) on the surface of the earth and the receiver (or source) at position r, the 3-D $\tau$-p travel time equation for the $n^{th}$ reflection is:

$$T_n = \vec{p}_r \cdot \vec{X}_n + \tau_n(\vec{p}_r) \quad ,$$

where $\vec{p}_r = (p_{r_x}, p_{r_y})$ is the horizontal slowness, $\vec{X} = (x,y)$, the source/receiver offset, and $\tau_n(\vec{p}_r)$ is the total vertical delay time. For a 1-D earth structure the vertical delay time can be written as the sum

$$\tau_n(p) = \sum_{j=1}^{n} 2\Delta z_j q_j \quad , \tag{1}$$

where $\Delta z_j$ and $q_j$ are the interval thicknesses and vertical slownesses respectively.

CMP data are commonly analyzed by assuming that the earth structure varies only with depth. This is usually a valid approximation because of source-receiver ray parameter averaging inherent in CMP data (Diebold and Stoffa, 1981). For 1-D velocity analysis, we use equation (1). First, replace $q_j$ by $(1 - p^2v_j^2)^{1/2}/v_j$ and then $2\Delta z_j /v_j$ by $\Delta t_j$, the two-way normal time in each layer. The result is:

$$\tau_n(p) = \sum_{j=1}^{n} \Delta t_j (1 - p^2v_j^2)^{1/2} \quad . \tag{2}$$

To solve for the interval velocity and two way normal time we can measure the delay times of any two reflection events such as $\tau_n$ and $\tau_{n-1}$ at the same two or more ray parameters. The differences between the vertical delay times $\Delta\tau_n(p) = \tau_n(p) - \tau_{n-1}(p)$ as a function of ray parameter can then be used to solve for the interval velocity.

The above method requires that we first interpret the $\tau$-p data to identify the delay time of the reflections, that is, we must 'pick' the event times. This is usually possible, but may be difficult in practice. To aid in the picking the interpreter can 'NMO' correct the $\tau$-p data (Stoffa

et al., 1981). That is, given the correct interval velocity function, the $n^{th}$ reflection event can be corrected to its total two-way normal time. The 1-D $\tau$-p normal moveout correction is:

$$\Delta T_n(p) = T0_n - \tau_n(p) \tag{3}$$

where $T0_n$ is the total two-way normal time, $T0_n = \sum_{j=1}^{n} \Delta t_j$. Thus,

$$\Delta T_n(p) = \sum_{j=1}^{n} \Delta t_j (1 - (1 - p^2 v_j^2)^{1/2}) \quad . \tag{4}$$

To actually do the NMO, we resample the $\tau$-p seismic wave form data for each plane wave seismogram, f(t,p):

$$F(T0_n, p) = f(\tau,p)\, \delta ( \tau - \sum_{j=1}^{n} \Delta t_j (1 - p^2 v_j^2)^{1/2}) \quad , \tag{5}$$

interpolating as required for discretely sampled data. This process is repeated for all $T0_n$'s and ray parameters of interest to construct the $\tau$-p NMO corrected data, $F(T0_n,p)$. For a 1-D earth, this process is equivalent to imaging the plane wave data directly to time or depth.

*Calculation of Interval Velocities*

An efficient method of implementing the velocity analysis is to superimpose the calculated delay time curves on the $\tau$-p seismic data using a computer graphics workstation. As the model is adjusted interactively by the interpreter the delay time curves can be quickly re-calculated and re-displayed. When the delay time curves calculated using equation (2) are coincident with the reflections in the $\tau$-p gather, the data have been correctly modeled. More specifically the method proceeds in a top down or layer striping fashion (Stoffa et al., 1991,

submitted). Beginning with the top most event of interest, the interpreter picks the delay time at p = 0.0 and makes an initial guess at the velocity (Figure 6a). A corresponding delay time curve is drawn and superimposed on the seismic data. If necessary the model is adjusted until the resulting delay time curve matches as closely as possible the seismic reflection event. At this point an NMO correction can be applied using equation (5) according to the present model which downward continues the plane wave data and makes a correctly modeled reflection event appear horizontal (Figure 6b). If further adjustment is needed the analysis procedure can continue in the NMO domain. When the reflection event has been properly NMO corrected the seismic data have been downward continued to the time or depth of this layer (Figure 6c) and the interpreter proceeds by choosing the vertical delay time $\tau$ at p= 0.0 for the next reflection event of interest. The procedure is repeated for every reflector of interest in the gather, resulting in each interpreted reflector in the gather being downward continued by the NMO process (Figure 6d). Each of the NMO corrected gathers done in this study is shown in the Appendix.

*Estimates of Uncertainties*

When the $\tau$-p interactive velocity analysis is complete, every reflection in the $\tau$-p gather should be horizontally aligned at the two way normal time or depth. Since the uncertainty of the measure is dependant on the model no single uncertainty can be assigned to the entire survey. Instead, an interpretation uncertainty can be estimated for each reflection in each profile. Delay time curves corresponding to velocities slightly higher and slightly lower than the chosen model velocity are drawn and compared to the reflection events. When the delay time curve is obviously above the reflection event, the corresponding velocity is taken as the upper bound of possible velocities for that layer. Similarly, when the curve is obviously below the reflection event the corresponding velocity is taken to be a lower bound. These bounds are listed for the four layer analysis in the Appendix.

Since the method itself is exact, the factors which affect the resolution of the method are simply those which affect the picking of the reflections. A source wavelet with a wide

frequency bandwidth, for example, is very narrow in time and will leave less doubt as to the actual delay time of the event. A wide range of offsets is also important. Wide aperture data can be characterized in $\tau$-p by very complete delay time curves, giving the interpreter more opportunity to match a theoretical delay time curve to the seismic data. This is analogous to matching hyperbolas to data in x-t where a wide aperture enables the interpreter to distinguish between subtle changes in velocity because of the increase in NMO differences with increasing offset.

## APPLICATION TO DATA COLLECTED RECENTLY IN THE BLAKE RIDGE

### *The Data*

The seismic data used in this study, line BA-6, were collected by The University of Texas Institute for Geophysics (UTIG) and have previously been conventionally processed. The data were acquired for UTIG by GECO, an offshore geophysical contractor, using a 177 L source towed array and a 6.0 km, 240 channel streamer. Although a stacking velocity analysis was already applied to line BA-6 as part of the standard processing, the primary intent was to create a coherent image for the entire 16 sec of data. In contrast, the focus of this study is to describe in as much detail as possible the interval velocities of the shallow sediments, (< 1km sub-bottom). Previously, stacking velocity analyses for line BA-6 were performed every 200 CMPs (i.e., every 2.5 km). In this study the $\tau$-p analyses described above were performed every 100 CMPs (i.e., every 1.25 km) on gathers having undergone a $\tau$-p transform by cylindrical slant stacking (Brysk and McCowan, 1986). The velocity of individual seismic stratigraphic intervals was then measured and mapped. Since the presence of clathrates in sediments increases the seismic velocity, a lateral increase in clathrate content of an interval should produce an increase in velocity for that interval.

### *Implementation of Velocity Analysis*

Since the purpose of the velocity survey was to resolve the vertical and lateral velocity variations in the sediments due to clathrate content, attempts were made to reduce the already

small lateral inhomogeneity in this nearly 1-D area due to changes in lithology. This was accomplished by choosing individual seismic stratigraphic units to serve as the intervals in the interval velocity analysis (compare Figure 7 with Figure 3). This enables the interval velocity of each geologic unit to be traced laterally and statistically analyzed for significant variations. Specifically, two sets of seismic stratigraphic boundaries were traced through the area of interest. In one set interpretable reflection events in the zone above a major unconformity were picked at intervals as thin as possible (~100 msec) for increased vertical resolution. The other set of sequence boundary picks is a subset of the first, where interval thickness was kept at about 400 ms. Thicker layers result in more easily defined elliptical trajectories and can therefore be picked with a higher degree of certainty, but the velocities derived will be the root mean square velocities of the interpreted interval.

## RESULTS

*Results of Interactive Velocity Analyses*

One of the products of the velocity analysis is a velocity cross section in depth of the pertinent part of line BA-6 which is shown in grey scale in Figure 8. These velocities were used to accurately depth migrate the seismic data using the split step Fourier method (Stoffa et al., 1990) resulting in the depth image of Figure 9. Immediately evident on the velocity cross section is a local area of high velocity from CMP 500 and 3.0 km depth to CMP 2000 and 2.8 km depth. This zone is located just above and is parallel to the BSR and very likely contains more hydrate than the surrounding sediment. The velocity in this zone is ~2.1 km/sec, much lower than that of pure hydrate, (3.8 km/sec) or even low estimates of hydrated sediment, (2.7 km/sec). Directly below the zone of elevated velocities is a zone of anomalously low velocities of about 1.6 km/sec possibly due to accumulated free methane gas in the sediment. A similar region of anomalously high velocities is seen at roughly the same sub-bottom depth further landward from CMP 2600 to 4000. The anomaly is not as strong here and no strong low velocity zone appears below the high velocity anomaly. There is possible evidence of a BSR at

2.85 km at CMP 3100 although the seismic data shows bedding in this area to be more nearly parallel to the bottom, making the determination difficult.

*Analysis of the Raw Interval Velocities*

Since one of the objectives of this study was to look for lateral changes in the velocity profile of the shallow sediments, the interval velocities were plotted vs. CMP (Figure 10). Here the bold curves represent the interval velocity in each sediment layer of the four layer analysis and the narrow lines correspond to the uncertainty bounds interpreted for each measurement, (velocities and uncertainties for the water column appear as 3 sub-parallel lines since all measurements were 1.5 km/sec +/- .005 km/sec). The bottom most bold line shows the velocity for the top most sediment layer, the next bold line up corresponds to the second layer and the top most bold line corresponds to the bottom most layer. Since each interval is a seismic stratigraphic interval and the area is very flat, changes in velocity due to change in lithology have been minimized. Under ideal conditions subtracting a constant velocity (e.g., the mean velocity) from each of the curves would leave us with the rapidly varying velocity variations, hopefully those associated with clathrate content. However a constant velocity, or even a linearly changing velocity does not adequately approximate the regional, slowly varying velocity trend in this section. Compare Figure 10 with Figure 7 and note the increase in velocity with depth. This is a background effect which is more slowly changing than the variations we expect from varying clathrate content. The change from transparent to reflective layers in the seismic data occurs over about 200 to 300 CMPs (2.5 to 3.8 km). To observe more rapid variations in the velocity we smoothed the data over 23.75 km and subtracted the smoothed data from the original. The smoothed data consist of wavenumber components with periods larger than 23.75 km and contain information on changes in depth and gross geological changes which obscure the variations we seek (Figure 11). Subtracting this from the original data allows us to observe the deviations from the background trend for each layer (Figure 12). Unfortunately almost all the velocity deviations are within the bounds of uncertainty and cannot be considered significant. A similar analysis was performed on the many layered analysis but

since uncertainties in the interval velocities are larger than those of the four layer analysis the results are even less informative.

Since the lateral variations in each of the layers were not very pronounced between neighboring analyses, the vertical velocity variations were examined by displaying all the interval velocities as a function of sub-bottom depth (Figures 13 through 19). The depth plotted is the depth to the center of the interval and the velocity is the corresponding interval velocity. As an objective means of fitting the data with a single curve, the data were binned into depth intervals of 0.1 km and the velocities within each bin were averaged. The depth to the center of each bin was plotted against the average of the interval velocities to obtain a velocity vs. depth curve.

The most confident interval velocities, those of the four layer model are shown in Figure 13. Since the intervals in this analysis are approximately 0.4 sec in duration this curve represents a relatively smooth background velocity trend and small velocity reversals are obscured. Note the small amount of scatter in the points indicating the relative lateral constancy of the sub-bottom velocity profile. Note also the break in slope in the velocity curve (solid line) at about 0.35 km. When compared to the velocity profile of a clastic section described by Hamilton (1980) the data suggest that the velocity gradient of the sediments down to ~0.35 km is very close to that of Hamilton but the overall velocity is about 0.1 km/sec slower. Below 0.35 km the velocity remains roughly constant down to 0.7 km where it increases sharply and converges with Hamilton's curve. (The apparent slight velocity reversal at about 0.75 km is probably due to the scarcity of interfaces interpreted at this depth.) Thus, we see an anomalously low velocity zone from 0.35 to 0.7 km sub-bottom depth when the analysis intervals are ~0.4 sec.

The velocity curve in the many layered analyses plot (Figure 14), shows a gradient increasing relative to the global curve in the shallow sediment, a sharp slope break at ~0.3 km and a ~0.1 km/sec velocity reversal from 0.3 km to 0.55 km. This suggests elevated velocities from 0.25 to 0.4 km, significantly reduced velocities in the sediments from 0.45 km to 0.6 km, and somewhat reduced velocities down to 0.9 km sub-bottom. Below ~1 km sub-bottom the

uncertainty in the data increases and small velocity reversals in the curve are not likely to be significant.

The analyses were then divided into two groups, those in areas were the BSR (solid line in Figure 7) is present, shown in Figure 15, and those performed in areas where no obvious BSR is present, shown in Figure 16. Where the BSR is present we see elevated velocities from 0.25 to 0.35 km followed by a strong velocity reversal starting at 0.35 km and 2.0 km/sec and going to 0.55 m and 1.7 km/sec, below which velocities monotonically increase. A very slight (perhaps insignificant) velocity reversal is seen at 0.3 km in analyses performed where no BSR is present, and a sharp slope break is seen at this depth. Note the high velocity at the point of the slope break is only slightly lower in the "No BSR" plot but the low velocity, just below the depth of the BSR is much higher than in the "BSR" plot. This may aid in determining quantities of methane present as discussed later.

A similar approach was attempted to distinguish between analyses performed in areas of seismic transparency or blanking (Figure 17) and areas of normal reflectivity (Figure 18). (Transparent zones are shown as stippled areas in Figure 7, and can be compared with the original seismic data in Figure 3). If the transparency is caused by large amounts of clathrate cement then these areas should have anomalously high velocities in the sediments above ~0.5 m and possibly anomalously low velocities in the sediments below ~0.5 km. However, the opposite effect is seen. A more significant velocity reversal occurs in areas of good reflectivity, and no such reversal is seen in the areas of seismic transparency.

The curves drawn through each of these subsets of the data are plotted together in Figure 19. Immediately apparent is the very good agreement (within 200 m/sec) of all the curves indicating that the analyses were performed consistently, and again confirming that the velocity profile of the entire area examined is laterally constant to within ~10%. Large lateral velocity anomalies do not exist in this area, but the largest anomaly, ~10%, is easily observed and it is associated with the presence of the BSR.

## DISCUSSION

To evaluate the significance of the velocity anomaly created by clathrates in the sediment we must first determine what the velocity would be near the depth of the BSR with no clathrate present. Even in areas where no BSR is present we see the same apparently anomalously high velocity of 2.1 km/sec so we base the clathrate free velocity on an extrapolation of the velocity of near surface sediment. We note from Figure 14 that the velocity vs. depth of sediments in the near surface (< 0.25 km) parallels the curve given by Hamilton (1980) for terrigenous sediment but ~0.1 km/sec slower. We assume that velocity of these sediments is unaffected by clathrate. A velocity ~0.1 km/sec slower than Hamilton's curve at 0.35 to 0.45 km is ~1.8 to 1.9 km/sec.

The acoustic velocity of sediments containing gas hydrate can be very high, greater than 2.7 km/sec, and the velocity of pure hydrate even higher, ~3.8 km/sec, much faster than the clathrate free velocity of 1.8 to 1.9 km/sec. However, no single shallow interval in our analyses showed this high a velocity. Instead we assume that clathrate is present in only a fraction of each anomalously high velocity seismic interval and we propose two simple models.

In the first model we assume that each interval measured consists of two sublayers, one containing hydrate cemented sediment, and one containing sediment with no hydrate, (consistent with DSDP results showing intermittent recovery of clathrate enriched sediment), and that the travel time of the measured interval is merely the sum of the travel times of the two types of sediment or equivalently the total slowness (reciprocal of velocity) is the sum of the slownesses weighted by their respective thicknesses,

$$z_{tot} / \alpha_{tot} = ( z_{normsed} / \alpha_{normsed} + z_{clathsed} / \alpha_{clathsed} )$$

where $\alpha_{tot}$ and $z_{tot}$ are the interval velocity and thickness of the layer, $\alpha_{normsed}$ and $z_{normsed}$ are the interval velocity and interval thickness for the sublayer containing no clathrate, and $\alpha_{clathsed}$ and $z_{clathsed}$ are the interval velocity and interval thickness for the sublayer of clathrate enriched cemented sediment. In this sediment we assume all of the pore spaces have been

filled with methane hydrate which has driven out the original pore fluids. Since the velocity of clathrate is similar to that of ice we assume that clathrate enriched sediment behaves similarly to frozen sediment whose velocity when saturated can be approximated by Wyllie's (1956) time average equation:

$$1/\alpha_{clathsed} = \phi / \alpha_{clath} + ( 1 - \phi ) / \alpha_{normsed}$$

where $\alpha_{clath}$ is the velocity of pure clathrate and $\phi$ is the porosity. Figure 20 shows a plot of $\alpha_{tot}$ vs. fraction enriched sediment for $\alpha_{normsed}$ = 1.8 and $\phi$ = 40% (left most solid line) and for $\alpha_{normsed}$ = 1.9 and $\phi$ = 30% (right most solid line). Note that the solid lines pass through the measured velocity $\alpha_{tot}$ = 2.1 km/sec (dashed line) at a fraction of ~0.65 (upper arrow). This suggests that for a layer with a velocity of 2.1 km/sec and a porosity of 30% to 40% whose velocity at this depth is normally 1.8 to 1.9 km/sec, the entire pore volume of ~65% of the layer has been replaced by clathrate. Given that many of these interpreted layers have a time thickness of 0.1 sec, and therefore a true thickness of ~0.1 km, the clathrate cemented layer, if it existed as a single layer would be ~0.065 km thick.

In the second model we assume that clathrate formation has excluded not only the pore fluids but also some of the matrix rock grains (also consistent with drilling results of intermittent recovery of pockets ~2 to 3 cm in size of pure clathrate). This layer is modeled by a sublayer of clathrate free sediment and a sublayer of pure methane hydrate. Again the total velocity is a weighted average of the slownesses of the two sublayers,

$$z_{tot} / \alpha_{tot} = ( z_{normsed} / \alpha_{normsed} + z_{clath} / \alpha_{clath} )$$

where $\alpha_{clath}$ and $z_{clath}$ are the interval velocity and interval thickness for the sublayer of pure methane hydrate. The results of this model are also shown in Figure 20 as dotted lines. We see that sediments with clathrate free velocities between 1.8 and 1.9 km/sec both converge to the velocity of pure clathrate as the rock becomes completely replaced by clathrate. To achieve

a velocity of 2.1 km/sec ~25% (lower arrow in Figure 20) of the layer must be replaced by pure clathrate. This corresponds to roughly the same total volume of clathrate as in the first model. Therefore when determining the volume of clathrate from the velocity in the manner discussed here either model works equally well. Both models indicate that for sediments in this area of the Blake Plateau with 30% to 40% porosity whose velocity is 2.1km/sec and whose clathrate free velocity is 1.8 to 1.9 km/sec, ~25% of the volume is occupied by clathrates.

## CONCLUSIONS

High resolution analysis of seismic interval velocities on Line BA-6 in the Blake Ridge area offshore southeastern U.S. have shown that there are no significant lateral variations in velocity associated with seismic transparent zones in the shallow sediments. However, differences in the velocity profiles do exist between areas with a BSR and those without. In all profiles we see slightly elevated velocities from ~0.3 - 0.4 km sub-bottom, just above the level of the BSR. Because of the density and velocity of methane hydrate no large reflection would be expected due to the presence of hydrate alone. In areas with a BSR this high velocity anomaly is enhanced and occurs in conjunction with a significant low velocity anomaly below the BSR suggesting a higher concentration of clathrate in the sediments just above the BSR. The models discussed above suggest that ~25% of the volume of these anomalously fast intervals consists of methane hydrate.

## REFERENCES


Brysk, H., and D. McCowan, 1986, A slant-stack procedure for point source data, *Geophysics*, V. 51, p. 1370-1386.

Carpenter, G., 1981, Coincident sediment slump/clathrate complexes on the U.S. Atlantic continental slope, *Geo-Marine Letters*, V. 1, p. 29-32.

Claypool, G. E., and I. R. Kaplan, 1974, The origin and distribution of methane in marine sediments, In Kaplan, I. R., (Ed.), Natural Gases in Marine Sediments: New York (Plenum), p. 94-129.

Diebold J. B., and P. L. Stoffa, 1981,The travel time equation, tau-p mapping and inversion of common midpoint data. *Geophysics*, V. 46, p. 238-254.

Diebold J. B., 1987, Three dimensional traveltime equation for dipping layers, *Geophysics*, V. 52, p. 1492-1500.

Dillon, W. P., and C. K. Paull, 1983, Marine gas hydrates-II: geophysical evidence, in Cox, J. L., (Ed), Hydrates: Properties, Occurrences, and Recovery, Butterworth Publishers, Boston, p. 73-90.

Dillon, W. P., and P. Popenoe, 1988, The Blake Plateau Basin and Carolina Trough, in Sheridan, R. D., and J. A. Grow, (Eds.), The Geology of North America, Vol I-2, The Atlantic Continental Margin: U.S., The Geological Society of America, Boulder, CO, p. 291-328.

Field, M. E., and K. A. Kvenvolden, 1985, Gas hydrates on the northern California continental margin, *Geology*, V. 13, p. 517-520.

Hamilton, E. L., 1976, Variations of density and porosity with depth in deep sea sediments. , *J. Sedimentary Petrology*, V. 46, No. 2, p. 280-300.

Hamilton, E. L., 1980, Geoacoustic modeling of the sea floor, *J. Acoust. Soc. Am.*, V. 68, No. 5, p. 1313-1340.

Hammond, R. D. and J. R. Gaither, 1983, Anomalous seismic character-Bering Sea shelf, *Geophysics*, V. 48, No. 5, p. 590-605.

Hein, J. R., D. W. Scholl, J. A. Barron, M. J. Jones, and J. Miller, 1978, Diagenesis of late Cenozoic diatomaceous deposits and formation of the bottom simulating reflector in the southern Bering Sea, *Sedimentology*, V. 25, p. 155-181.

Kvenvolden, K. A., 1984, Comparison of marine gas hydrates in sediments of an active and passive continental margin, *Marine and Petroleum Geology*, V. 2, p. 65-71.

Kvenvolden, K. A., 1988, Methane hydrate - a major reservoir of carbon in the shallow geoshpere?, *Chemical Geology*, V. 71, p. 41-51.

Kvenvolden, K. A., and L. A. Barnard, 1983, Gas hydrates of the Blake outer ridge, site 533 deep sea drilling project leg 76, In R. E. Sheridan, F. Gradstein et al., (Eds.), Init. Rep. Deep Sea Drill. Proj., V. 76, U.S. Govt. Print. Off., Washington, D.C., p. 353-365.

Kvenvolden, K. A., and T. J. McDonald, 1985, Gas hydrates of the middle America trench-deep sea drilling project leg 84, In R. von Huene, J. Aubouin et al., (Eds.), Init. Rep. Deep Sea Drill. Proj., V. 84, U.S. Govt. Print. Off., Washington, D.C., p. 667-682.

Lancelot, Y., and J. I. Ewing, 1973, Correlation of natural gas zonation and carbonate diagenesis in tertiary sediments from the north-west Atlantic, In C. D. Hollister, and J. I. Ewing et al., (Eds.), Init. Rep. Deep Sea Drill. Proj., V. 11, U.S. Govt. Print. Off., Washington, D.C., p. 791-799.

Mathews, M. A. and R. von Huene, 1985, Site 570 methane hydrate zone, In R. von Huene, J. Aubouin et al., (Eds.), Init. Rep. Deep Sea Drill. Proj., V. 84, U.S. Govt. Print. Off., Washington, D.C., p. 773-790.

Paull, C. K., and W. P. Dillon, 1981, Appearance and distribution of the gas hydrate reflection in the Blake ridge region, offshore southeastern United States, Map, U.S. Geological Survey, Reston, VA.

Pearson, C., J. Murphy, and R. Hermes, 1986, Acoustic resistivity measurements on rock samples containing tetrahydrofuran hydrates: laboratory analogues to natural gas hydrate deposits, *J. Geophys. Res.*, V. 91, N. B14, p. 14132-14138.

Shipley, T. H., M. H. Houston, R. T. Buffler, F. J. Shaub, K. J. McMillen, J. W. Ladd, and J. L. Worzel, 1979, Seismic evidence for widespread possible gas hydrate horizons on continental slopes and rises, *AAPG Bulletin*, V. 63, p. 2204-2213.

Shipley, T. H., and B. M. Didyk, 1982, Occurrence of methane hydrates offshore southern Mexico, In J. S. Watkins, J. C. Moore, et al. (Eds.), Init. Rep. Deep Sea Drill. Proj., V. 66, U.S. Govt. Print. Off., Washington, D.C., p. 547-555.

Stoffa, P. L., P. Buhl, J. B. Diebold, and F. Wenzel, 1981, Direct Mapping of seismic data to the domain of intercept time and ray parameter: A plane wave decomposition, *Geophysics*, V. 46, p. 255-267.

Stoffa, P. L., J. T. Fokkema, R. M. deLuna Freire, and W. P. Kessinger, Split step Fourier migration, *Geophysics*, V. 55, No. 4, p. 410-421.

Stoll, R. D., J. Ewing, and G. M. Bryan, 1971, Anomalous wave velocities in sediments containing gas hydrates, *J. Geophys. Res.*, V. 76, No. 8, p. 2090-2094.

Tucholke, B. E., G. M. Bryan, and J. I. Ewing, 1977, Gas-hydrate horizons detected in seismic-profiler data from the western north Atlantic, *AAPG Bulletin*, V. 61, No. 5, p. 698-707.

Whalley, E., 1980, Speed of longitudinal sound in clathrate hydrates, *J. Geoph. Res.*, V. 85, p. 2539-2542.

Wyllie, M. R. J., A. R. Gregory, and L. W. Gardner, 1956, Elastic wave velocities in heterogeneous and porous media, *Geophysics*, V. 21, p. 41-70.

Yamano, M., S. Uyeda, Y. Aoki, and T. H. Shipley, 1982, Estimate of heat flow derived from gas hydrates, *Geology*, V. 10, p. 339-343.

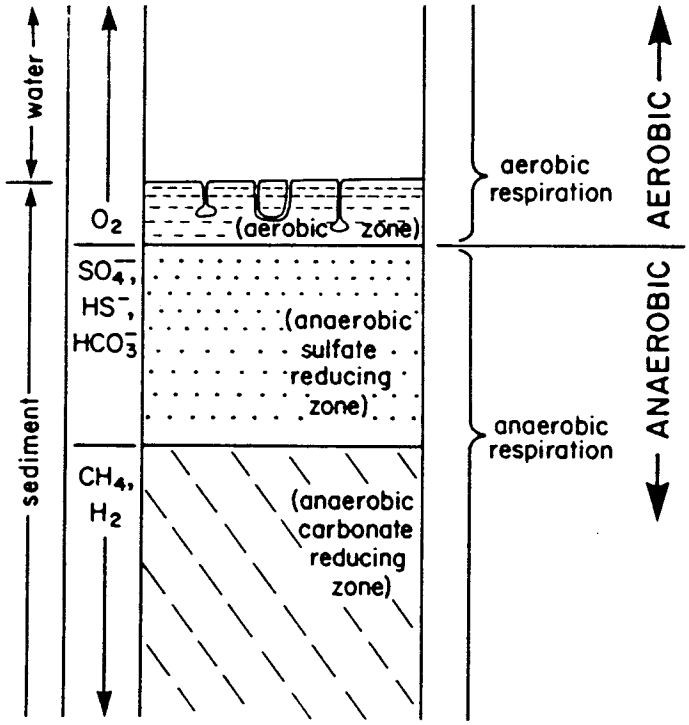


Figure 1. Methane production in the shallow sub-bottom sediments occurs in the lower most of three successive ecological zones, an aerobic zone, an anaerobic sulfate reducing zone, and an anaerobic carbonate reducing zone. Depth to the top of the third zone is likely to be 10's of meters. (From Claypool and Kaplan, 1974)

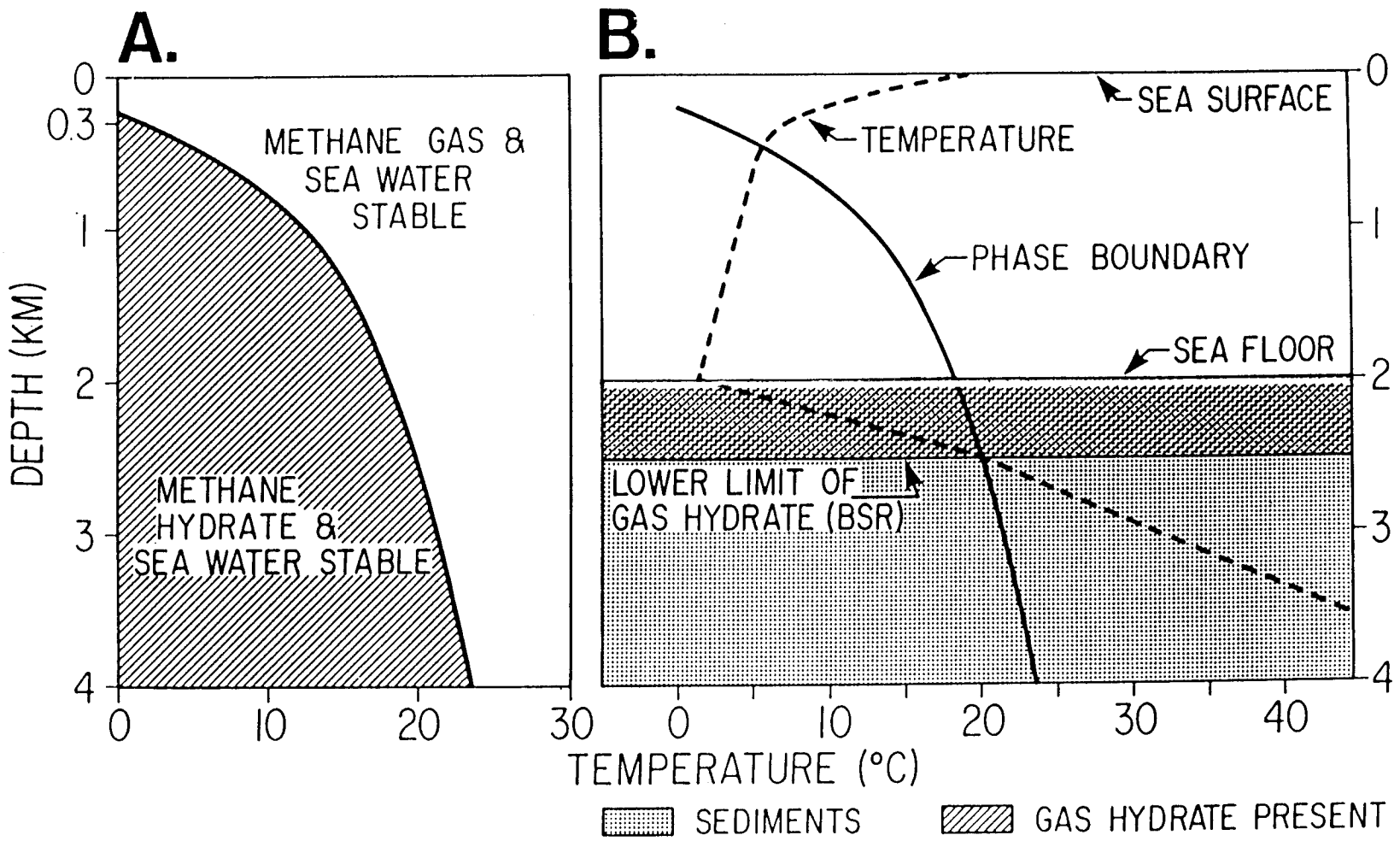


Figure 2. A) The stability of methane as a hydrate is sensitive to pressure and temperature. Higher hydrostatic pressures and lower temperatures increase the stability of methane as a hydrate. B) The hydrate/gas phase boundary (solid line) and a typical temperature profile (dashed line) are shown for deep marine sediments. The area of the diagram which is both to the left of the phase boundary and to the right of the temperature profile is the pressure-temperature region where methane is stable as a hydrate with sea water. (From Dillon and Paul, 1983)

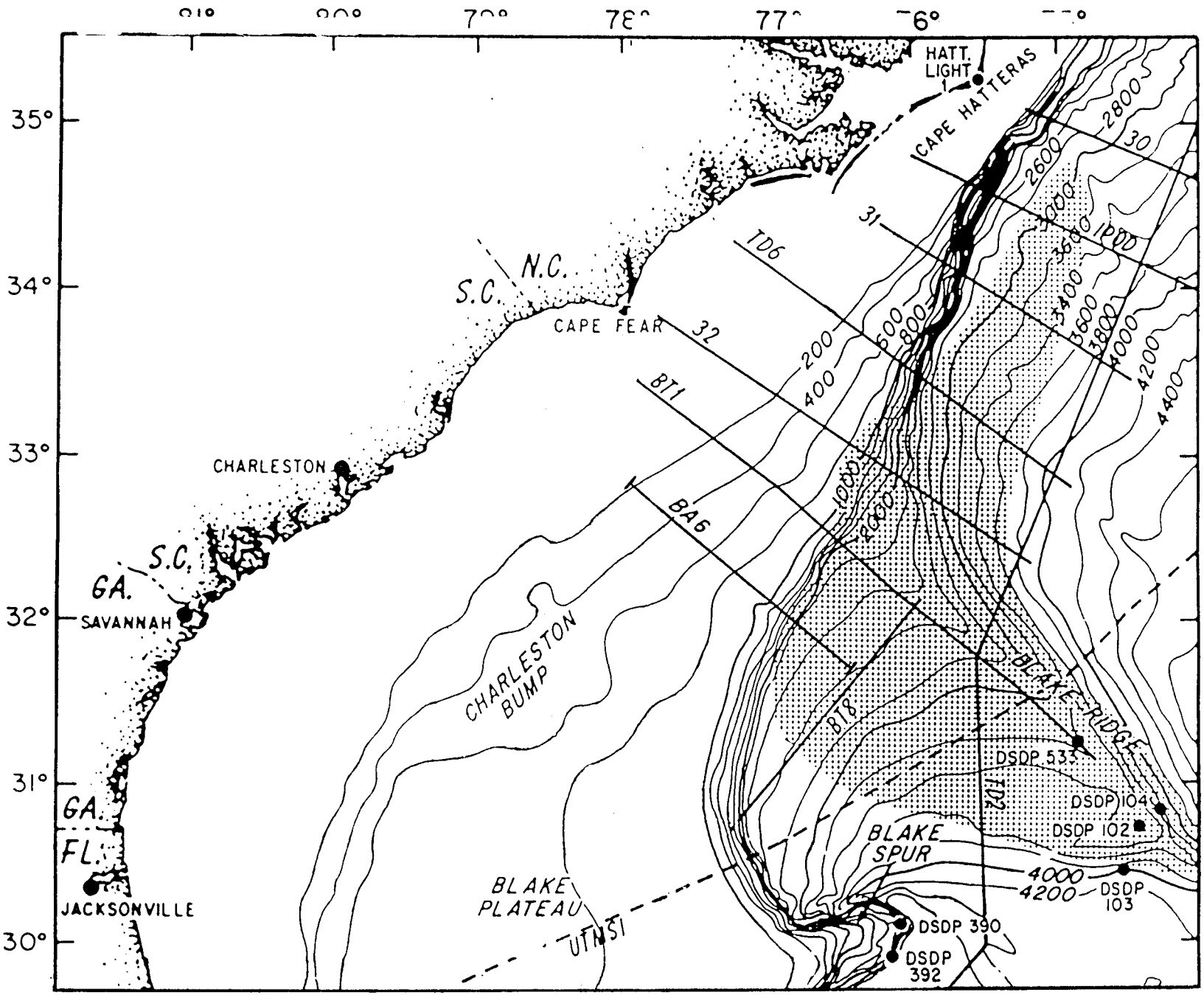


Figure 3. The seismic line used in this study is marked BA6 in the diagram of the southeastern Atlantic coast of the U.S. Only the portion of the line deeper than 1500 m was examined. The stippled area indicates the presence of a BSR mapped by Paull and Dillon, 1981 using single and multi-channel seismic lines, some of which are shown here. Note the four DSDP sites in areas where a BSR is expected. (From Dillon, 1988)

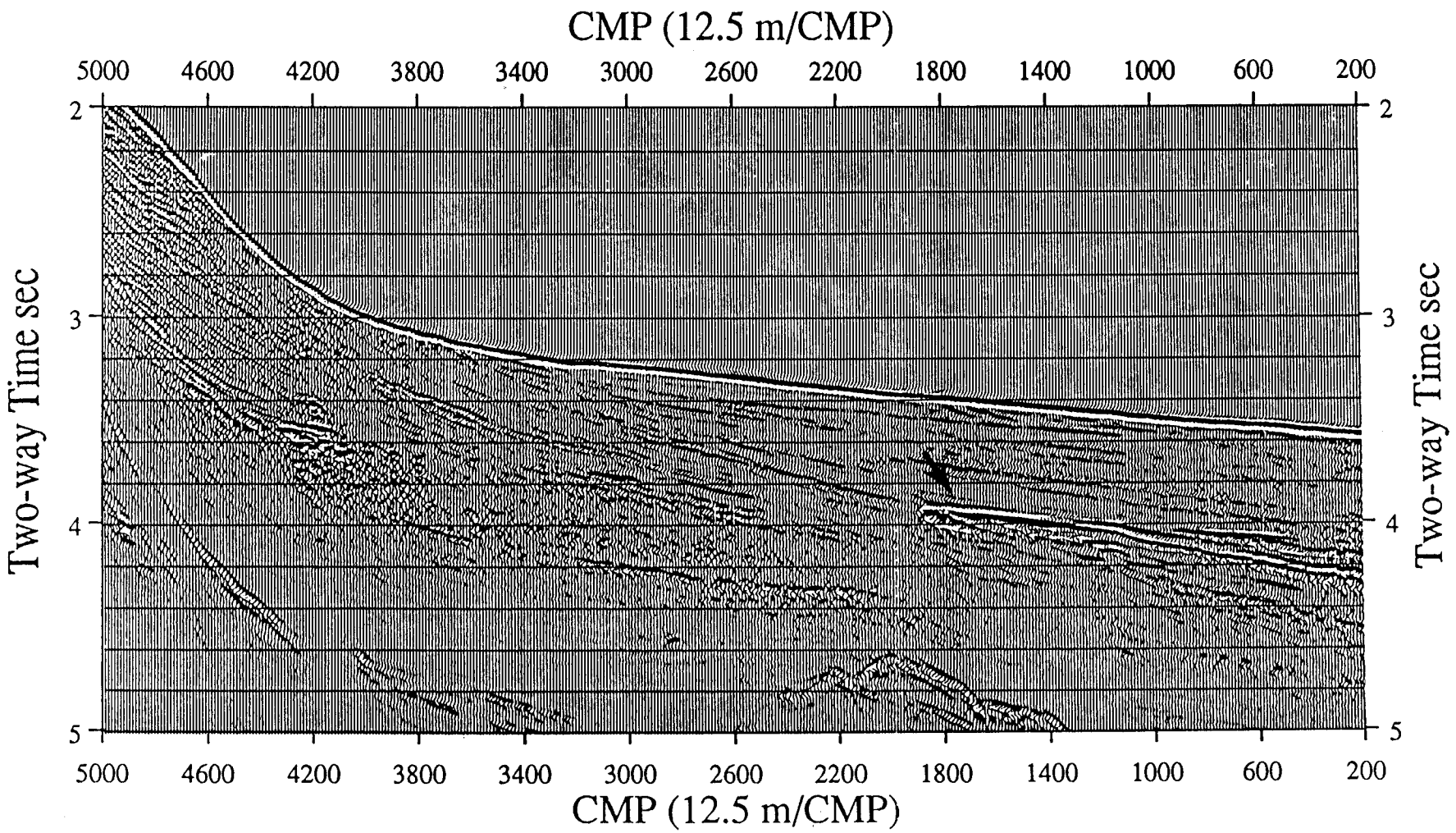


Figure 4. The seaward portion of BA6 after conventional processing but unmigrated. Note the strong BSR from 4.080 s at CMP 500 to 3.920 s at CMP 1800, (arrow) and a possible BSR at 3.750 s at CMP 3100.

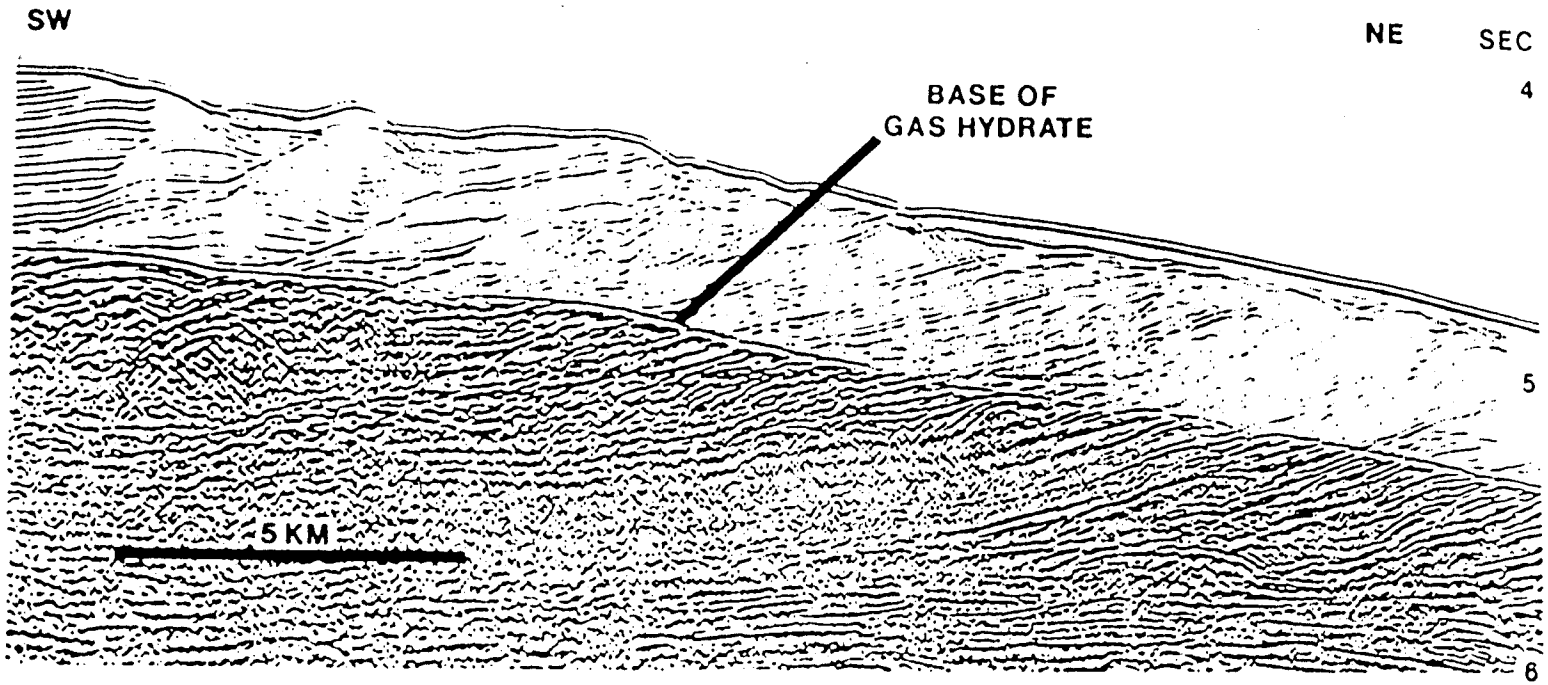


Figure 5. This seismic section from the Blake Outer Ridge shows a sharp contrast in reflectivity between almost transparent sediment above the BSR to very reflective sediments below. (From Shipley et al., 1979)

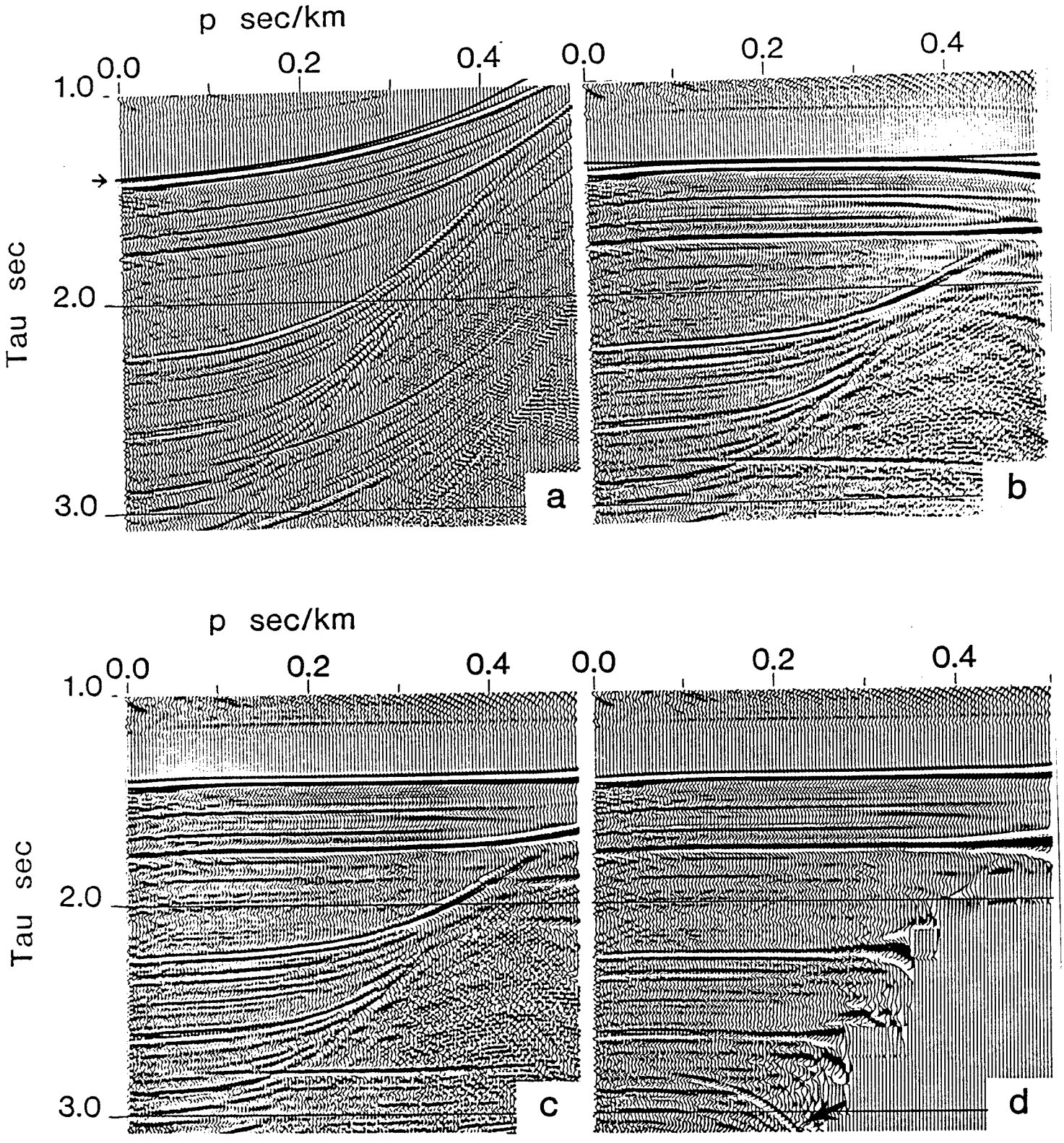


Figure 6. a) The raw τ-p gather (CMP 4900) is displayed on a graphics screen and the interpreter picks a τ at p = 0.0 (arrow) and chooses a velocity. A delay time curve corresponding to the picked velocity and $\tau_o$ is then superimposed on the seismic data (solid line). b) An NMO correction is applied to the data according to the current model. In this example the velocity has been overestimated and adjustment takes place in the corrected domain. c) The water bottom reflection has been correctly modeled and the next layer for analysis is chosen. d) When all layers have been interpreted the reflections in the seismic data will be correctly moved out. (Note the easily distinguished multiple at 2.8 sec at the arrow.)

# Velocity Analysis Intervals

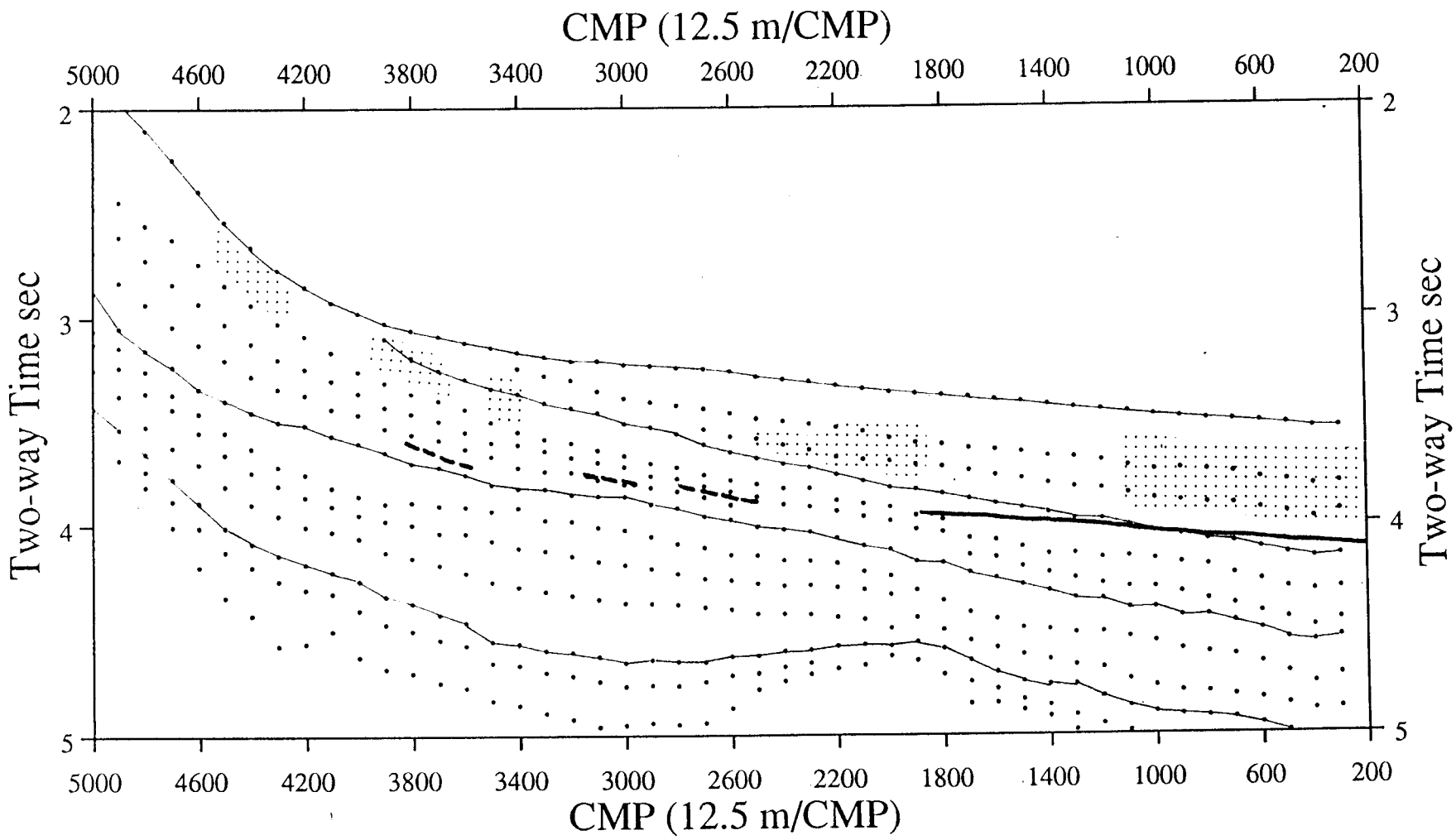


Figure 7. The points (dots) shown here mark the geologic interval boundaries used for the velocity analyses. The interval boundaries of the four layer analyses are marked with a solid line. The location of the BSR is indicated with a heavy solid line and possible BSRs are indicated with a heavy dashed line. Areas of seismic transparency or "blanking" in the shallow section are stippled. Compare with Figure 4.

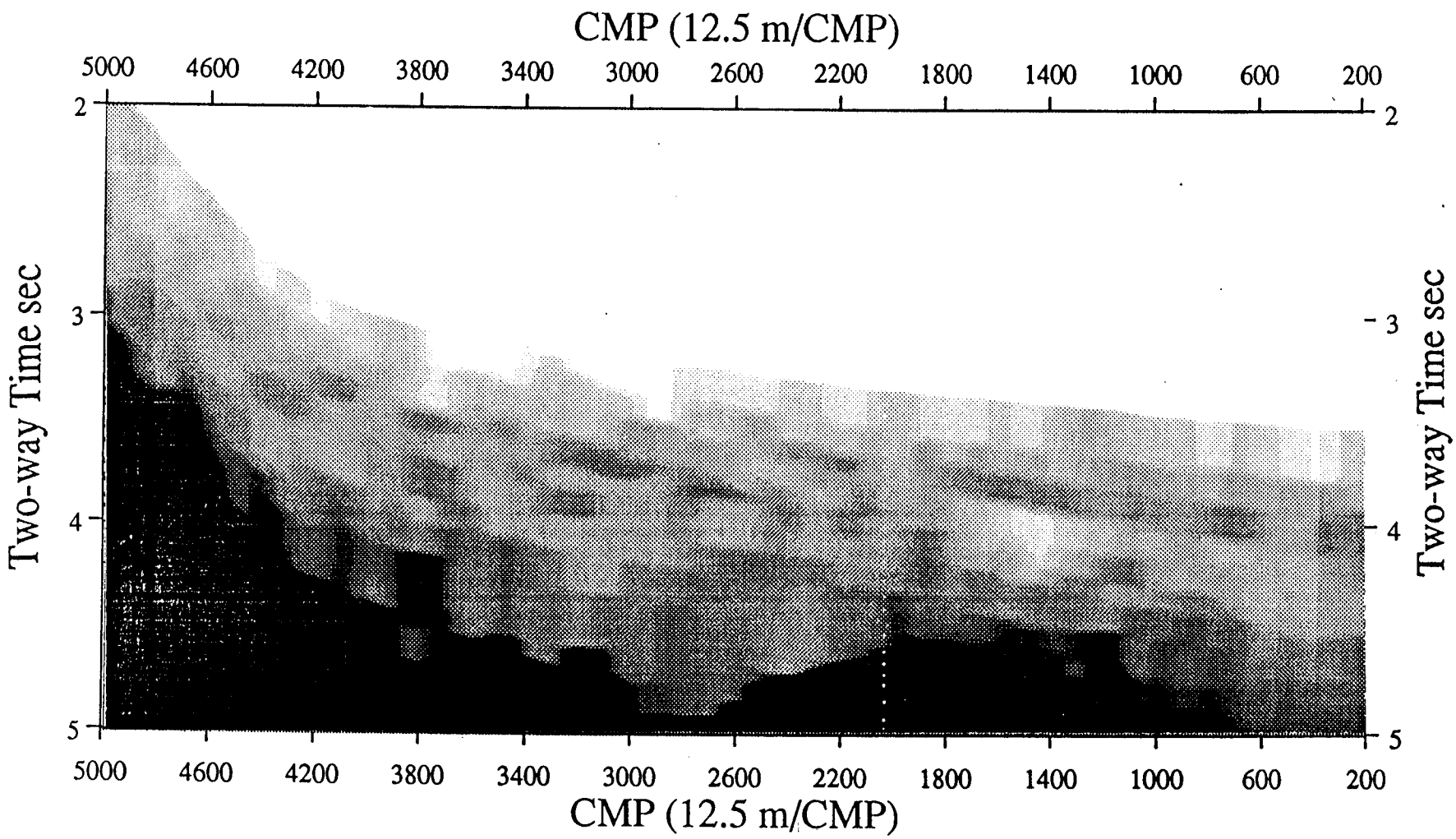


Figure 8. After smoothing with a filter 0.06 sec in time and 2.5 km long laterally the final result of the many layered analysis is shown here with higher velocities indicated by darker shades (black > = 2.5 km/sec, white < = 1.5. Note the relatively fast band parallel to and just above the BSR.

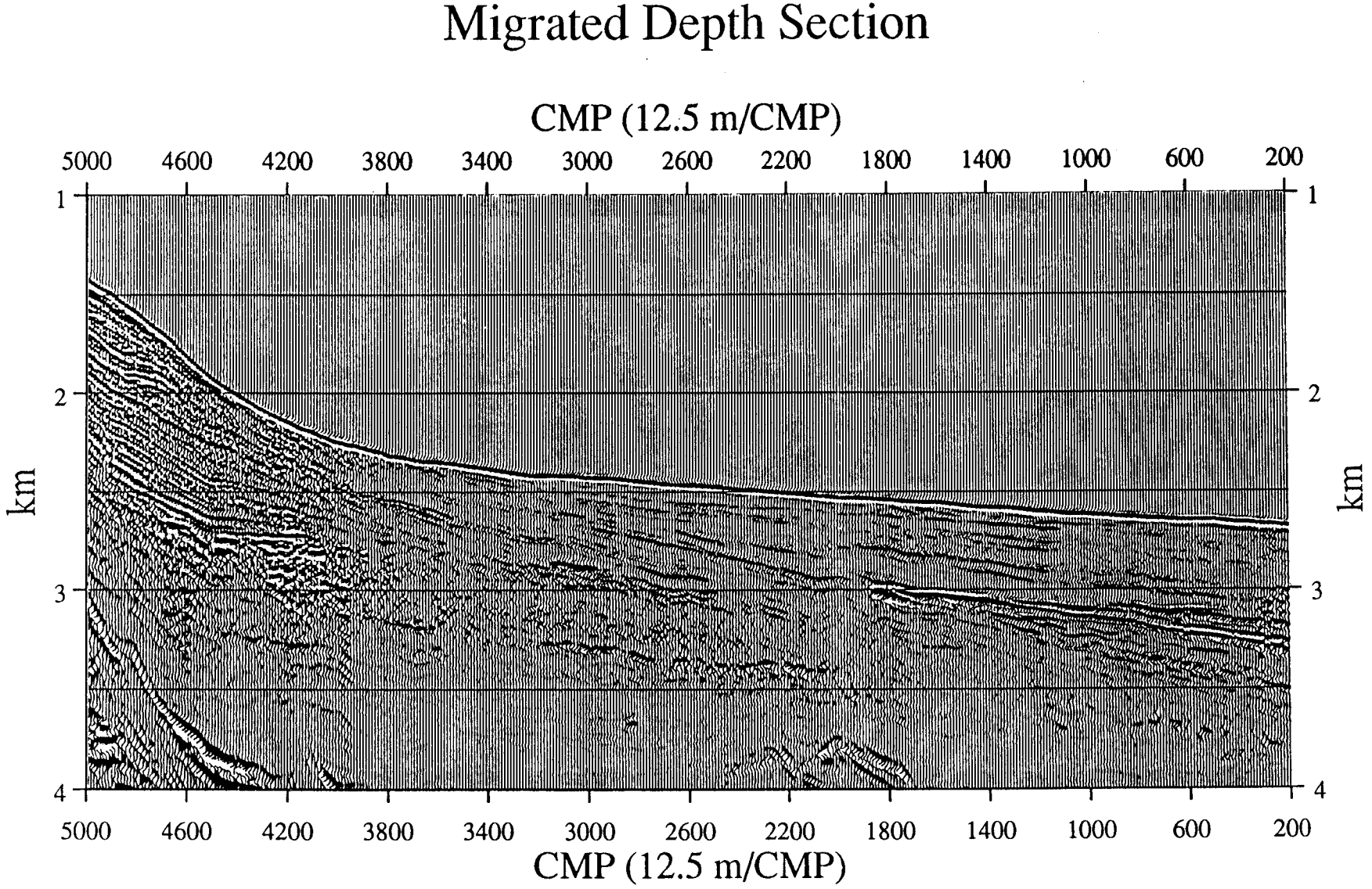


Figure 9. Accurate interval velocities allow for an accurate depth migration of the seismic data. Note the nearly constant sub-bottom depth of the BSR.

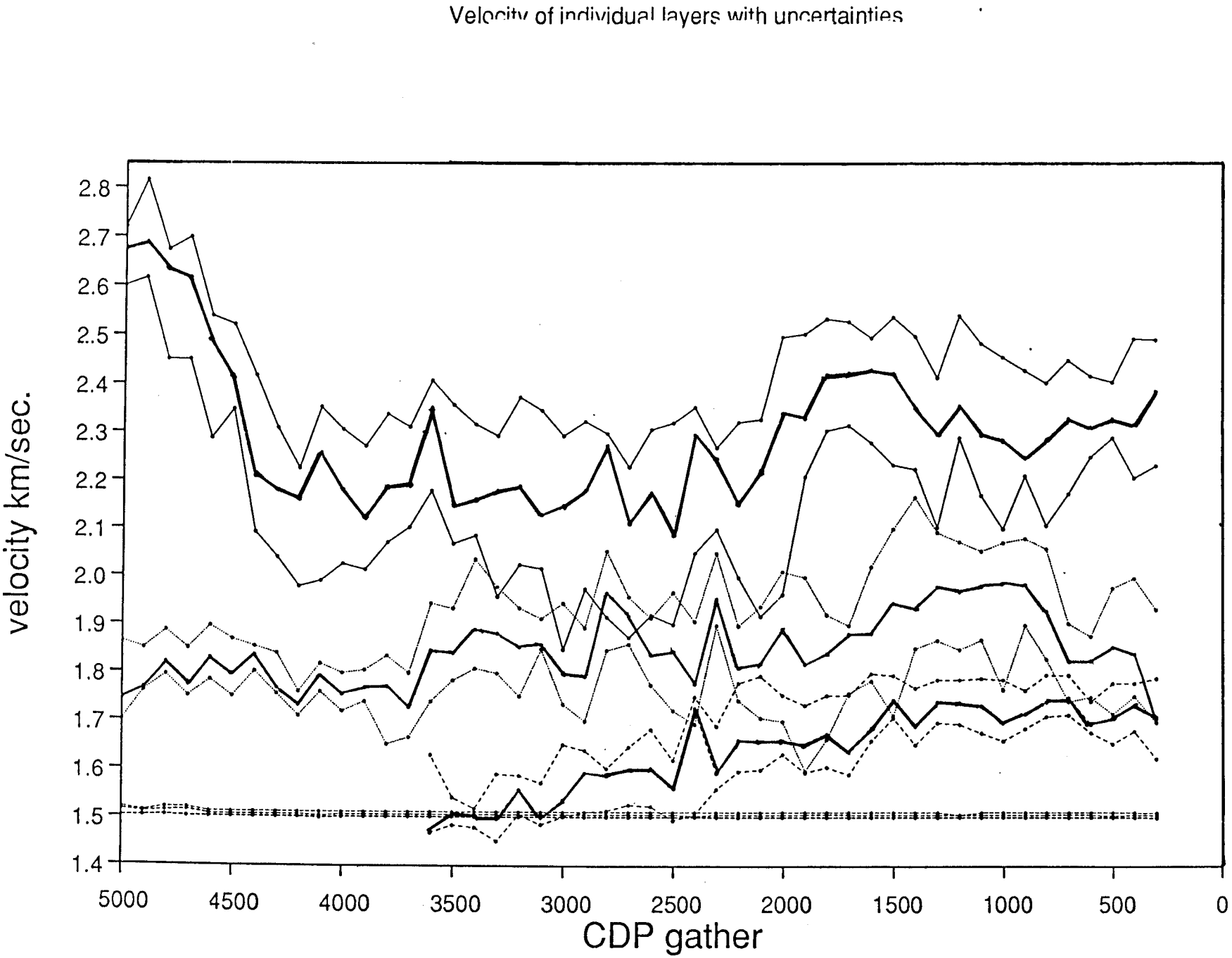


Figure 10. The interval velocities of the four layer analysis are plotted vs. CMP. The bold curves represent the interval velocity in each sediment layer of the four layer analysis, (velocities for the water column appear as 3 sub-parallel lines since all measurements were 1.5 km/sec +/- .005 km/sec), and the narrow lines correspond to the uncertainty bounds interpreted for each measurement. The bottom most bold line shows the velocity for the top most sediment layer, and the next bold line up corresponds to the second layer and the top most bold line corresponds to the bottom most layer.

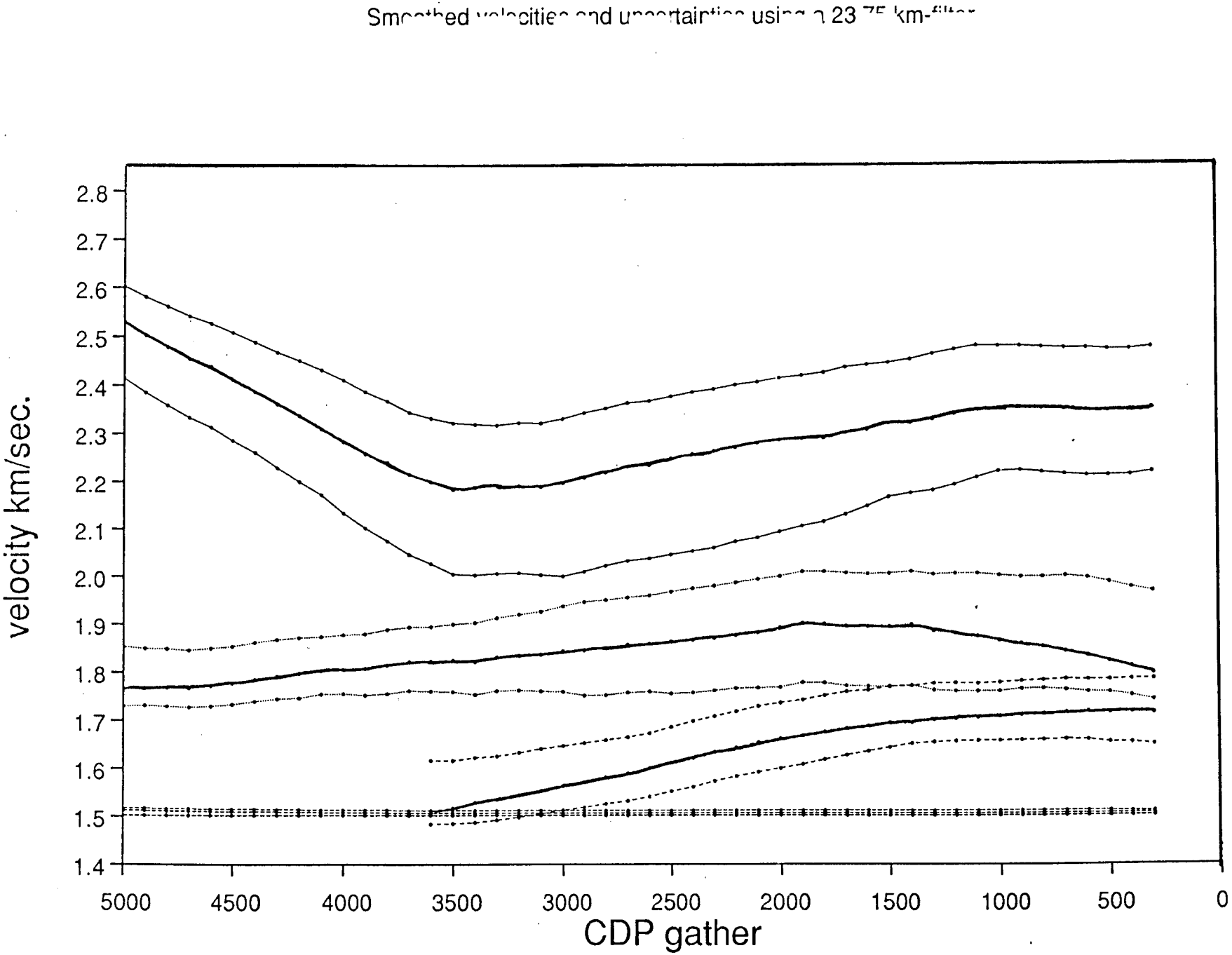


Figure 11. Here the interval velocities of the four layer analysis are smoothed over 23.75 km and the uncertainties are adjusted to the smooth curve. Again the bottom most bold line shows the velocity for the top most sediment layer, and the next bold line up corresponds to the second layer and the top most bold line corresponds to the bottom most layer.

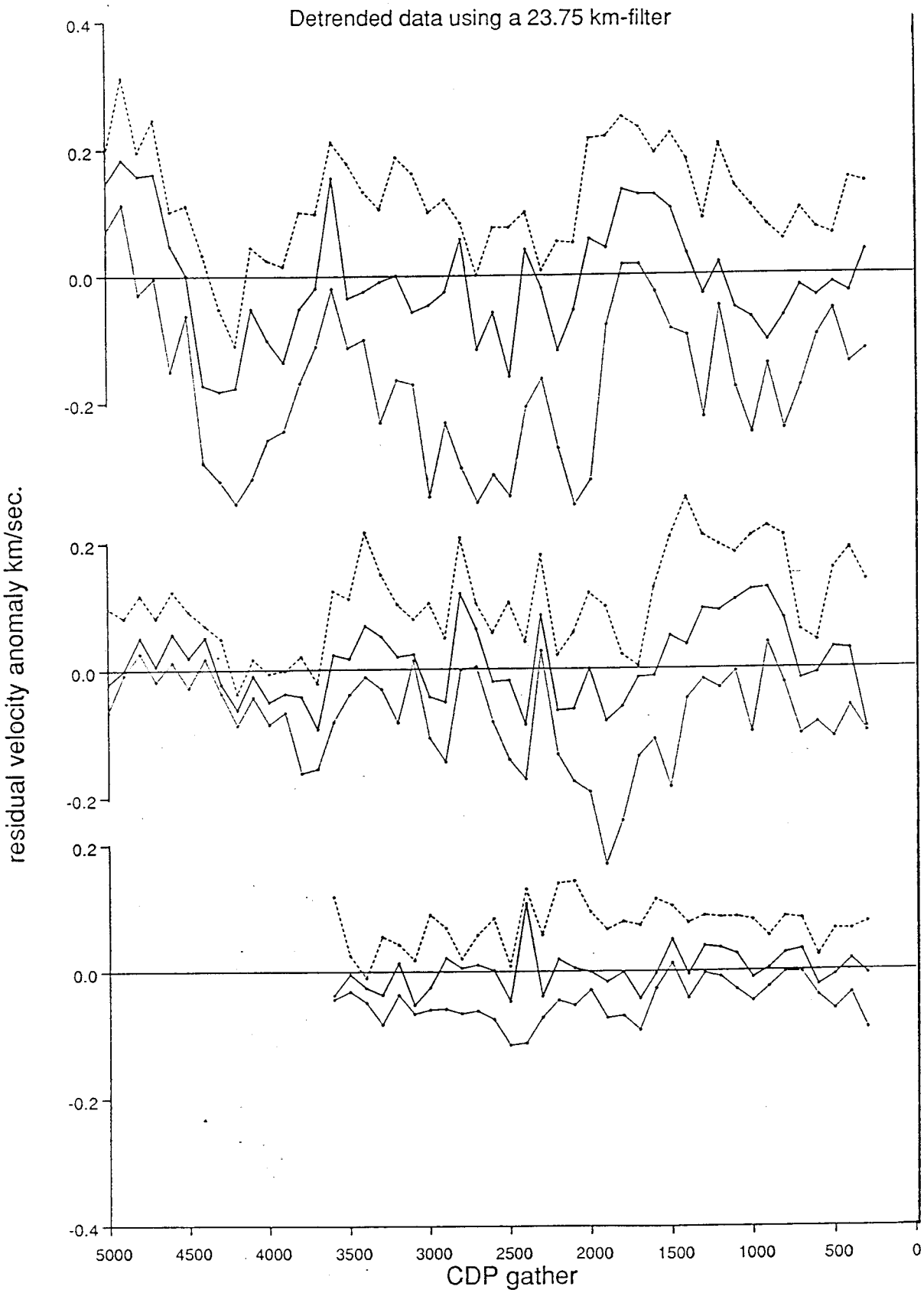


Figure 12. The smooth curves of Figure 11 have been subtracted from the raw data of Figure 10 to enhance the more rapid lateral variations we expect from changing reflectivity. Unfortunately most of the variations are within the uncertainty. The top figure corresponds to the bottom most sediment layer; the center figure corresponds to the middle sediment layer; and the bottom figure corresponds to the topmost sediment layer.

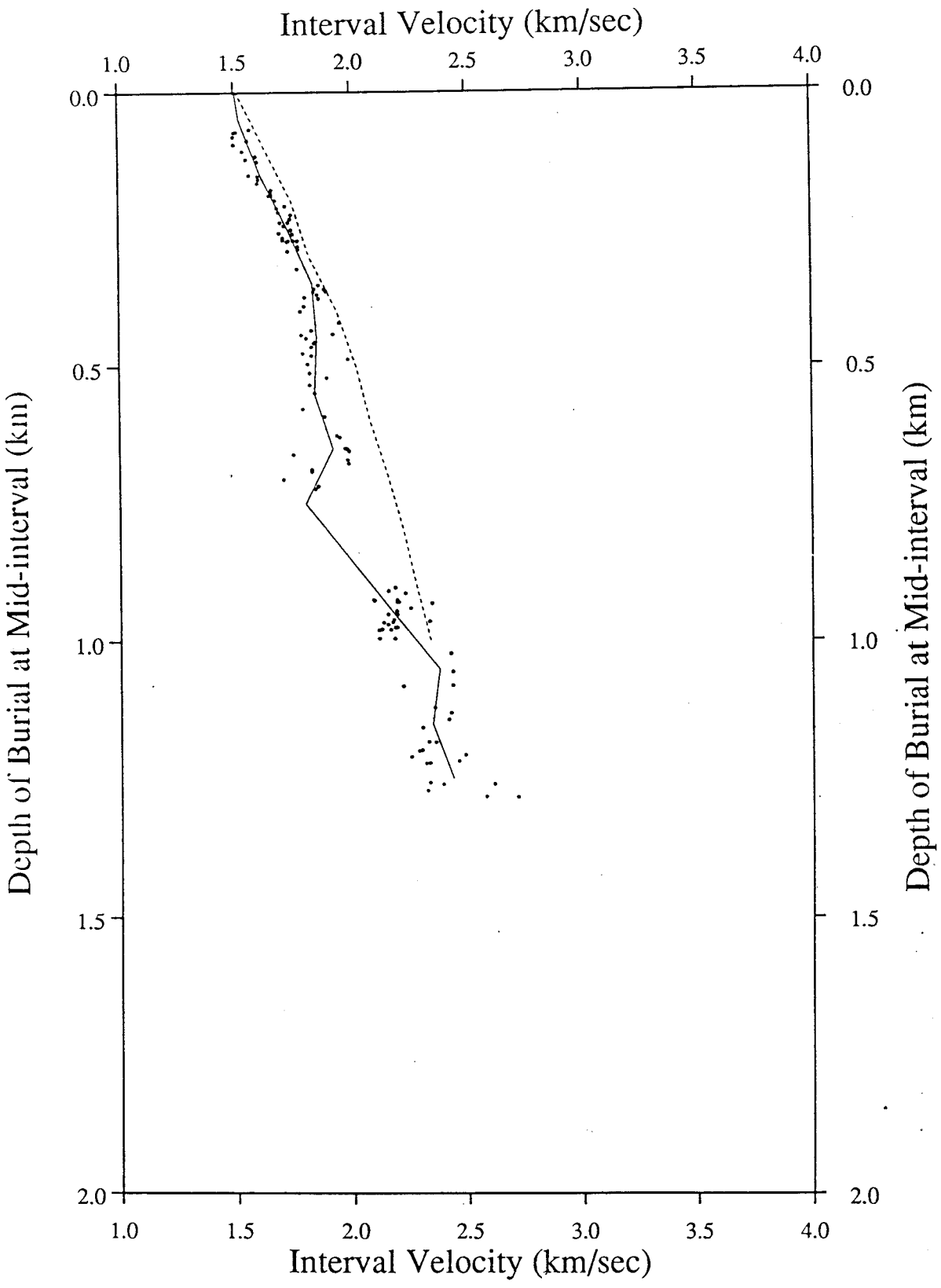


Figure 13. Depth from the sea bottom to the center of the interval vs. the corresponding interval velocity. The solid line shown was obtained by averaging velocities within bins (see text), and the dashed line represents an average for clastic sediments, (Hamilton, 1980). The data points are those from the analyses done with four intervals.

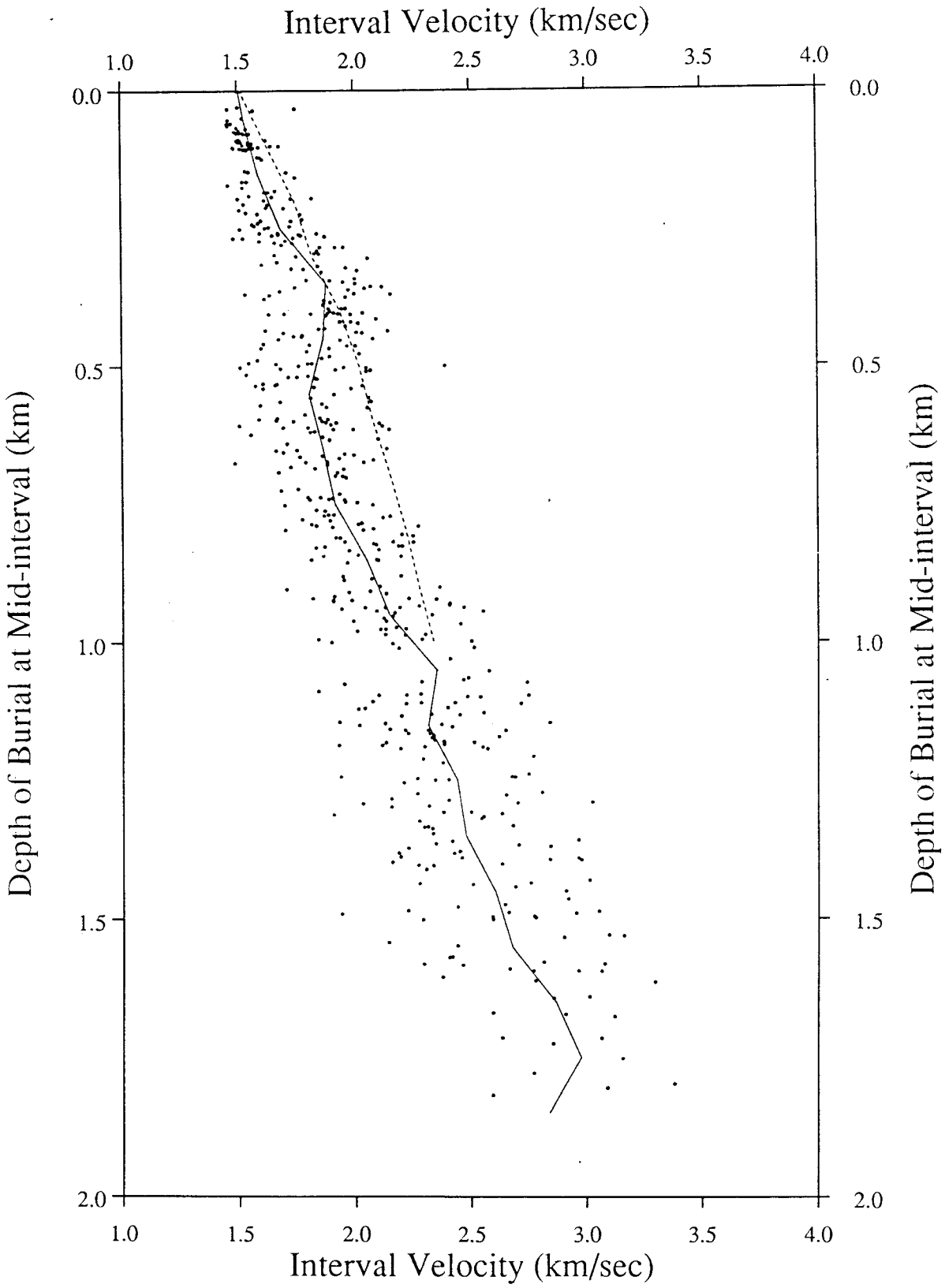


Figure 14. Interval velocity vs. depth of burial for the analyses done for many layers. Note the slightly elevated velocities just above 450 m, the depth corresponding to the BSR, and significantly depressed velocities below this depth.

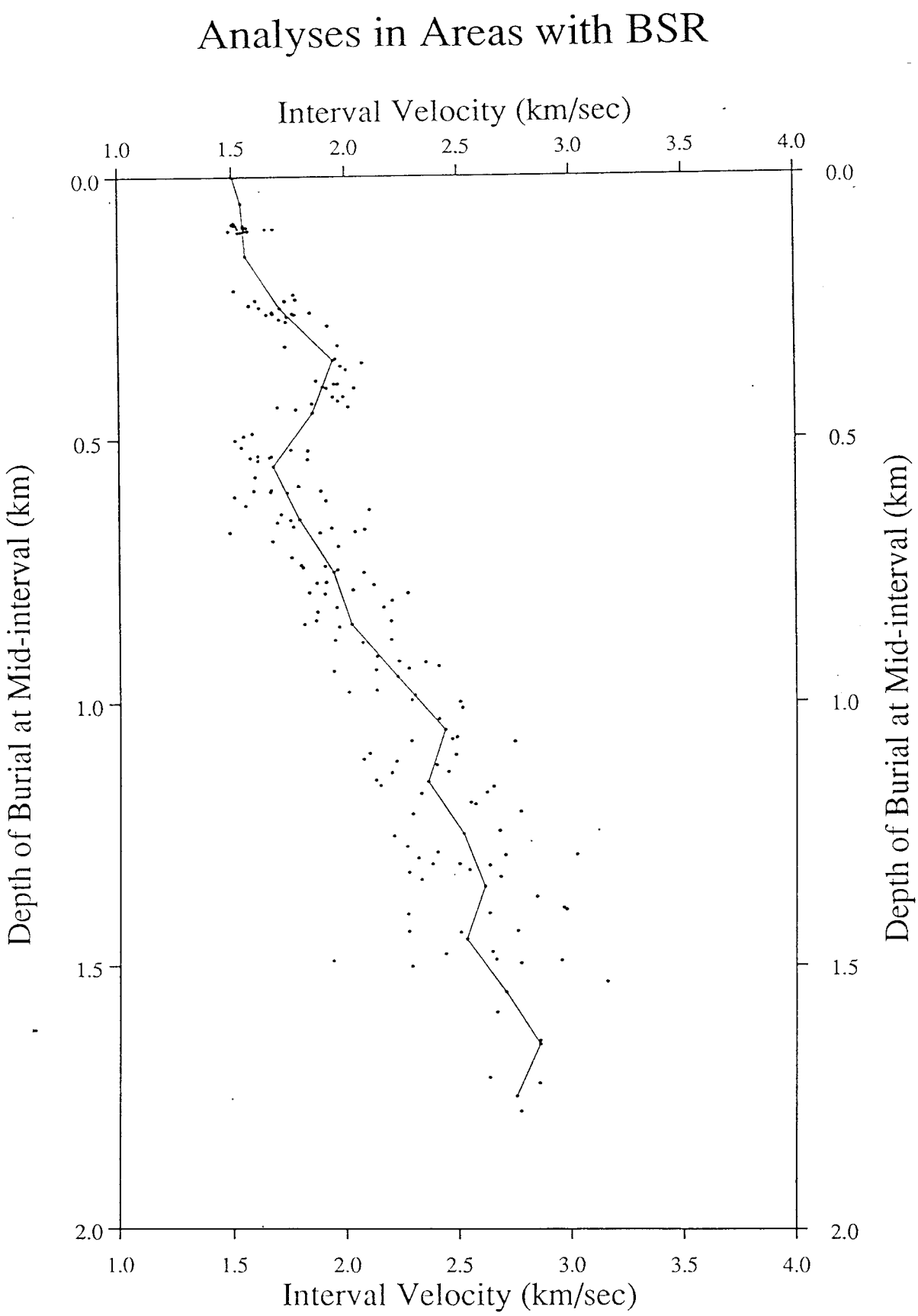


Figure 15. Interval velocity vs. depth of burial for the analyses done in areas where the BSR is present. Note the strong velocity reversal just below the depth corresponding to the BSR.

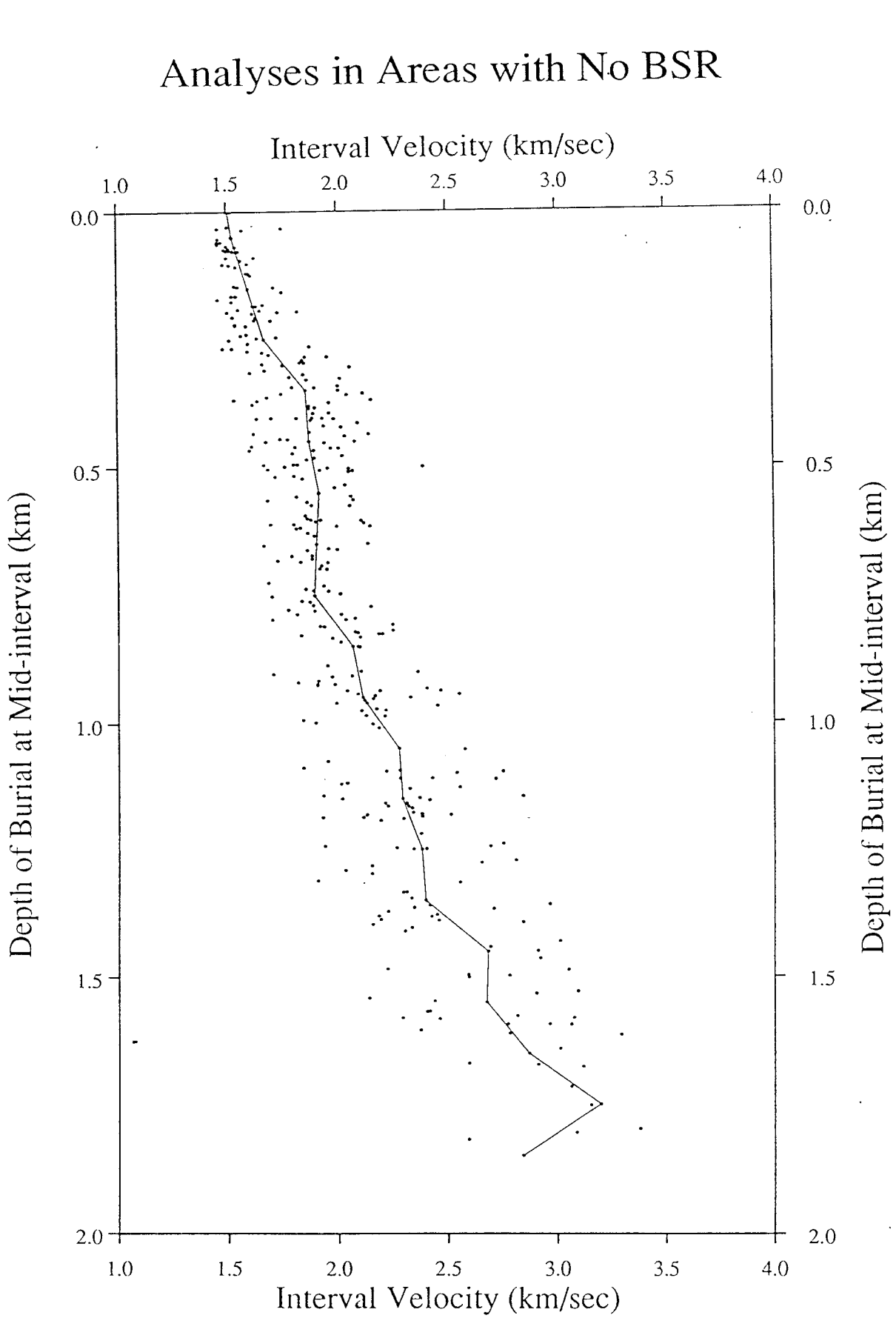


Figure 16. Interval velocity vs. depth of burial for the analyses done in areas where no BSR is present.

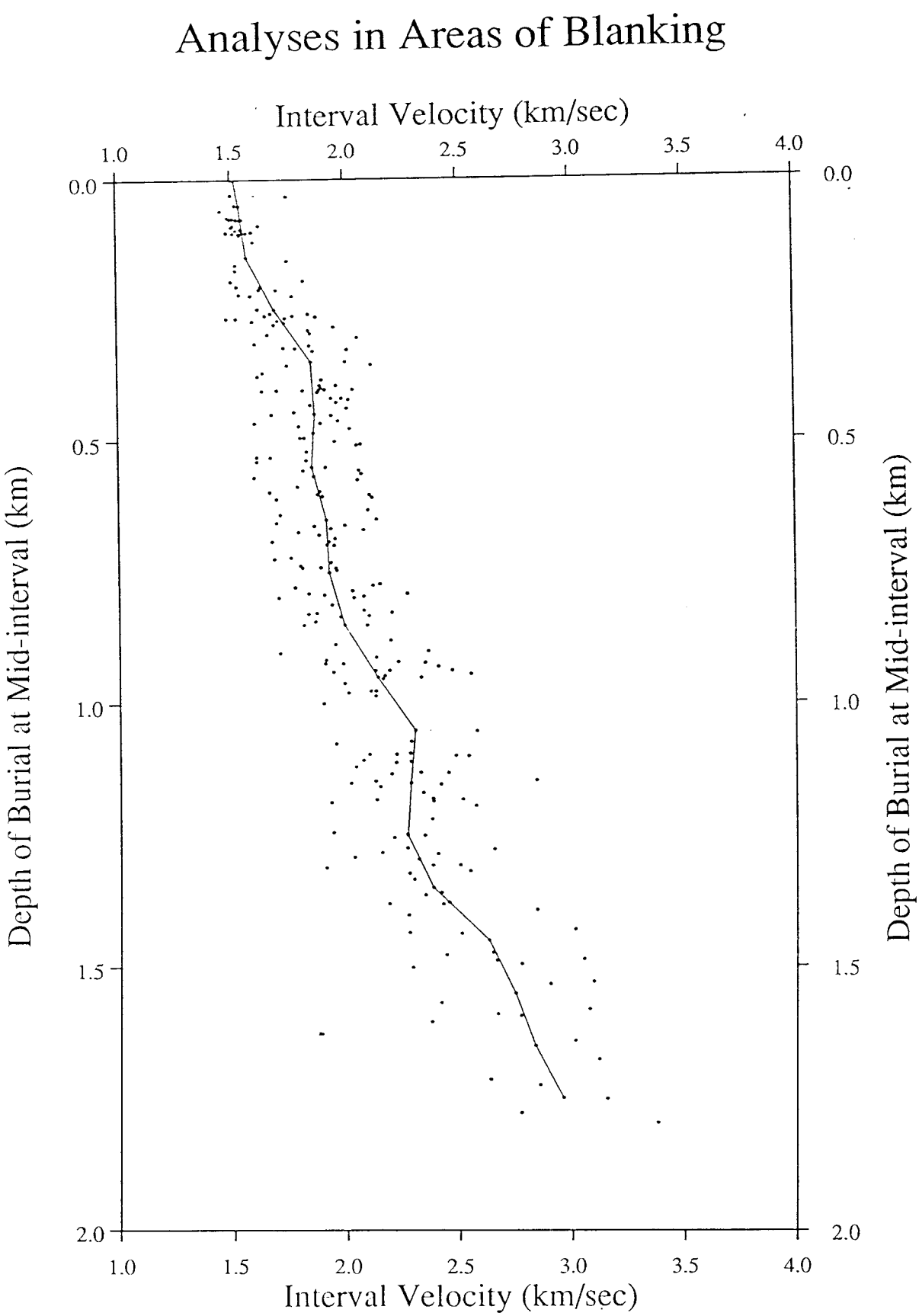


Figure 17. Interval velocity vs. depth of burial for the analyses done in areas of seismic transparency.

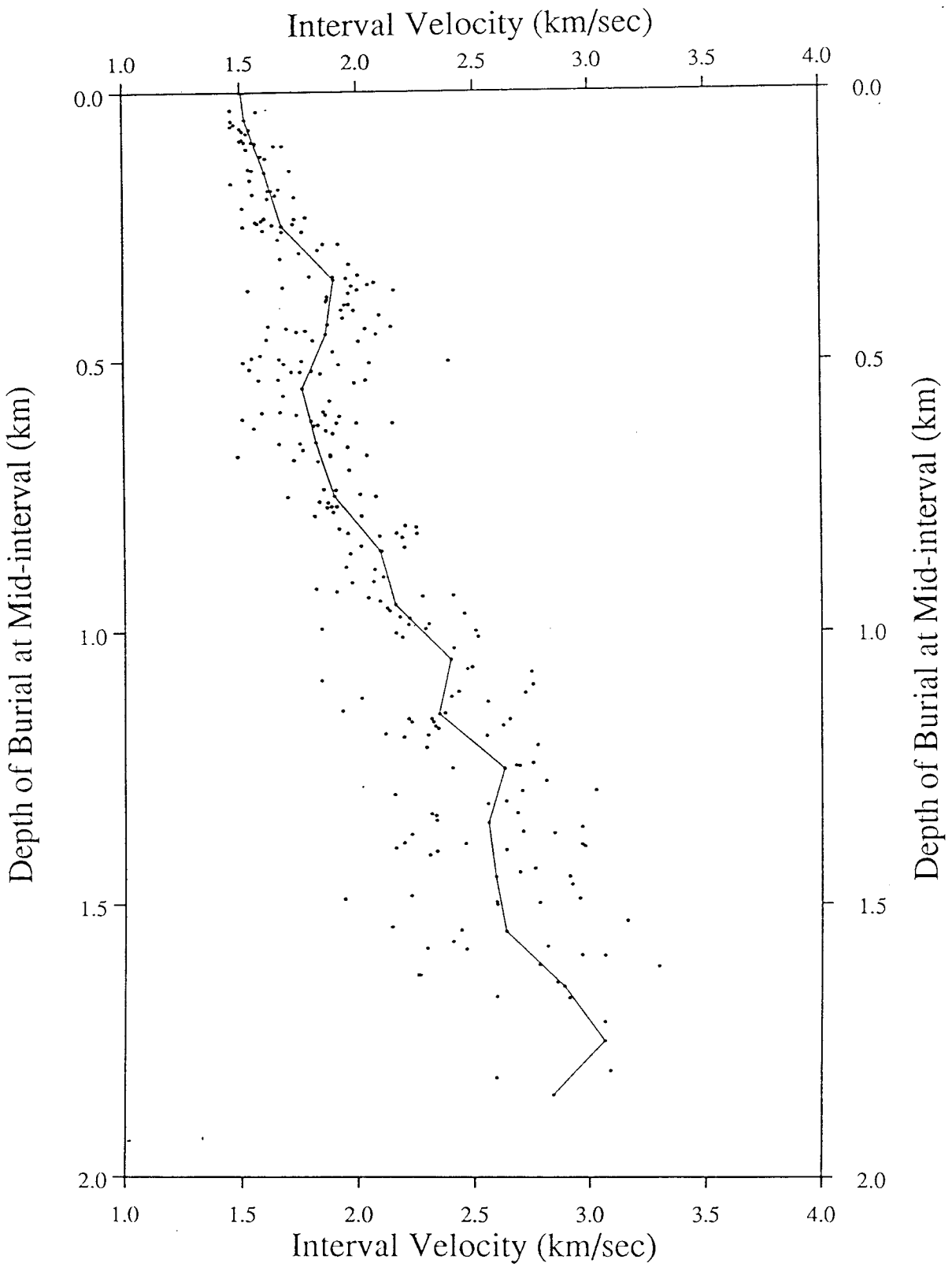


Figure 18. Interval velocity vs. depth of burial for the analyses done in areas of typical seismic reflectivity.

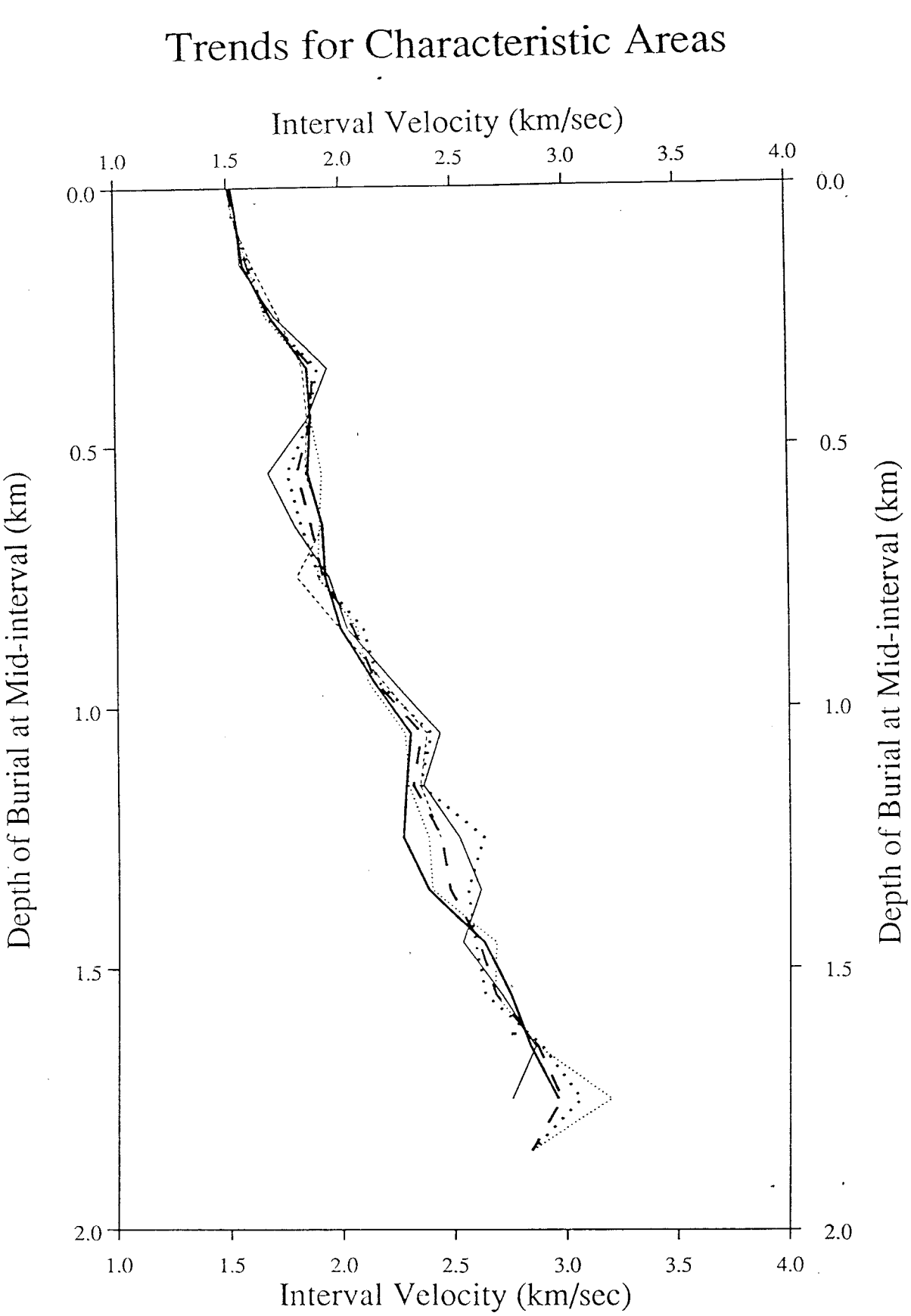


Figure 19. A comparison of curves from the data and subsets of data shown in Figures 13-18. The correspondence is as follows: (light dashed line) four layer analyses; (heavy dashed line) many layer analyses; (light solid line) analyses in area of BSR; (light dotted line) analyses in area of no BSR; (heavy solid line) analyses in area seismic transparency; and (heavy dotted line) analyses in area of typical reflectivity. Note the strong velocity reversal in the area of the BSR.

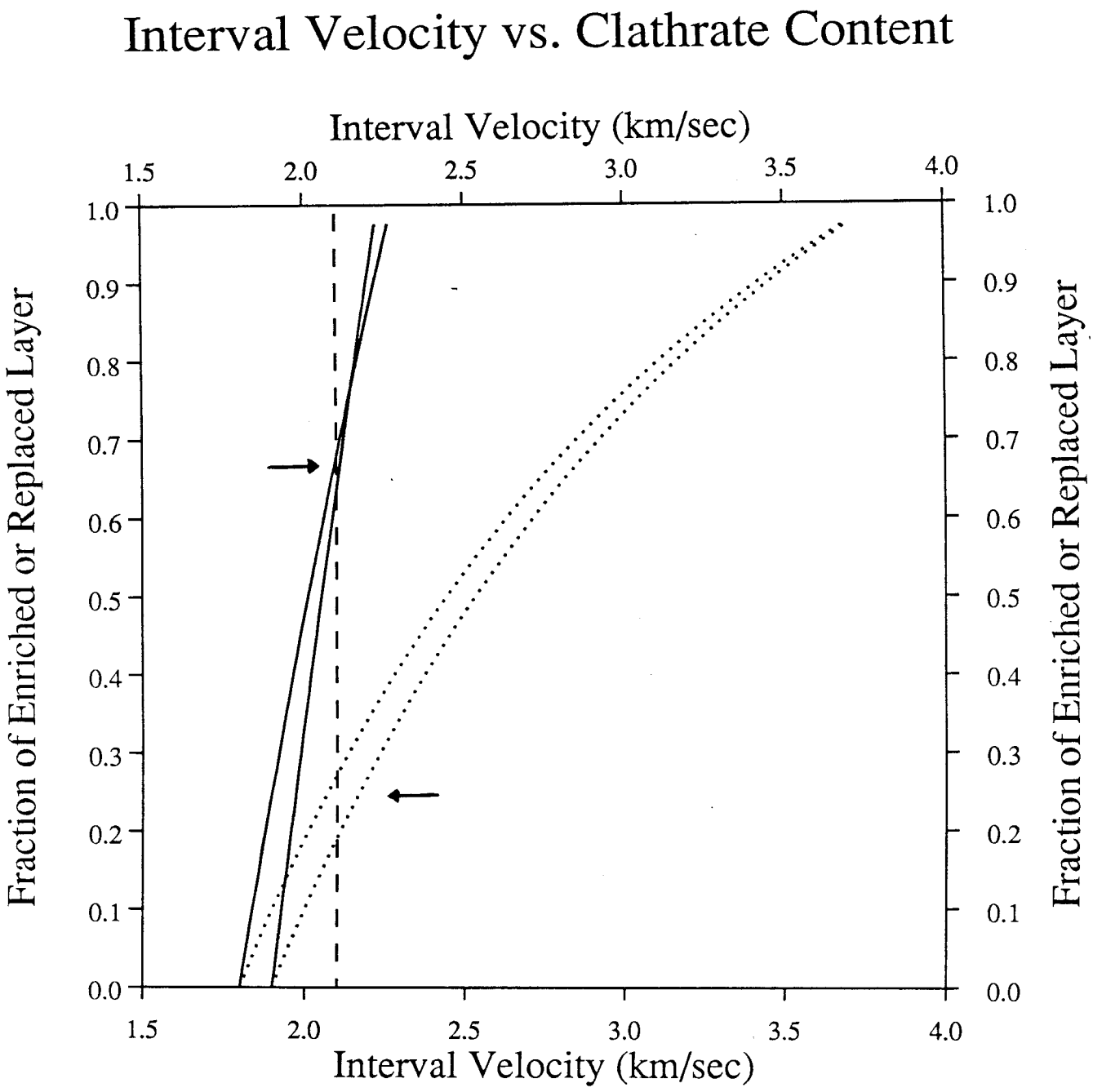


Figure 20. In one possible model a layer is made up of two sublayers, one of clathrate free sediment and one where pore spaces are increasing filled with clathrate. The solid lines show the increase in velocity of the total interval for two sediment types, velocity 1.8 and porosity 40% (left most) to velocity 1.9 km/sec and porosity 30% (right most). The second model consists of a sublayer of clathrate free sediment and a sublayer of pure clathrate. The dotted lines show velocity of the total layer vs. fraction of the layer occupied by clathrate (see text).

# APPENDIX

This Appendix consists of 48 tables of velocity each followed by a figure. In the first column of the table is the two way travel time (at normal incidence) to the bottom of each layer. In the second column is the interval velocity for that layer. For the few layer analysis the third and fourth columns contain the lower and upper velocity estimates respectively, obtained from uncertainty estimates. The corresponding figures show the velocity profile and the NMO corrected $\tau$-p CMP gather. The solid bold line is the interval velocity estimate from the many layered analysis, and the thin dotted lines are the estimate from the few layer analysis. The left and right most dotted lines represent the uncertainties associated with the picked interval velocities. The NMO correction for the seismic data is based on the velocities of the many layer model.

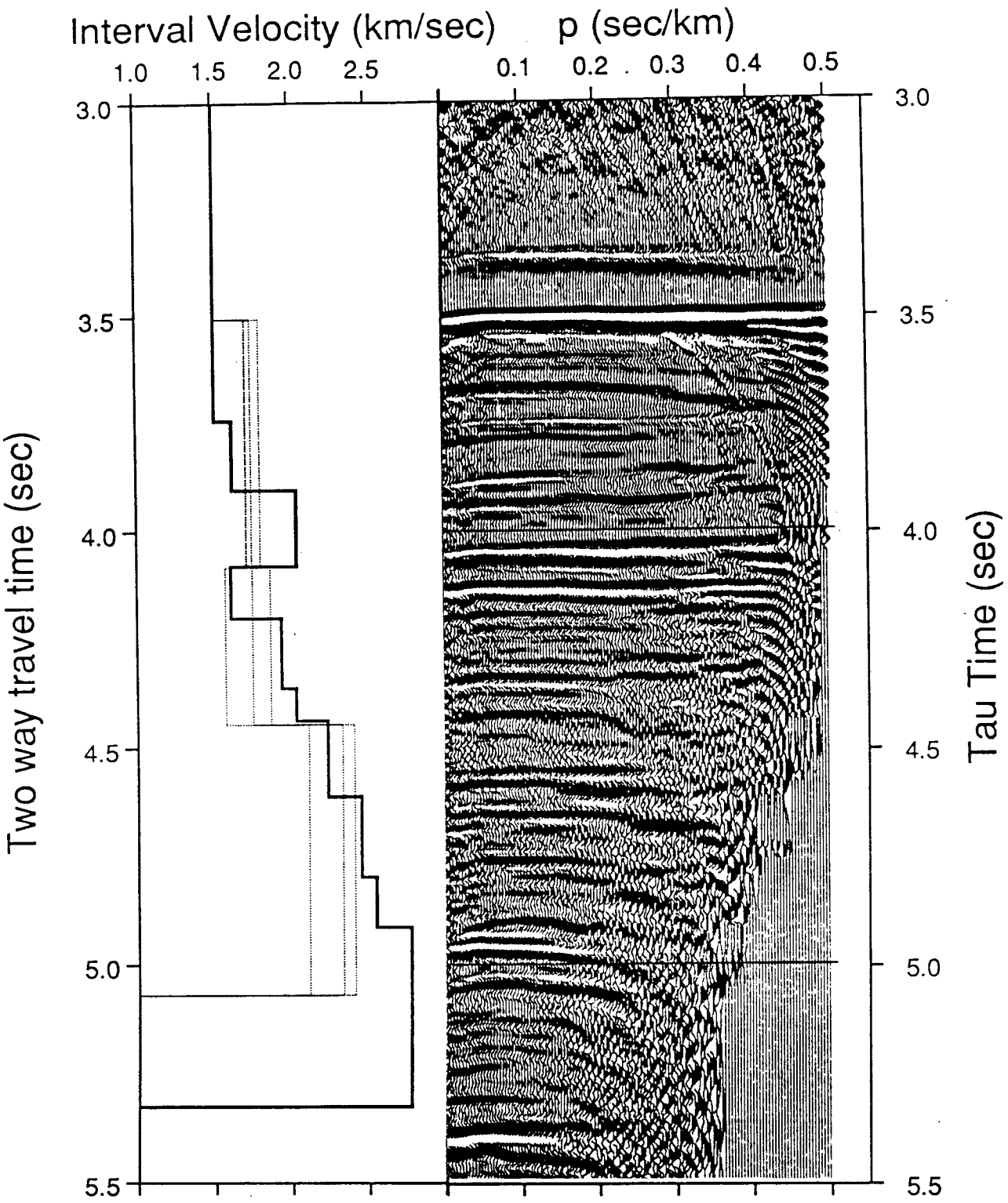
Interval Velocity (km/sec)
1.0
1.5
2.0
2.5
p (sec/km)
0.1
0.2
0.3
0.4
0.5
3.0
3.5
4.0
4.5
5.0
5.5
Two way travel time (sec)
Tau Time (sec)

## CDP 1002

| T0 sec | Interval Velocity km/sec | Lower Velocity Bound km/sec | Upper Velocity Bound km/sec |
|---|---|---|---|
| 3.478 | 1.507 | 1.502 | 1.512 |
| 4.038 | 1.697 | 1.660 | 1.787 |
| 4.399 | 1.988 | 1.766 | 2.072 |
| 5.040 | 2.282 | 2.101 | 2.456 |

| T0 sec | Interval Velocity km/sec |
|---|---|
| 3.478 | 1.506 |
| 3.741 | 1.570 |
| 3.880 | 1.740 |
| 4.039 | 1.913 |
| 4.168 | 1.609 |
| 4.303 | 1.711 |
| 4.398 | 1.958 |
| 4.558 | 2.195 |
| 4.769 | 2.481 |
| 4.894 | 2.497 |
| 5.045 | 2.437 |
| 5.264 | 2.854 |

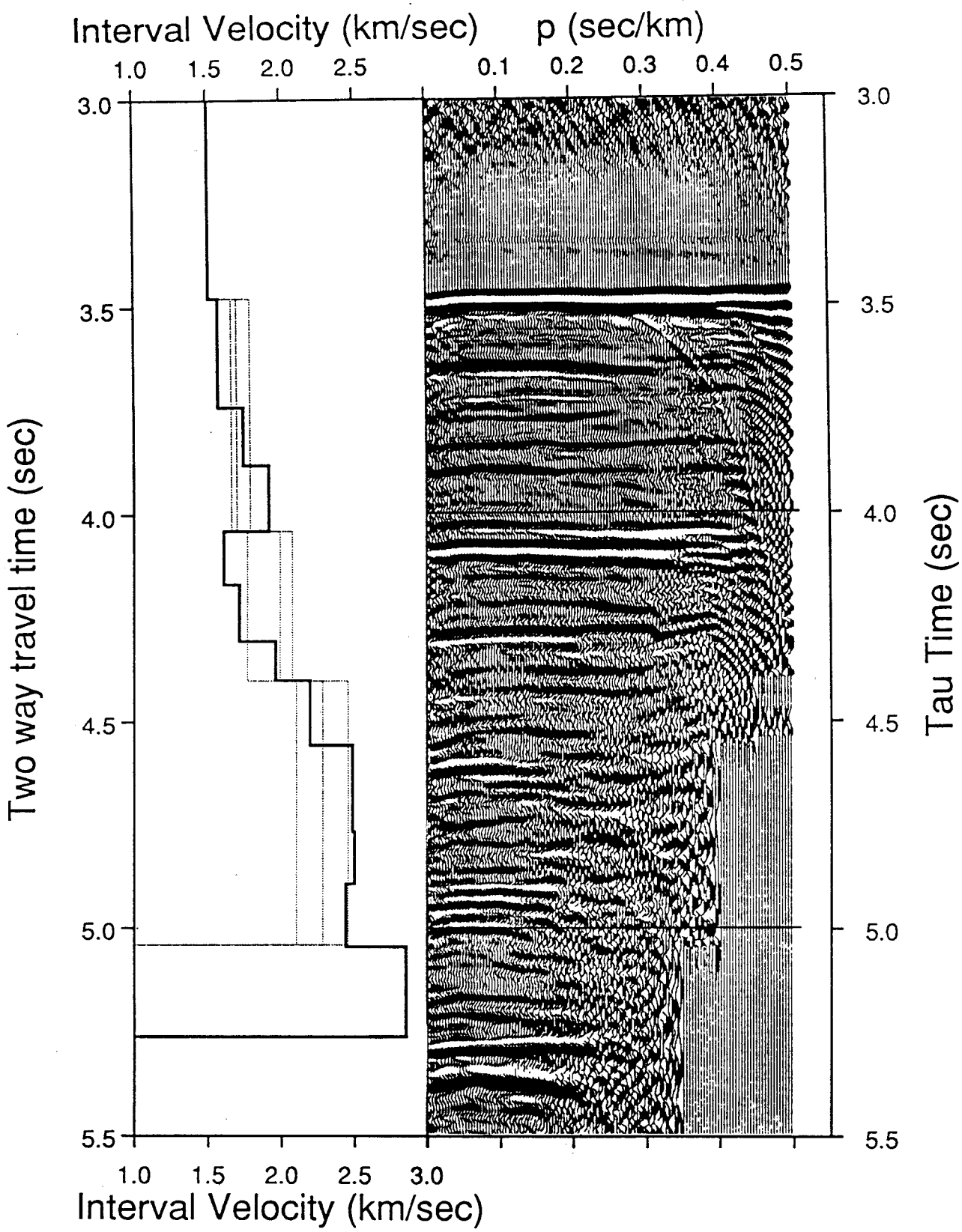
Interval Velocity (km/sec)
p (sec/km)
1.0
1.5
2.0
2.5
0.1
0.2
0.3
0.4
0.5
3.0
3.5
4.0
4.5
5.0
5.5
Two way travel time (sec)
Tau Time (sec)
Interval Velocity (km/sec)

## CDP 1102

| T0 sec | Interval Velocity km/sec | Lower Velocity Bound km/sec | Upper Velocity Bound km/sec |
|---|---|---|---|
| 3.461 | 1.507 | 1.502 | 1.512 |
| 4.011 | 1.732 | 1.676 | 1.790 |
| 4.402 | 1.982 | 1.870 | 2.055 |
| 4.984 | 2.295 | 2.170 | 2.484 |

| T0 sec | Interval Velocity km/sec |
|---|---|
| 3.461 | 1.510 |
| 3.719 | 1.524 |
| 3.853 | 1.841 |
| 4.006 | 1.963 |
| 4.156 | 1.669 |
| 4.299 | 2.080 |
| 4.400 | 1.902 |
| 4.539 | 2.348 |
| 4.739 | 2.070 |
| 4.865 | 2.401 |
| 4.985 | 2.504 |
| 5.101 | 2.664 |

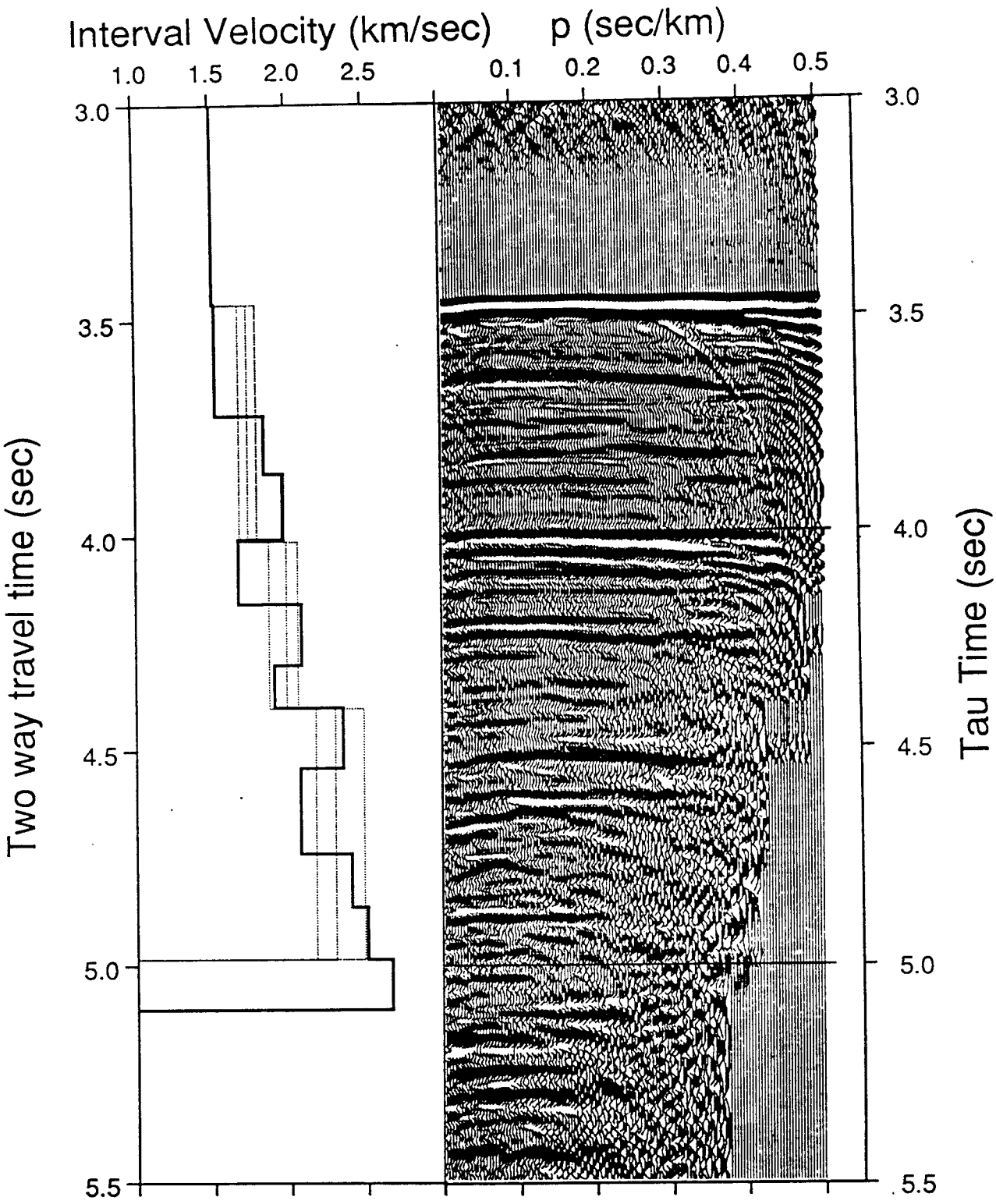
Interval Velocity (km/sec)
1.0
1.5
2.0
2.5
p (sec/km)
0.1
0.2
0.3
0.4
0.5
3.0
3.5
4.0
4.5
5.0
5.5
Two way travel time (sec)
Tau Time (sec)

## CDP 1202

| T0 sec | Interval Velocity km/sec | Lower Velocity Bound km/sec | Upper Velocity Bound km/sec |
|---|---|---|---|
| 3.452 | 1.507 | 1.502 | 1.507 |
| 3.984 | 1.739 | 1.694 | 1.787 |
| 4.363 | 1.971 | 1.850 | 2.074 |
| 4.953 | 2.357 | 2.290 | 2.542 |

| T0 sec | Interval Velocity km/sec |
|---|---|
| 3.450 | 1.509 |
| 3.692 | 1.645 |
| 3.830 | 1.765 |
| 3.976 | 1.866 |
| 4.160 | 1.660 |
| 4.285 | 2.037 |
| 4.357 | 1.867 |
| 4.514 | 1.945 |
| 4.683 | 2.741 |
| 4.818 | 3.022 |
| 4.950 | 2.953 |
| 5.028 | 2.856 |

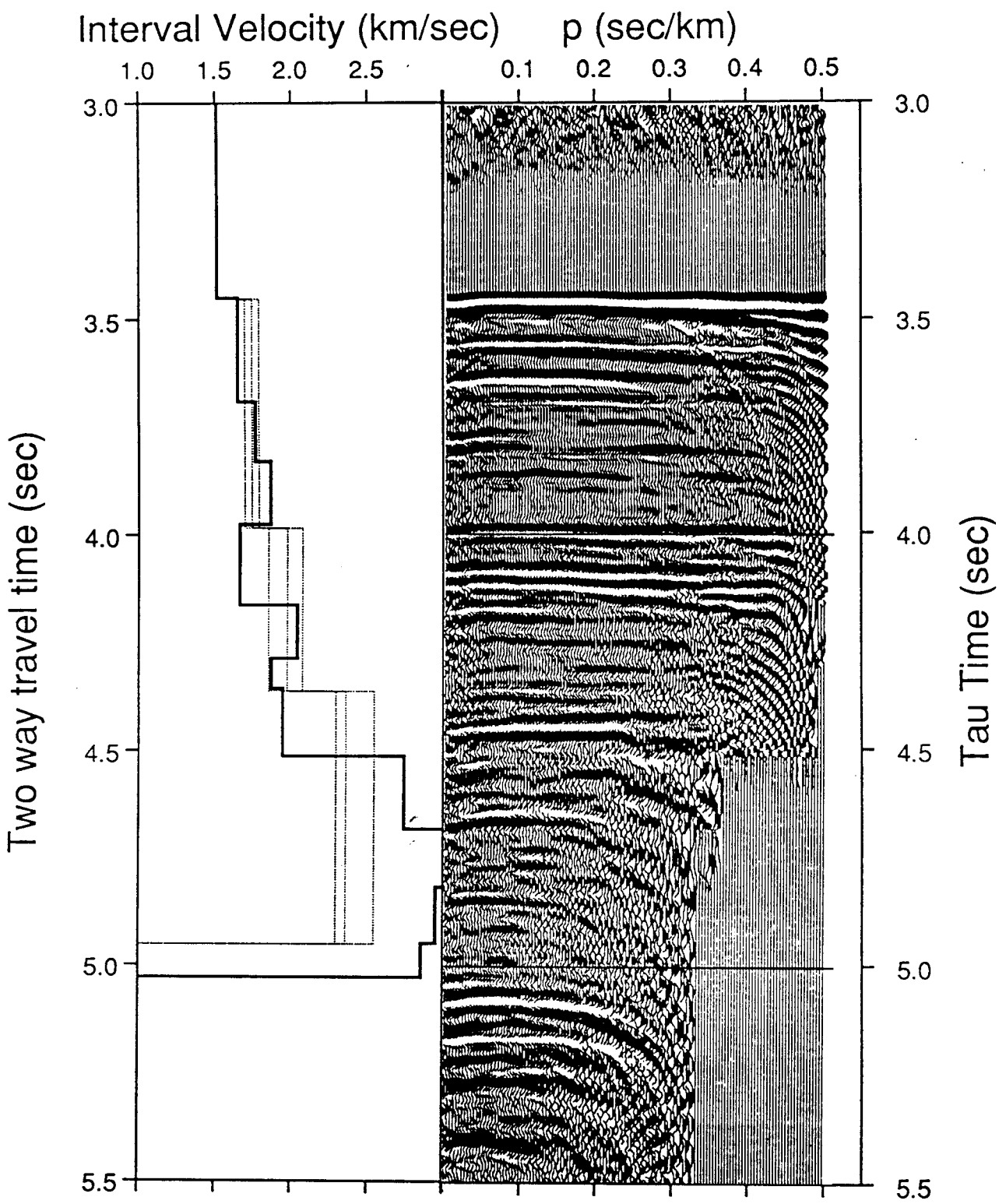
Interval Velocity (km/sec)
p (sec/km)
1.0
1.5
2.0
2.5
0.1
0.2
0.3
0.4
0.5
3.0
3.5
4.0
4.5
5.0
5.5
Two way travel time (sec)
Tau Time (sec)

## CDP 1302

| T0 sec | Interval Velocity km/sec | Lower Velocity Bound km/sec | Upper Velocity Bound km/sec |
|---|---|---|---|
| 3.443 | 1.507 | 1.502 | 1.512 |
| 3.975 | 1.740 | 1.697 | 1.787 |
| 4.353 | 1.980 | 1.869 | 2.094 |
| 4.910 | 2.297 | 2.104 | 2.415 |

| T0 sec | Interval Velocity km/sec |
|---|---|
| 3.439 | 1.504 |
| 3.677 | 1.681 |
| 3.821 | 1.677 |
| 3.973 | 1.946 |
| 4.141 | 1.575 |
| 4.257 | 1.752 |
| 4.350 | 2.074 |
| 4.515 | 2.068 |
| 4.667 | 2.485 |
| 4.759 | 2.289 |
| 4.906 | 2.842 |
| 4.978 | 3.159 |

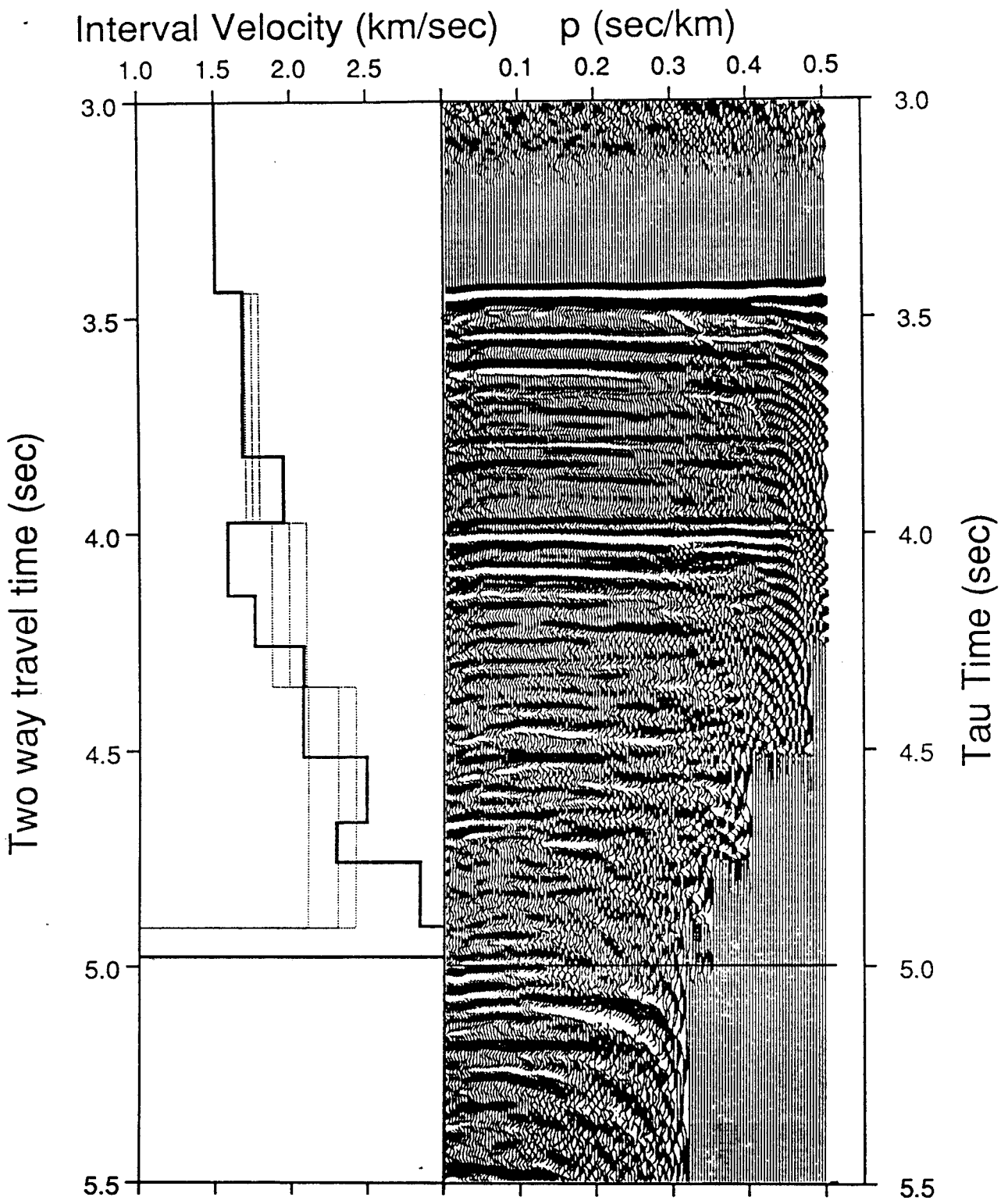
Interval Velocity (km/sec)
p (sec/km)
1.0
1.5
2.0
2.5
0.1
0.2
0.3
0.4
0.5
3.0
3.5
4.0
4.5
5.0
5.5
Two way travel time (sec)
Tau Time (sec)

## CDP 1402

| T0 sec | Interval Velocity km/sec | Lower Velocity Bound km/sec | Upper Velocity Bound km/sec |
|---|---|---|---|
| 3.425 | 1.507 | 1.502 | 1.512 |
| 3.946 | 1.690 | 1.652 | 1.770 |
| 4.329 | 1.936 | 1.852 | 2.166 |
| 4.855 | 2.353 | 2.225 | 2.500 |

| T0 sec | Interval Velocity km/sec |
|---|---|
| 3.424 | 1.508 |
| 3.671 | 1.564 |
| 3.803 | 1.573 |
| 3.945 | 2.001 |
| 4.142 | 1.536 |
| 4.231 | 1.555 |
| 4.316 | 1.963 |
| 4.500 | 2.195 |
| 4.641 | 2.406 |
| 4.760 | 2.548 |
| 4.859 | 2.679 |
| 4.911 | 2.757 |

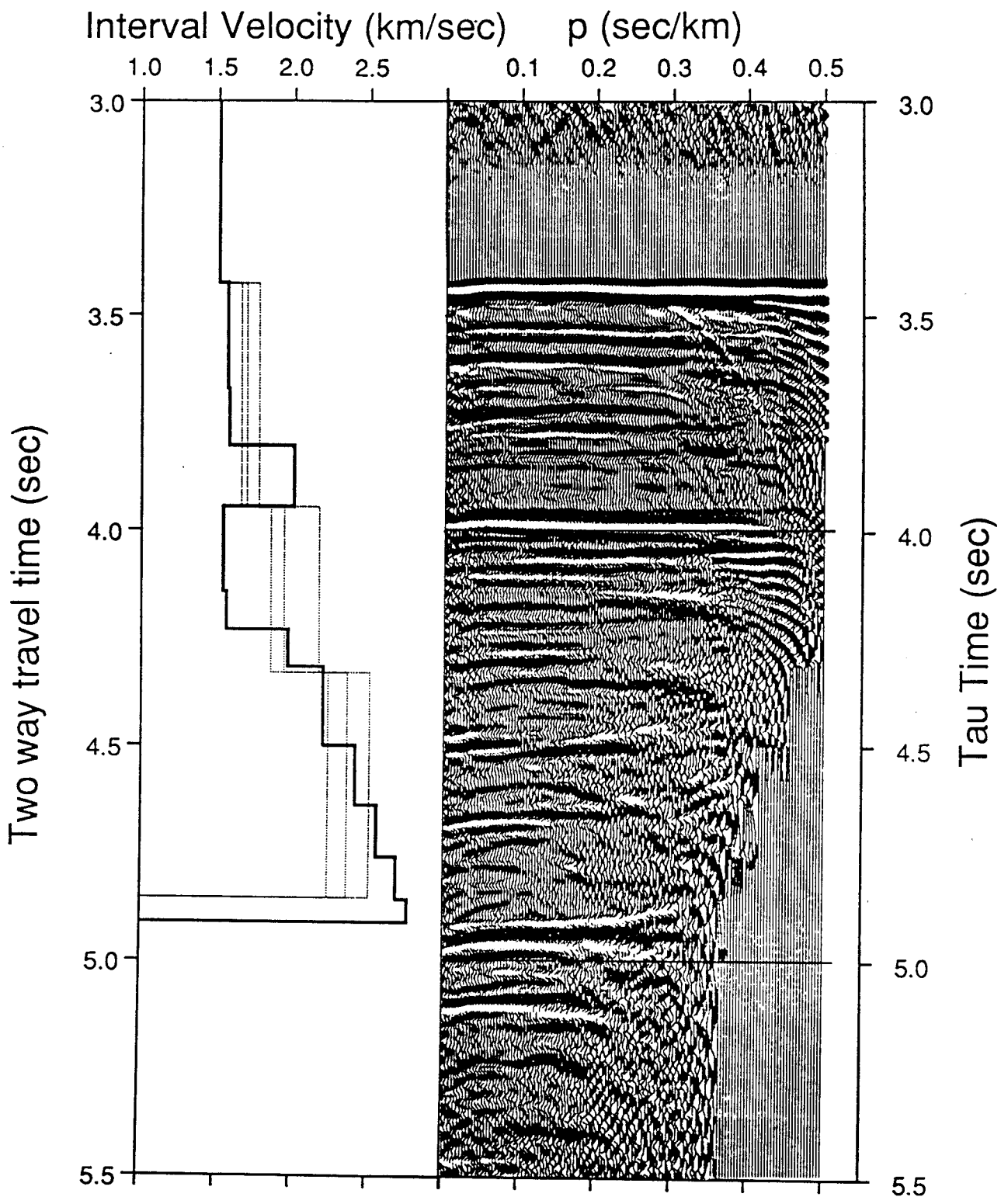
Interval Velocity (km/sec)
p (sec/km)
1.0
1.5
2.0
2.5
0.1
0.2
0.3
0.4
0.5
3.0
3.5
4.0
4.5
5.0
5.5
Two way travel time (sec)
Tau Time (sec)

## CDP 1502

| T0 sec | Interval Velocity km/sec | Lower Velocity Bound km/sec | Upper Velocity Bound km/sec |
|---|---|---|---|
| 3.407 | 1.507 | 1.502 | 1.512 |
| 3.921 | 1.744 | 1.707 | 1.796 |
| 4.293 | 1.947 | 1.711 | 2.101 |
| 4.820 | 2.422 | 2.234 | 2.539 |

| T0 sec | Interval Velocity km/sec |
|---|---|
| 3.410 | 1.508 |
| 3.651 | 1.501 |
| 3.778 | 1.732 |
| 3.921 | 1.974 |
| 4.106 | 1.509 |
| 4.202 | 1.505 |
| 4.286 | 1.484 |
| 4.493 | 2.163 |
| 4.619 | 2.510 |
| 4.745 | 2.619 |
| 4.831 | 2.631 |
| 4.882 | 2.631 |

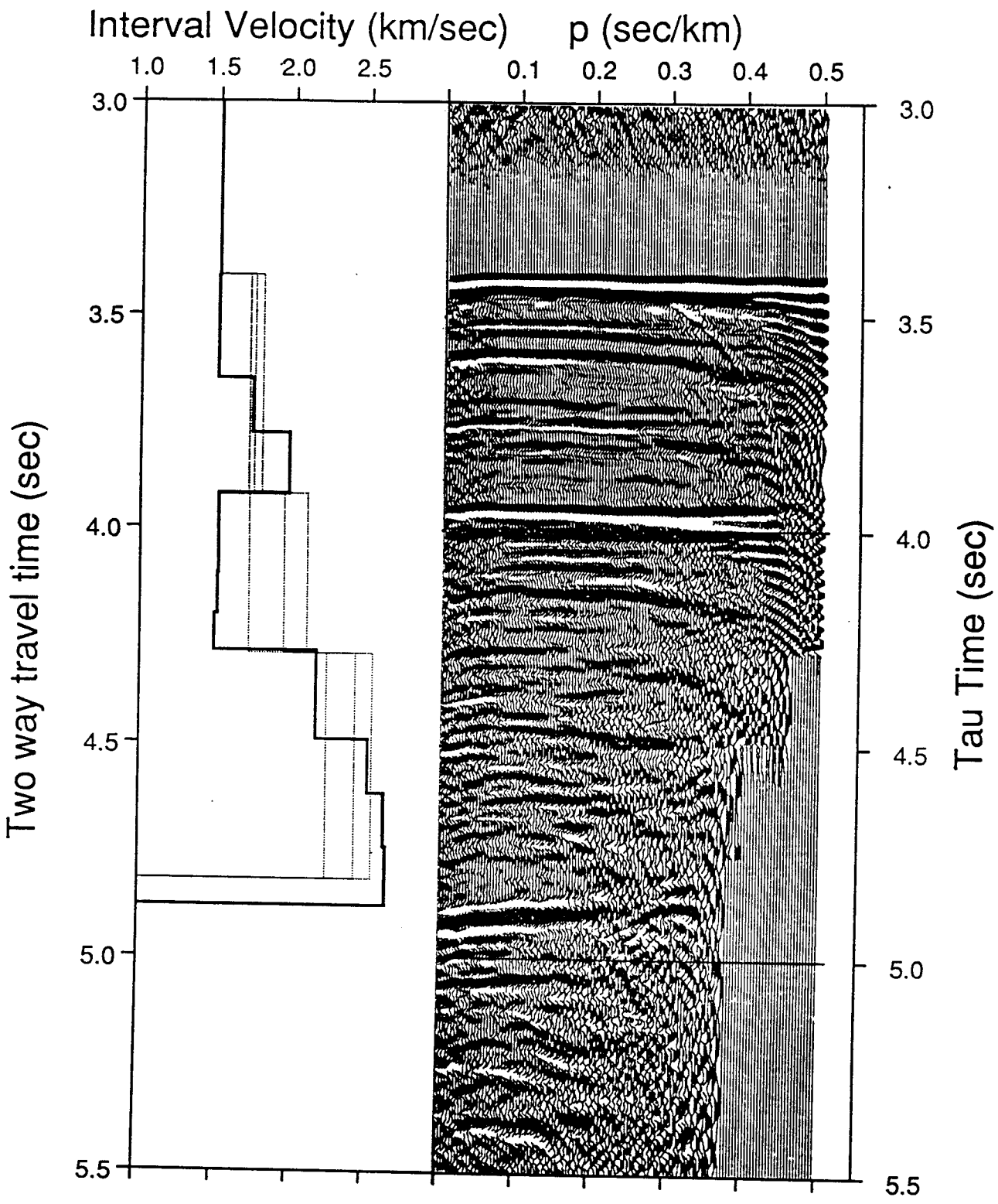
Interval Velocity (km/sec)
1.0
1.5
2.0
2.5
p (sec/km)
0.1
0.2
0.3
0.4
0.5
3.0
3.5
4.0
4.5
5.0
5.5
Two way travel time (sec)
Tau Time (sec)

## CDP 1602

| T0 sec | Interval Velocity km/sec | Lower Velocity Bound km/sec | Upper Velocity Bound km/sec |
|---|---|---|---|
| 3.397 | 1.507 | 1.502 | 1.512 |
| 3.900 | 1.684 | 1.684 | 1.800 |
| 4.257 | 1.884 | 1.785 | 2.022 |
| 4.784 | 2.431 | 2.280 | 2.497 |

| T0 sec | Interval Velocity km/sec |
|---|---|
| 3.400 | 1.503 |
| 3.640 | 1.551 |
| 3.762 | 1.602 |
| 3.899 | 2.071 |
| 4.075 | 1.546 |
| 4.154 | 1.668 |
| 4.254 | 1.881 |
| 4.450 | 1.955 |
| 4.585 | 2.500 |
| 4.702 | 2.647 |
| 4.782 | 2.701 |
| 4.846 | 2.975 |

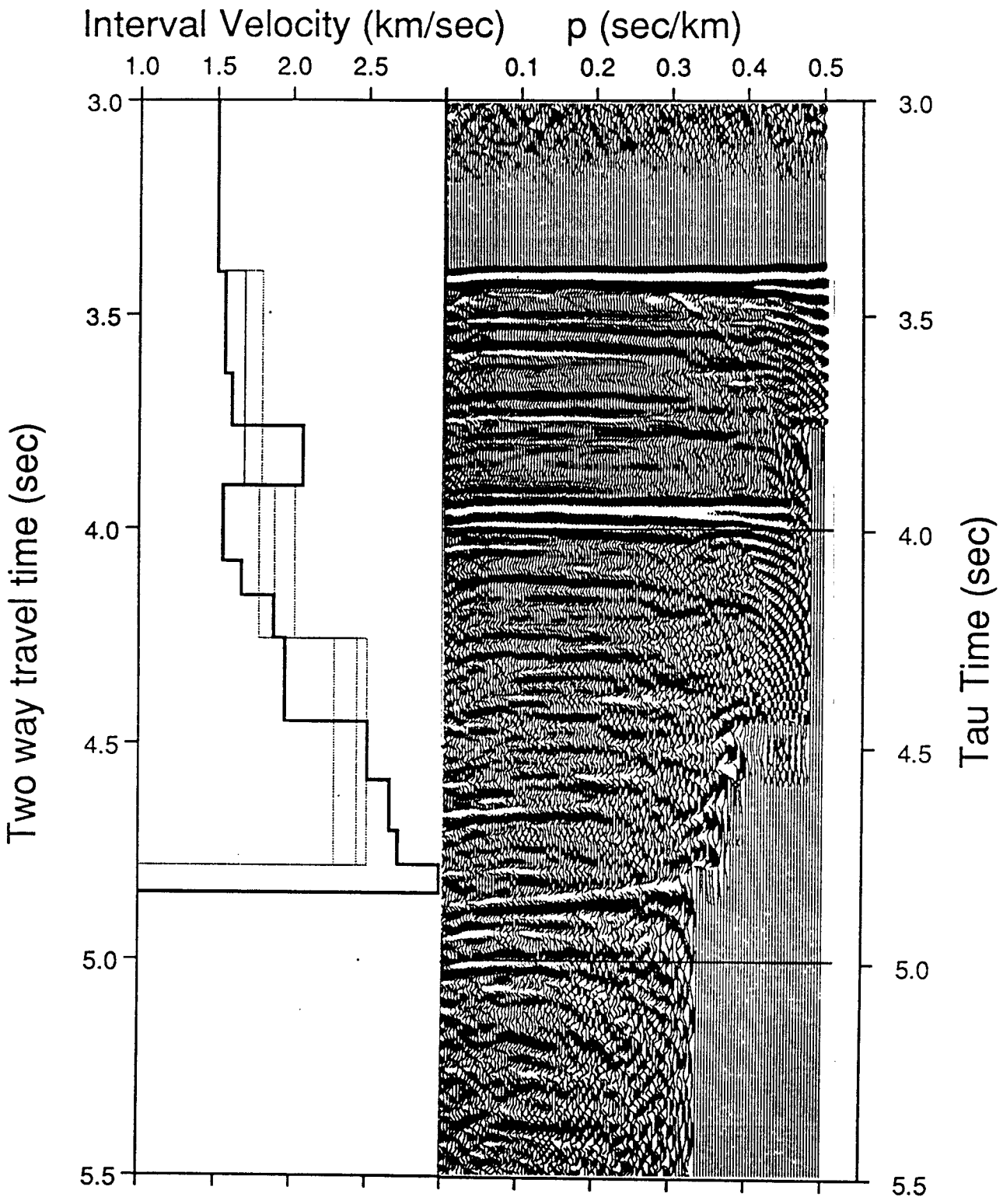
Interval Velocity (km/sec)
p (sec/km)
1.0
1.5
2.0
2.5
0.1
0.2
0.3
0.4
0.5
3.0
3.5
4.0
4.5
5.0
5.5
Two way travel time (sec)
Tau Time (sec)

## CDP 1702

| T0 sec | Interval Velocity km/sec | Lower Velocity Bound km/sec | Upper Velocity Bound km/sec |
|---|---|---|---|
| 3.388 | 1.507 | 1.502 | 1.512 |
| 3.874 | 1.718 | 1.680 | 1.754 |
| 4.232 | 1.790 | 1.700 | 1.871 |
| 4.753 | 2.431 | 2.316 | 2.530 |

| T0 sec | Interval Velocity km/sec |
|---|---|
| 3.387 | 1.507 |
| 3.631 | 1.518 |
| 3.740 | 1.780 |
| 3.874 | 1.953 |
| 4.065 | 1.583 |
| 4.145 | 1.589 |
| 4.227 | 1.764 |
| 4.417 | 2.199 |
| 4.550 | 2.301 |
| 4.643 | 2.396 |
| 4.747 | 2.676 |
| 4.851 | 2.962 |

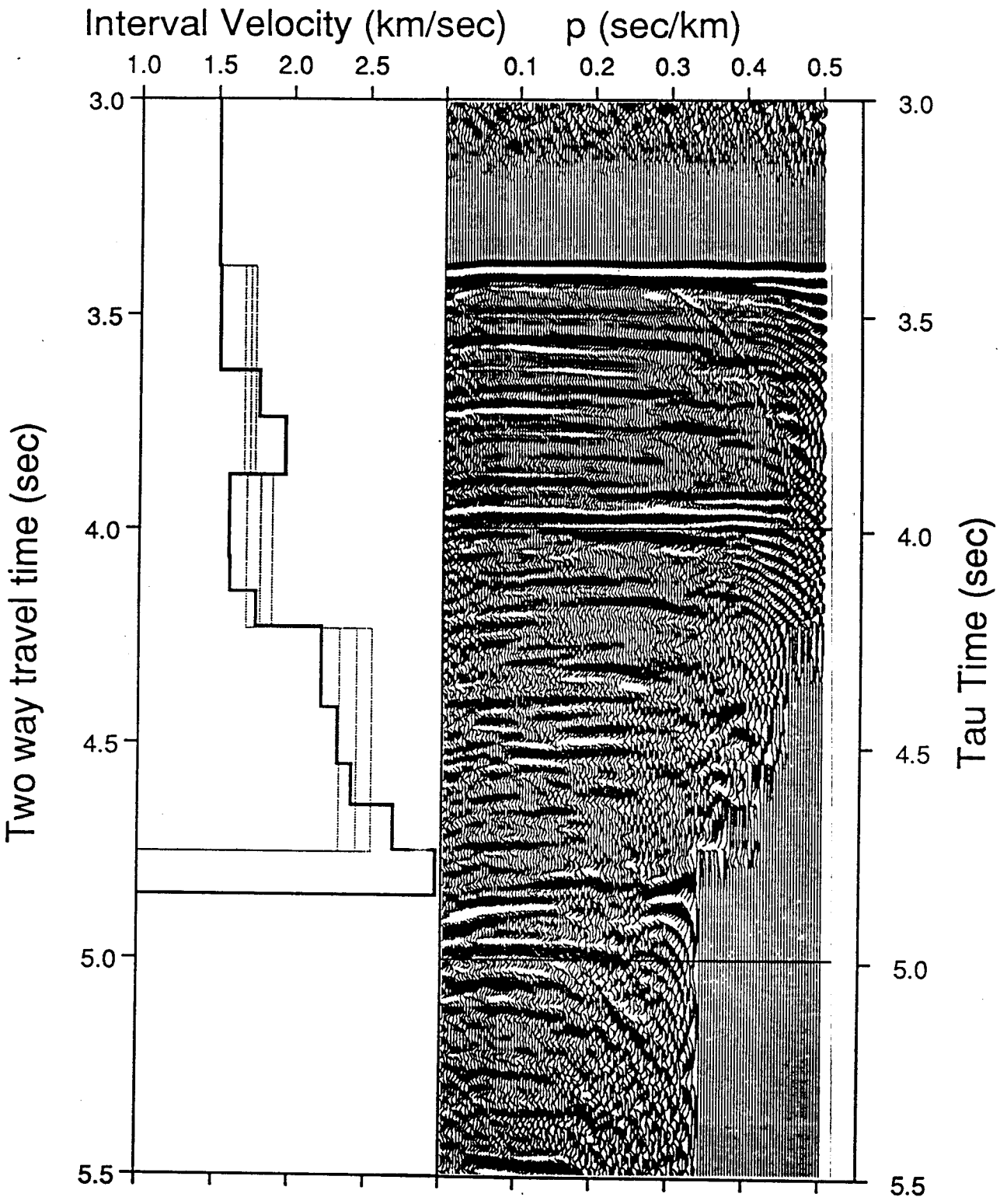
Interval Velocity (km/sec)
p (sec/km)
1.0
1.5
2.0
2.5
0.1
0.2
0.3
0.4
0.5
3.0
3.5
4.0
4.5
5.0
5.5
Two way travel time (sec)
Tau Time (sec)

## CDP 1802

| T0 sec | Interval Velocity km/sec | Lower Velocity Bound km/sec | Upper Velocity Bound km/sec |
|---|---|---|---|
| 3.378 | 1.508 | 1.502 | 1.512 |
| 3.850 | 1.674 | 1.605 | 1.753 |
| 4.183 | 1.841 | 1.663 | 1.923 |
| 4.711 | 2.422 | 2.305 | 2.536 |

| T0 sec | Interval Velocity km/sec |
|---|---|
| 3.378 | 1.506 |
| 3.612 | 1.508 |
| 3.719 | 1.508 |
| 3.850 | 1.965 |
| 3.977 | 1.695 |
| 4.036 | 1.754 |
| 4.182 | 1.909 |
| 4.361 | 1.909 |
| 4.500 | 2.273 |
| 4.589 | 2.464 |
| 4.712 | 2.768 |

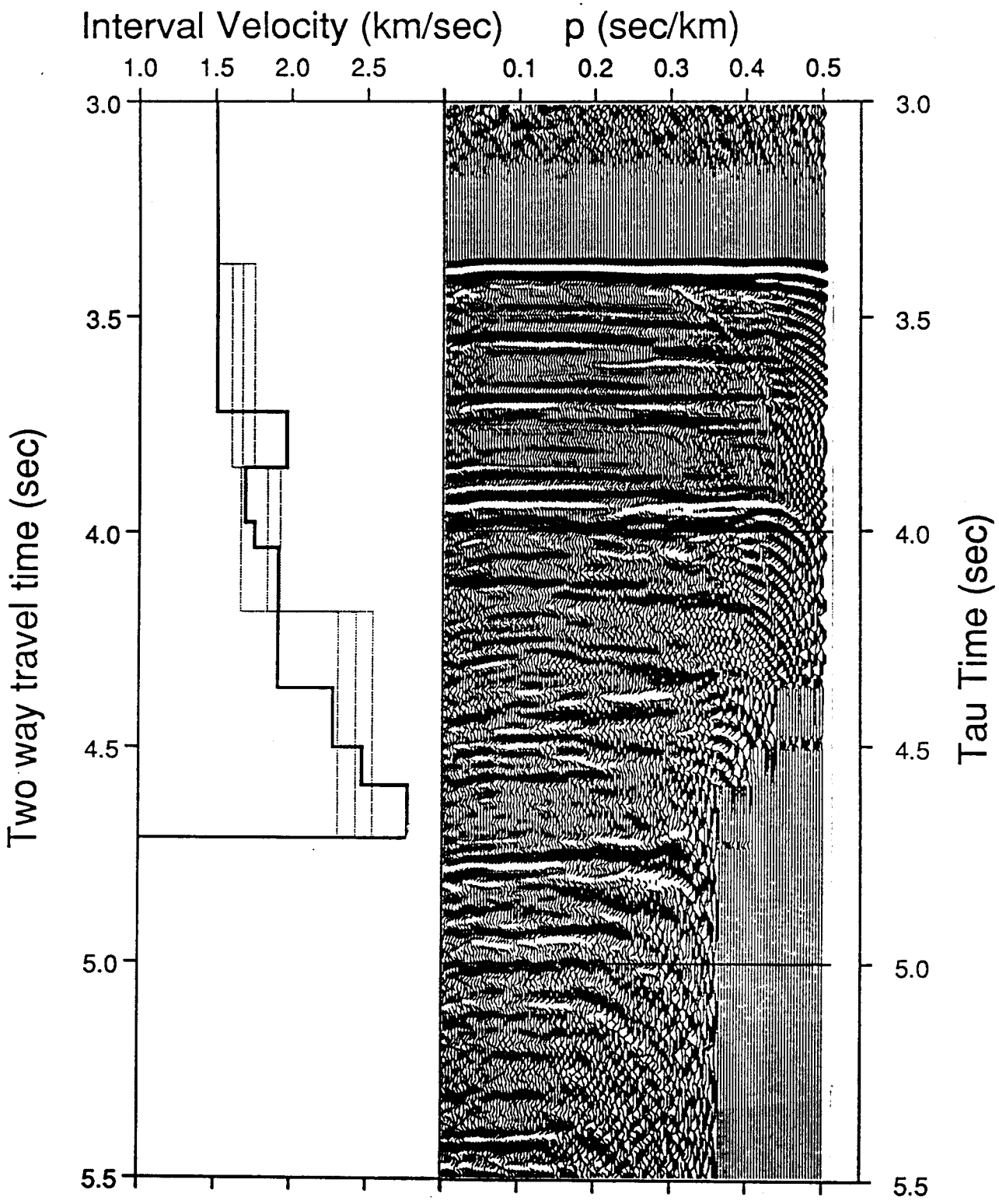
Interval Velocity (km/sec)
p (sec/km)
1.0
1.5
2.0
2.5
0.1
0.2
0.3
0.4
0.5
3.0
3.5
4.0
4.5
5.0
5.5
Two way travel time (sec)
Tau Time (sec)

## CDP 1902

| T0 sec | Interval Velocity km/sec | Lower Velocity Bound km/sec | Upper Velocity Bound km/sec |
|---|---|---|---|
| 3.371 | 1.507 | 1.502 | 1.512 |
| 3.830 | 1.651 | 1.594 | 1.733 |
| 4.171 | 1.820 | 1.597 | 2.000 |
| 4.642 | 2.331 | 2.210 | 2.505 |

| T0 sec | Interval Velocity km/sec |
|---|---|
| 3.369 | 1.505 |
| 3.604 | 1.512 |
| 3.708 | 1.771 |
| 3.829 | 1.731 |
| 3.954 | 1.848 |
| 4.022 | 1.830 |
| 4.174 | 2.099 |
| 4.311 | 2.271 |
| 4.441 | 2.127 |
| 4.555 | 2.283 |
| 4.645 | 2.568 |

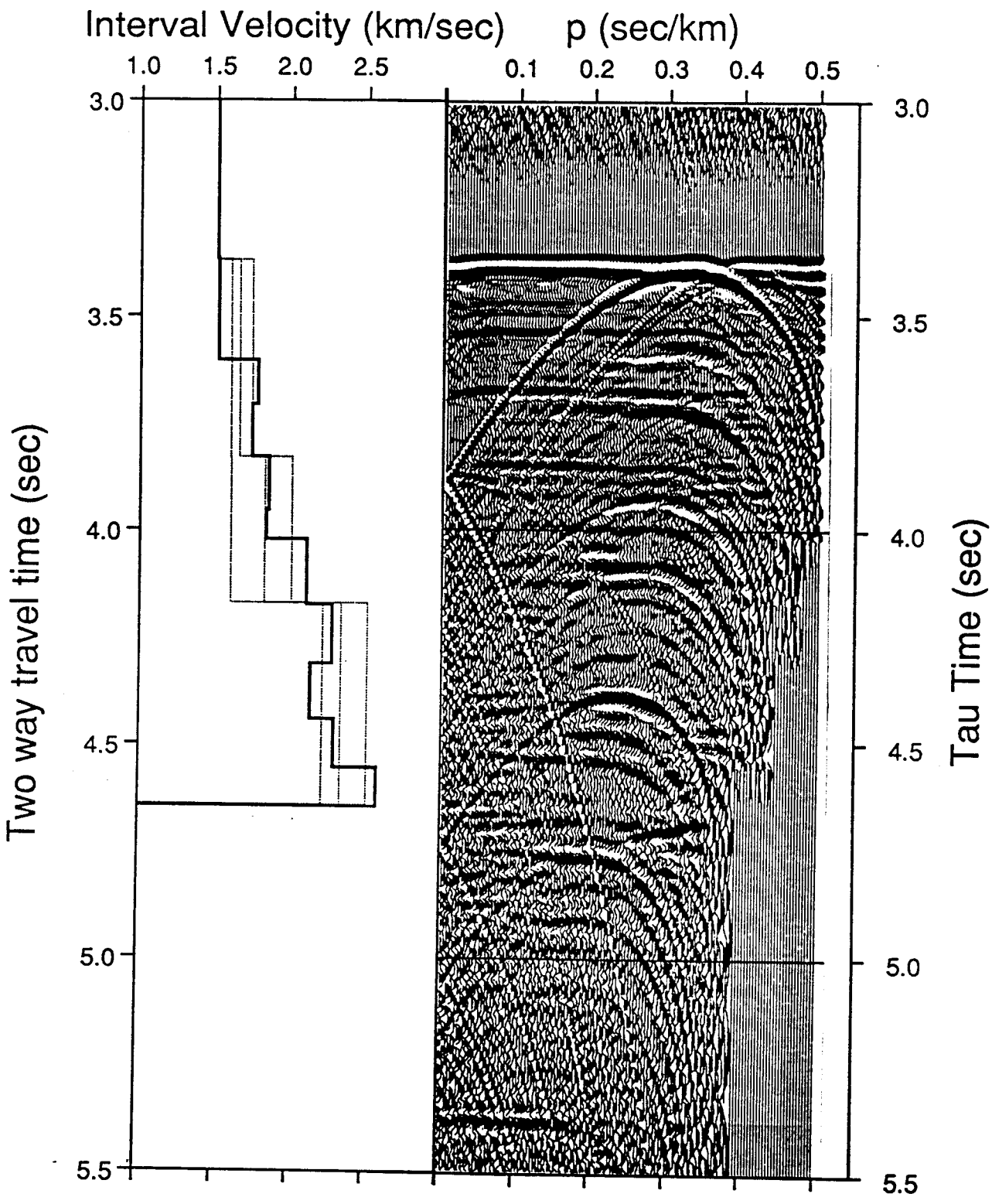
Interval Velocity (km/sec)
p (sec/km)
1.0
1.5
2.0
2.5
0.1
0.2
0.3
0.4
0.5
3.0
3.5
4.0
4.5
5.0
5.5
Two way travel time (sec)
Tau Time (sec)

## CDP 2002

| T0 sec | Interval Velocity km/sec | Lower Velocity Bound km/sec | Upper Velocity Bound km/sec |
|---|---|---|---|
| 3.359 | 1.507 | 1.502 | 1.512 |
| 3.815 | 1.661 | 1.632 | 1.754 |
| 4.115 | 1.893 | 1.700 | 2.012 |
| 4.574 | 2.342 | 1.965 | 2.499 |

| T0 sec | Interval Velocity km/sec |
|---|---|
| 3.361 | 1.506 |
| 3.582 | 1.624 |
| 3.692 | 1.537 |
| 3.821 | 1.605 |
| 3.915 | 1.634 |
| 3.981 | 1.796 |
| 4.119 | 1.860 |
| 4.243 | 1.926 |
| 4.332 | 2.033 |
| 4.492 | 2.549 |
| 4.576 | 2.537 |
| 4.623 | 2.511 |

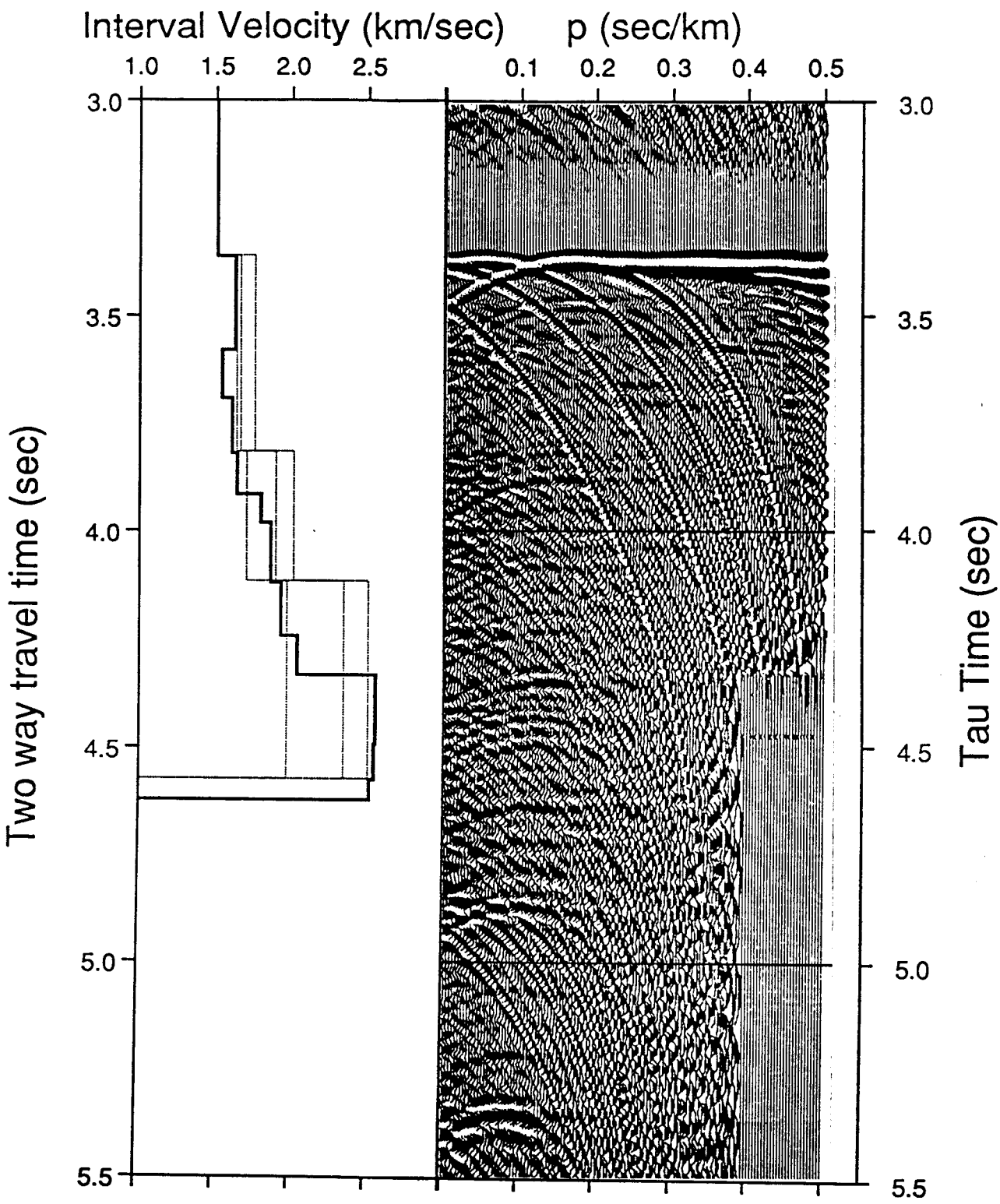
Interval Velocity (km/sec)
1.0
1.5
2.0
2.5
p (sec/km)
0.1
0.2
0.3
0.4
0.5
3.0
3.5
4.0
4.5
5.0
5.5
Two way travel time (sec)
Tau Time (sec)

## CDP 2102

| T0 sec | Interval Velocity km/sec | Lower Velocity Bound km/sec | Upper Velocity Bound km/sec |
|---|---|---|---|
| 3.343 | 1.506 | 1.502 | 1.512 |
| 3.789 | 1.659 | 1.690 | 1.795 |
| 4.101 | 1.821 | 1.707 | 1.940 |
| 4.567 | 2.224 | 1.920 | 2.329 |

| T0 sec | Interval Velocity km/sec |
|---|---|
| 3.347 | 1.507 |
| 3.550 | 1.529 |
| 3.686 | 1.700 |
| 3.790 | 1.846 |
| 3.899 | 2.016 |
| 3.961 | 2.051 |
| 4.099 | 1.898 |
| 4.222 | 1.934 |
| 4.309 | 1.972 |
| 4.451 | 2.160 |
| 4.571 | 2.219 |
| 4.667 | 2.376 |

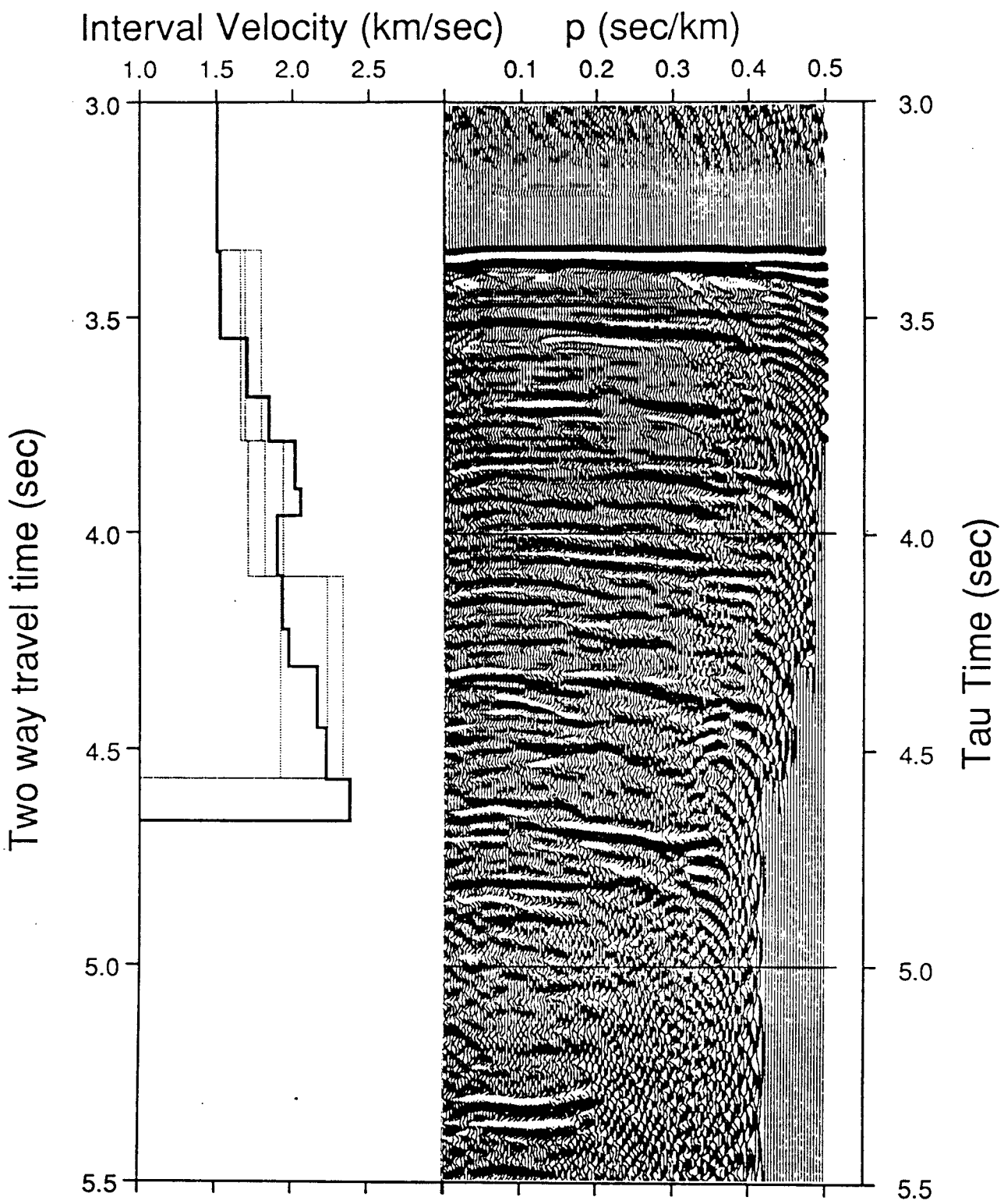
Interval Velocity (km/sec)
p (sec/km)
1.0
1.5
2.0
2.5
0.1
0.2
0.3
0.4
0.5
3.0
3.5
4.0
4.5
5.0
5.5
Two way travel time (sec)
Tau Time (sec)

## CDP 2202

| T0 sec | Interval Velocity km/sec | Lower Velocity Bound km/sec | Upper Velocity Bound km/sec |
|---|---|---|---|
| 3.326 | 1.507 | 1.502 | 1.512 |
| 3.756 | 1.661 | 1.596 | 1.780 |
| 4.063 | 1.812 | 1.743 | 1.899 |
| 4.572 | 2.152 | 2.000 | 2.323 |

| T0 sec | Interval Velocity km/sec |
|---|---|
| 3.328 | 1.507 |
| 3.531 | 1.500 |
| 3.673 | 1.527 |
| 3.758 | 2.059 |
| 3.883 | 1.815 |
| 3.934 | 1.860 |
| 4.063 | 2.055 |
| 4.182 | 1.917 |
| 4.296 | 1.935 |
| 4.440 | 2.329 |
| 4.574 | 2.282 |
| 4.683 | 2.341 |

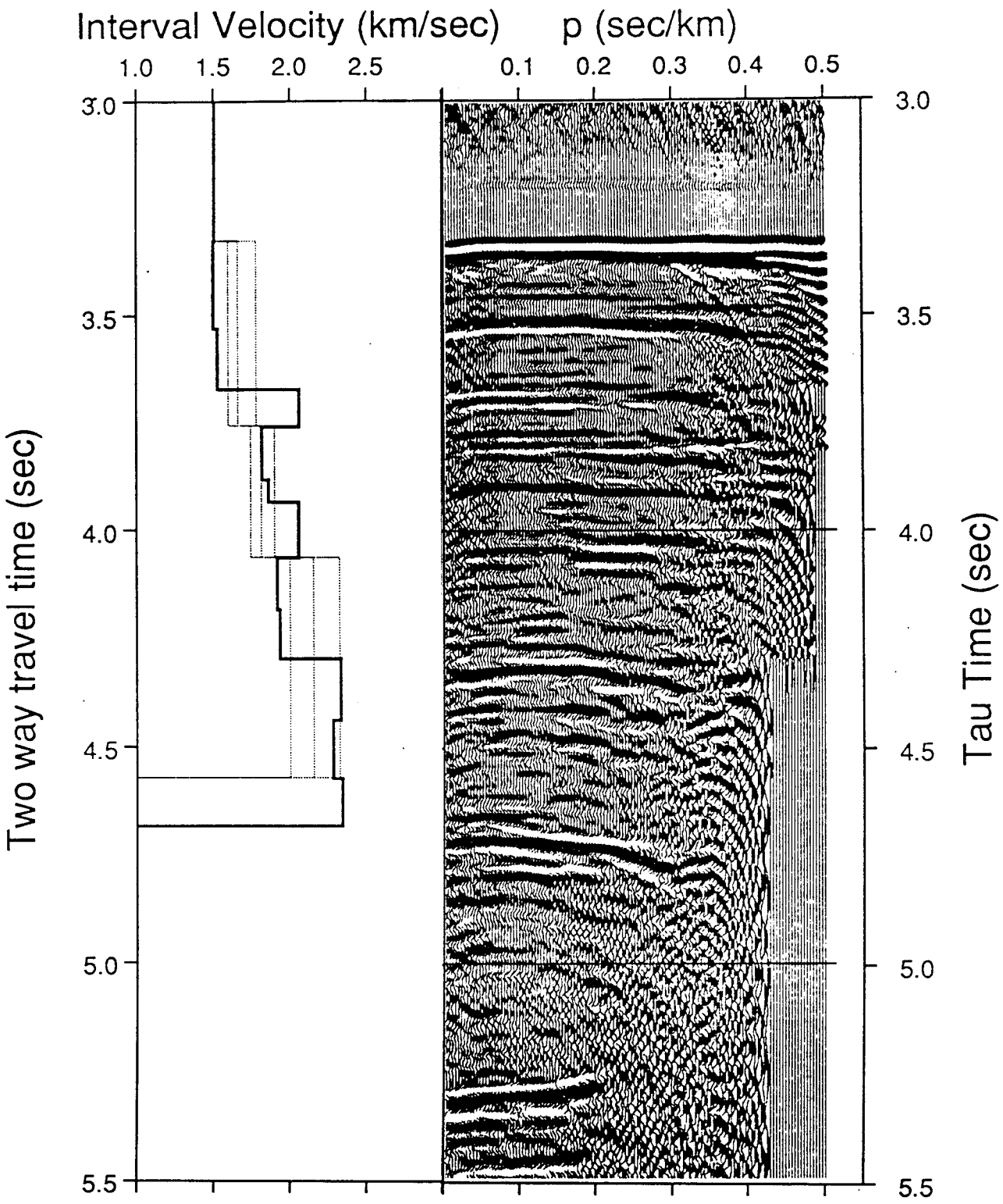
Interval Velocity (km/sec)
p (sec/km)
1.0
1.5
2.0
2.5
0.1
0.2
0.3
0.4
0.5
3.0
3.5
4.0
4.5
5.0
5.5
Two way travel time (sec)
Tau Time (sec)

## CDP 2302

| T0 sec | Interval Velocity km/sec | Lower Velocity Bound km/sec | Upper Velocity Bound km/sec |
|---|---|---|---|
| 3.314 | 1.507 | 1.502 | 1.512 |
| 3.731 | 1.600 | 1.560 | 1.690 |
| 4.040 | 1.986 | 1.900 | 2.050 |
| 4.597 | 2.187 | 2.100 | 2.241 |

| T0 sec | Interval Velocity km/sec |
|---|---|
| 3.312 | 1.506 |
| 3.515 | 1.545 |
| 3.637 | 1.631 |
| 3.723 | 1.849 |
| 3.824 | 1.897 |
| 3.912 | 1.599 |
| 4.033 | 1.813 |
| 4.171 | 1.789 |
| 4.285 | 2.078 |
| 4.427 | 1.984 |
| 4.594 | 1.951 |
| 4.655 | 1.928 |
| 4.710 | 2.264 |

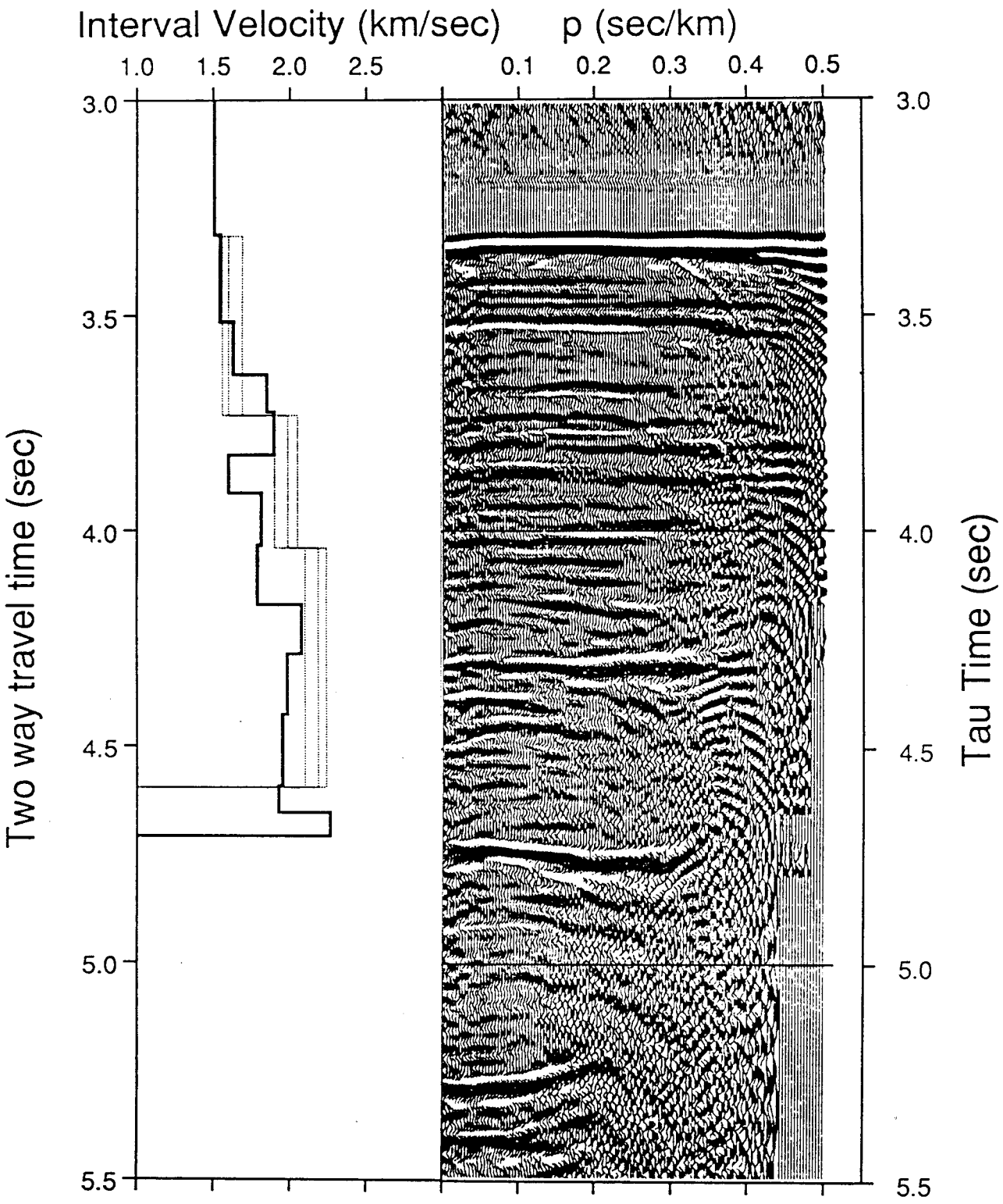
Interval Velocity (km/sec)
p (sec/km)
1.0
1.5
2.0
2.5
0.1
0.2
0.3
0.4
0.5
3.0
3.5
4.0
4.5
5.0
5.5
Two way travel time (sec)
Tau Time (sec)

## CDP 2402

| T0 sec | Interval Velocity km/sec | Lower Velocity Bound km/sec | Upper Velocity Bound km/sec |
|---|---|---|---|
| 3.309 | 1.507 | 1.502 | 1.512 |
| 3.708 | 1.604 | 1.508 | 1.671 |
| 4.024 | 1.829 | 1.694 | 1.909 |
| 4.602 | 2.189 | 2.050 | 2.355 |

| T0 sec | Interval Velocity km/sec |
|---|---|
| 3.301 | 1.506 |
| 3.500 | 1.552 |
| 3.613 | 1.503 |
| 3.705 | 1.954 |
| 3.825 | 1.614 |
| 3.901 | 1.969 |
| 4.023 | 2.071 |
| 4.170 | 1.948 |
| 4.288 | 2.101 |
| 4.423 | 1.989 |
| 4.600 | 2.038 |
| 4.673 | 1.935 |
| 4.742 | 1.905 |

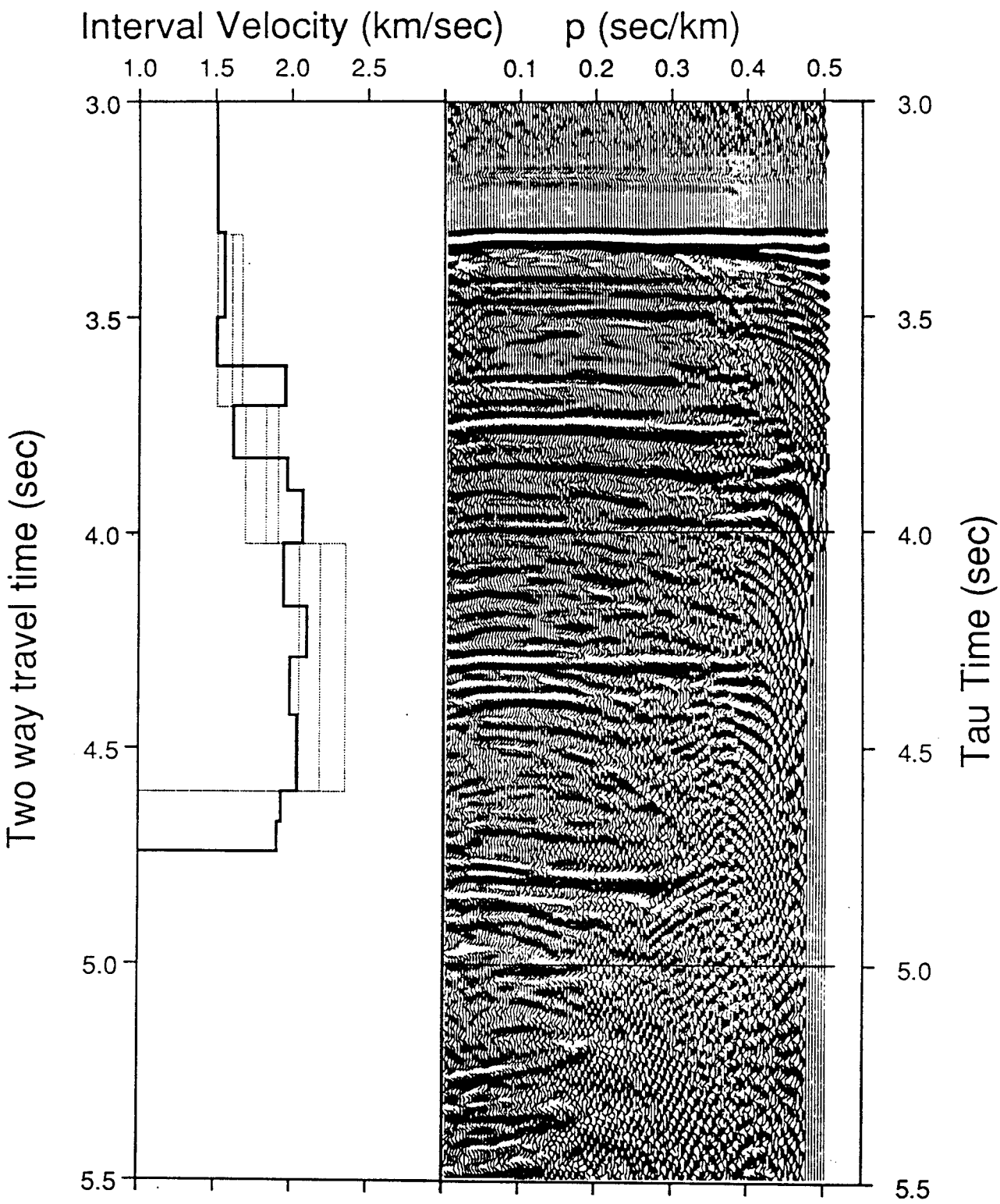
Interval Velocity (km/sec)
p (sec/km)
1.0
1.5
2.0
2.5
0.1
0.2
0.3
0.4
0.5
3.0
3.5
4.0
4.5
5.0
5.5
Two way travel time (sec)
Tau Time (sec)

## CDP 2502

| T0 sec | Interval Velocity km/sec | Lower Velocity Bound km/sec | Upper Velocity Bound km/sec |
|---|---|---|---|
| 3.287 | 1.507 | 1.502 | 1.512 |
| 3.676 | 1.564 | 1.495 | 1.620 |
| 4.005 | 1.846 | 1.722 | 1.969 |
| 4.613 | 2.088 | 1.902 | 2.322 |

| T0 sec | Interval Velocity km/sec |
|---|---|
| 3.287 | 1.506 |
| 3.486 | 1.513 |
| 3.584 | 1.821 |
| 3.678 | 1.690 |
| 3.804 | 1.637 |
| 3.865 | 1.940 |
| 4.009 | 1.912 |
| 4.145 | 1.952 |
| 4.278 | 2.203 |
| 4.424 | 2.106 |
| 4.619 | 2.014 |
| 4.704 | 2.030 |
| 4.781 | 2.423 |

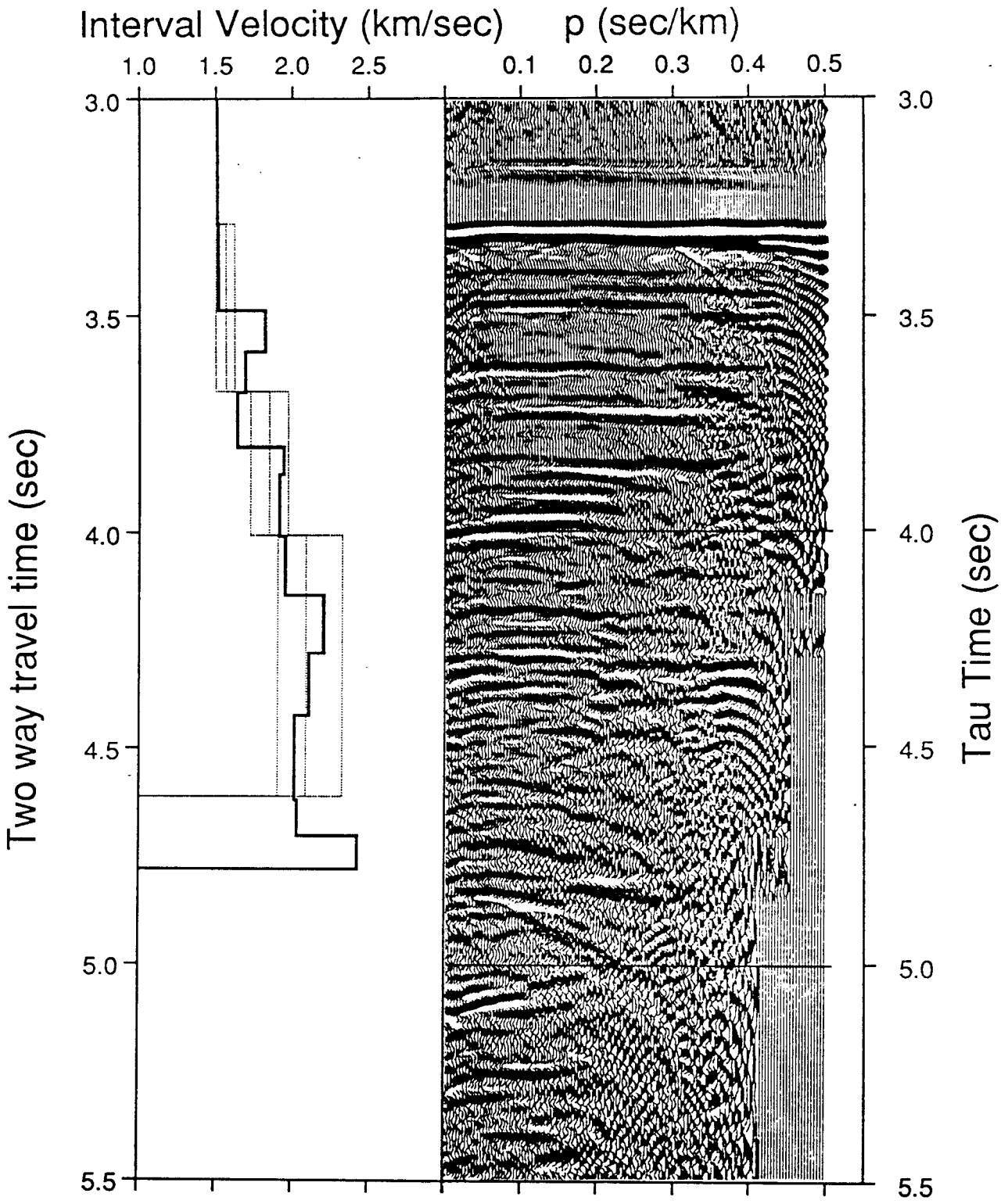
Interval Velocity (km/sec)
p (sec/km)
1.0
1.5
2.0
2.5
0.1
0.2
0.3
0.4
0.5
3.0
3.5
4.0
4.5
5.0
5.5
Two way travel time (sec)
Tau Time (sec)

## CDP 2602

| T0 sec | Interval Velocity km/sec | Lower Velocity Bound km/sec | Upper Velocity Bound km/sec |
|---|---|---|---|
| 3.263 | 1.507 | 1.502 | 1.512 |
| 3.648 | 1.602 | 1.524 | 1.683 |
| 3.973 | 1.839 | 1.776 | 1.916 |
| 4.624 | 2.176 | 1.922 | 2.308 |

| T0 sec | Interval Velocity km/sec |
|---|---|
| 3.260 | 1.508 |
| 3.460 | 1.528 |
| 3.573 | 1.616 |
| 3.648 | 1.660 |
| 3.784 | 1.681 |
| 3.841 | 1.739 |
| 3.904 | 2.049 |
| 3.974 | 1.682 |
| 4.141 | 1.881 |
| 4.262 | 2.249 |
| 4.401 | 2.132 |
| 4.624 | 2.319 |
| 4.713 | 2.331 |
| 4.869 | 2.222 |

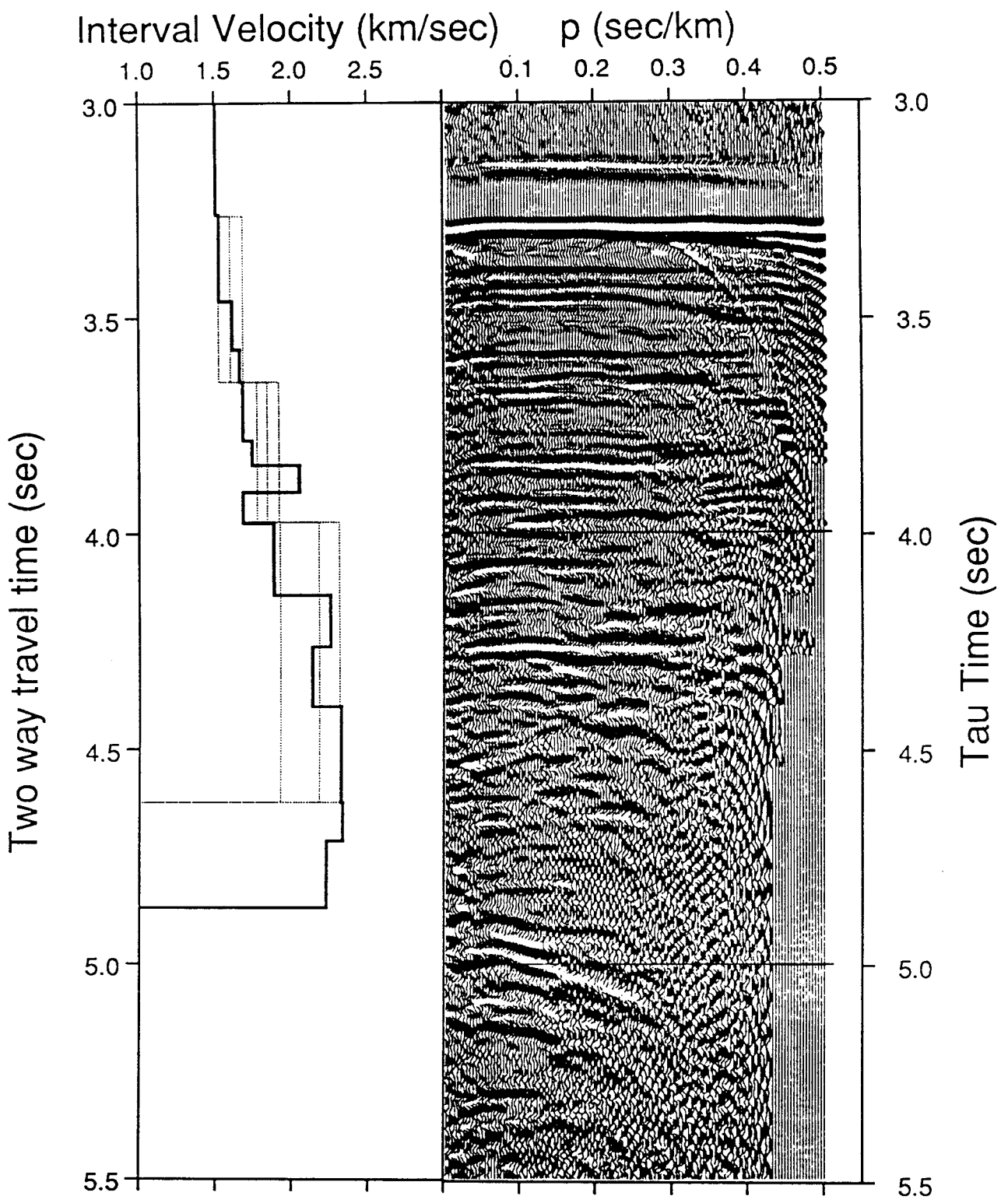
Interval Velocity (km/sec)
1.0
1.5
2.0
2.5
p (sec/km)
0.1
0.2
0.3
0.4
0.5
3.0
3.5
4.0
4.5
5.0
5.5
Two way travel time (sec)
Tau Time (sec)

## CDP 2702

| T0 sec | Interval Velocity km/sec | Lower Velocity Bound km/sec | Upper Velocity Bound km/sec |
|---|---|---|---|
| 3.251 | 1.507 | 1.502 | 1.512 |
| 3.568 | 1.600 | 1.527 | 1.647 |
| 3.959 | 1.920 | 1.861 | 1.960 |
| 4.652 | 2.113 | 1.875 | 2.230 |

| T0 sec | Interval Velocity km/sec |
|---|---|
| 3.249 | 1.510 |
| 3.440 | 1.511 |
| 3.538 | 1.633 |
| 3.609 | 1.510 |
| 3.756 | 1.796 |
| 3.813 | 2.034 |
| 3.866 | 2.389 |
| 3.957 | 1.879 |
| 4.108 | 1.726 |
| 4.254 | 2.089 |
| 4.390 | 2.217 |
| 4.650 | 2.192 |
| 4.745 | 2.192 |
| 4.937 | 2.140 |

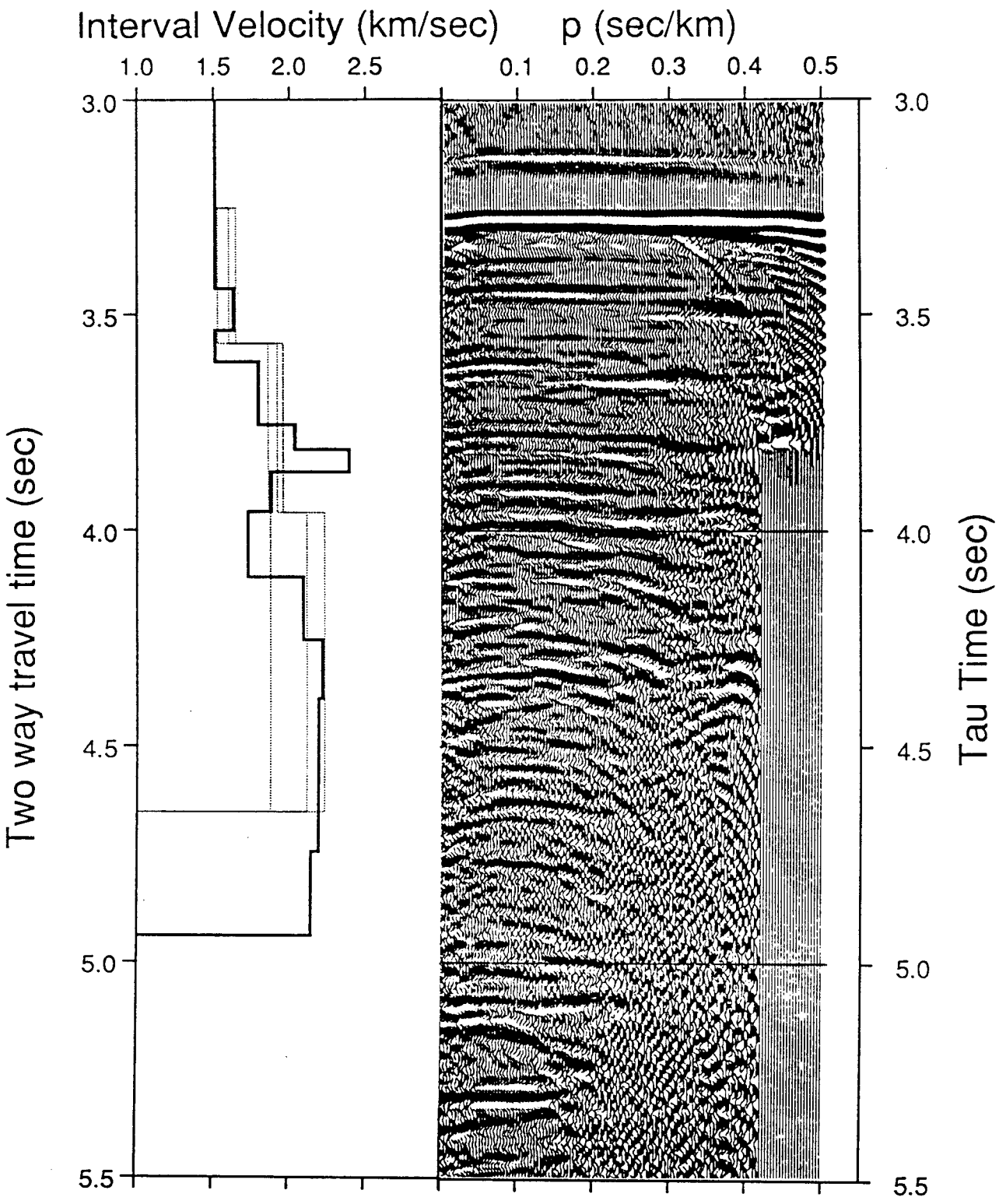
Interval Velocity (km/sec)
1.0
1.5
2.0
2.5
p (sec/km)
0.1
0.2
0.3
0.4
0.5
3.0
3.5
4.0
4.5
5.0
5.5
Two way travel time (sec)
Tau Time (sec)

## CDP 2802

| T0 sec | Interval Velocity km/sec | Lower Velocity Bound km/sec | Upper Velocity Bound km/sec |
|---|---|---|---|
| 3.245 | 1.507 | 1.502 | 1.512 |
| 3.561 | 1.552 | 1.515 | 1.602 |
| 3.921 | 1.948 | 1.848 | 2.055 |
| 4.649 | 2.111 | 1.918 | 2.298 |

| T0 sec | Interval Velocity km/sec |
|---|---|
| 3.244 | 1.508 |
| 3.423 | 1.540 |
| 3.560 | 1.553 |
| 3.720 | 1.671 |
| 3.775 | 1.932 |
| 3.839 | 2.005 |
| 3.918 | 2.034 |
| 4.088 | 1.956 |
| 4.230 | 1.916 |
| 4.377 | 2.121 |
| 4.648 | 2.295 |
| 4.761 | 2.303 |
| 4.945 | 2.292 |

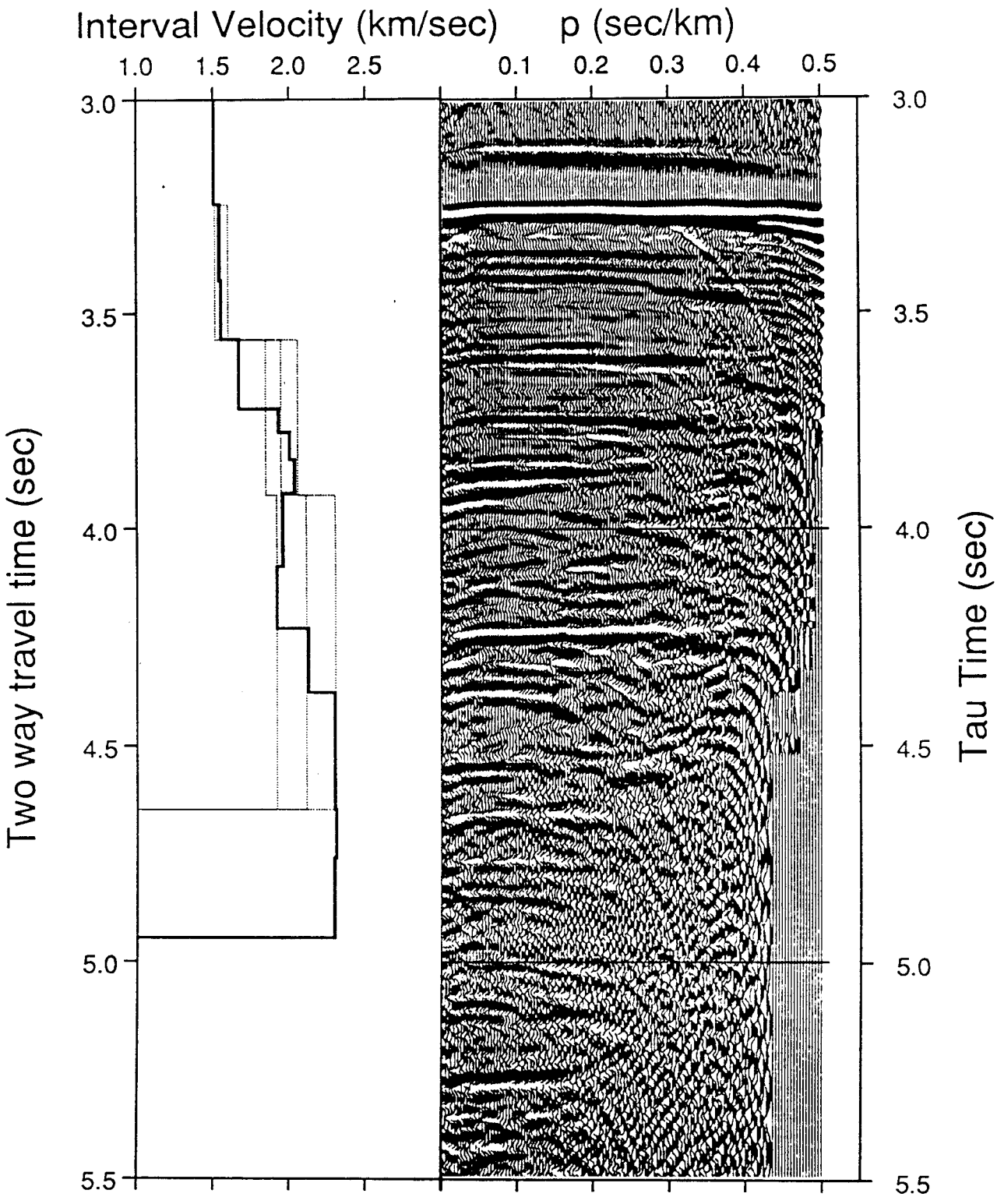
Interval Velocity (km/sec)
1.0
1.5
2.0
2.5
p (sec/km)
0.1
0.2
0.3
0.4
0.5
3.0
3.5
4.0
4.5
5.0
5.5
Two way travel time (sec)
Tau Time (sec)

CDP 2902

| T0 sec | Interval Velocity km/sec | Lower Velocity Bound km/sec | Upper Velocity Bound km/sec |
|---|---|---|---|
| 3.236 | 1.507 | 1.502 | 1.512 |
| 3.529 | 1.594 | 1.512 | 1.640 |
| 3.901 | 1.782 | 1.700 | 1.895 |
| 4.639 | 2.170 | 1.976 | 2.325 |

| T0 sec | Interval Velocity km/sec |
|---|---|
| 3.232 | 1.506 |
| 3.406 | 1.461 |
| 3.527 | 1.461 |
| 3.701 | 1.831 |
| 3.763 | 1.983 |
| 3.818 | 1.809 |
| 3.899 | 1.840 |
| 4.054 | 1.891 |
| 4.208 | 1.891 |
| 4.373 | 2.040 |
| 4.640 | 2.339 |
| 4.760 | 2.334 |
| 4.938 | 2.461 |

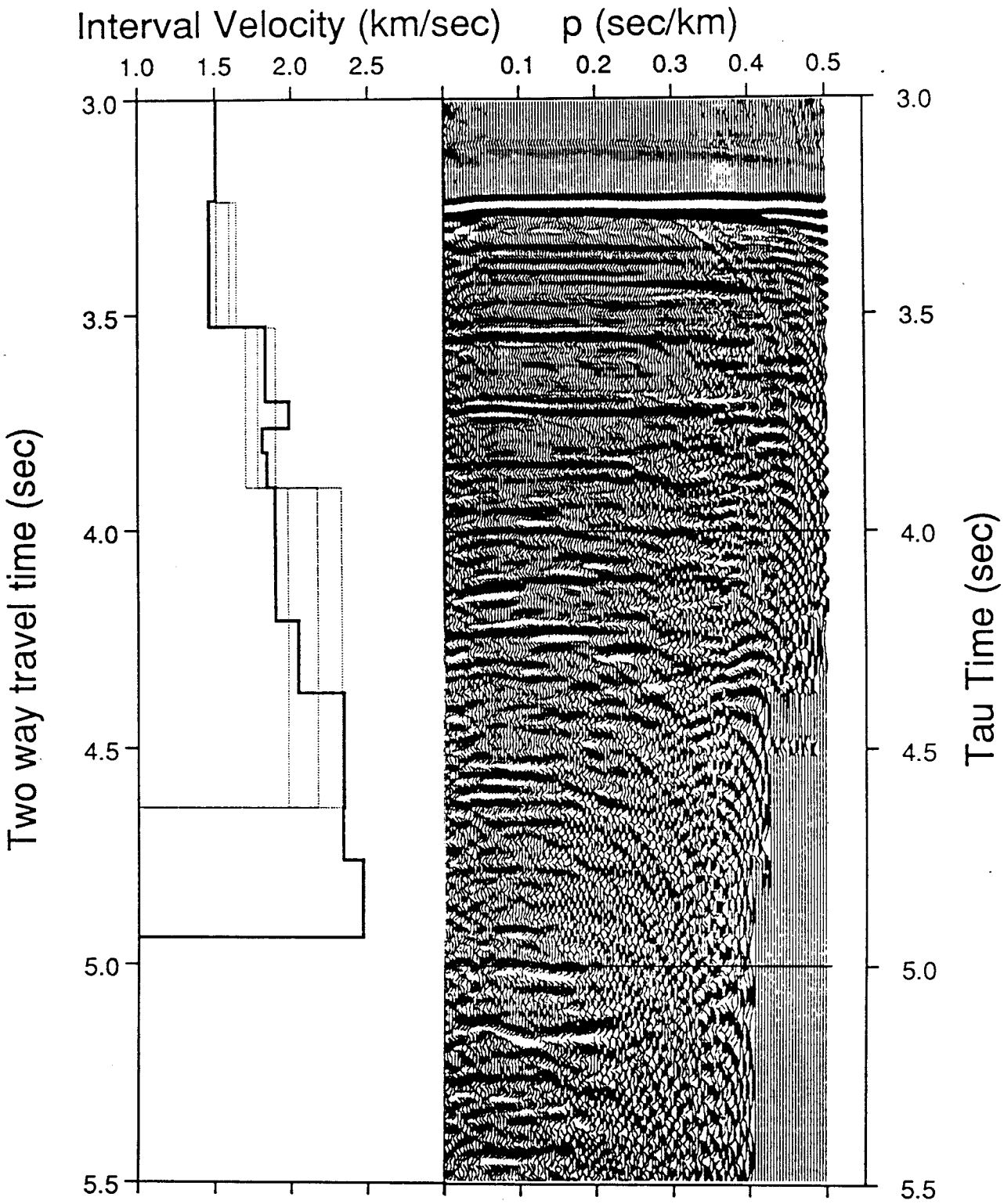
Interval Velocity (km/sec)
p (sec/km)
1.0
1.5
2.0
2.5
0.1
0.2
0.3
0.4
0.5
3.0
3.5
4.0
4.5
5.0
5.5
Two way travel time (sec)
Tau Time (sec)

## CDP 3002

| T0 sec | Interval Velocity km/sec | Lower Velocity Bound km/sec | Upper Velocity Bound km/sec |
|---|---|---|---|
| 3.228 | 1.507 | 1.502 | 1.512 |
| 3.507 | 1.537 | 1.502 | 1.652 |
| 3.862 | 1,800 | 1.735 | 1.947 |
| 4.638 | 2.150 | 1.850 | 2.295 |

| T0 sec | Interval Velocity km/sec |
|---|---|
| 3.228 | 1.507 |
| 3.387 | 1.476 |
| 3.509 | 1.542 |
| 3.665 | 1.854 |
| 3.716 | 1.870 |
| 3.804 | 2.080 |
| 3.861 | 1.717 |
| 4.022 | 1.830 |
| 4.187 | 1.886 |
| 4.370 | 2.090 |
| 4.652 | 2.112 |
| 4.764 | 2.157 |
| 4.950 | 2.402 |

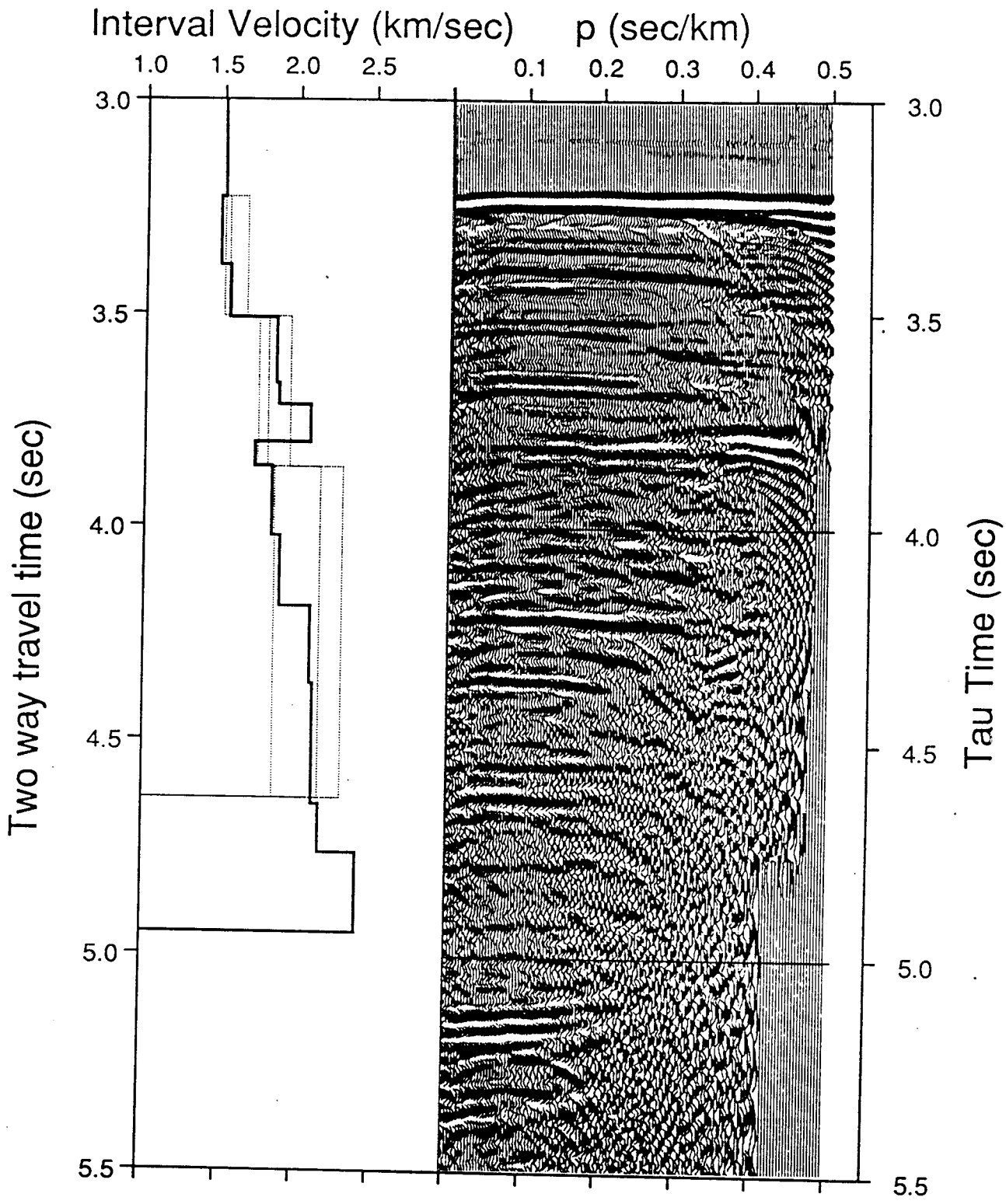
Interval Velocity (km/sec)
1.0
1.5
2.0
2.5
p (sec/km)
0.1
0.2
0.3
0.4
0.5
3.0
3.5
4.0
4.5
5.0
5.5
Two way travel time (sec)
Tau Time (sec)

## CDP 3202

| T0 sec | Interval Velocity km/sec | Lower Velocity Bound km/sec | Upper Velocity Bound km/sec |
|---|---|---|---|
| 3.209 | 1.507 | 1.502 | 1.512 |
| 3.436 | 1.558 | 1.507 | 1.587 |
| 3.852 | 1.855 | 1.751 | 1.937 |
| 4.604 | 2.190 | 2.026 | 2.376 |

| T0 sec | Interval Velocity km/sec |
|---|---|
| 3.209 | 1.509 |
| 3.299 | 1.461 |
| 3.434 | 1.589 |
| 3.601 | 1.589 |
| 3.671 | 2.002 |
| 3.744 | 2.094 |
| 3.850 | 1.761 |
| 3.979 | 2.147 |
| 4.146 | 1.833 |
| 4.332 | 1.904 |
| 4.601 | 1.930 |
| 4.714 | 2.963 |
| 4.919 | 2.963 |

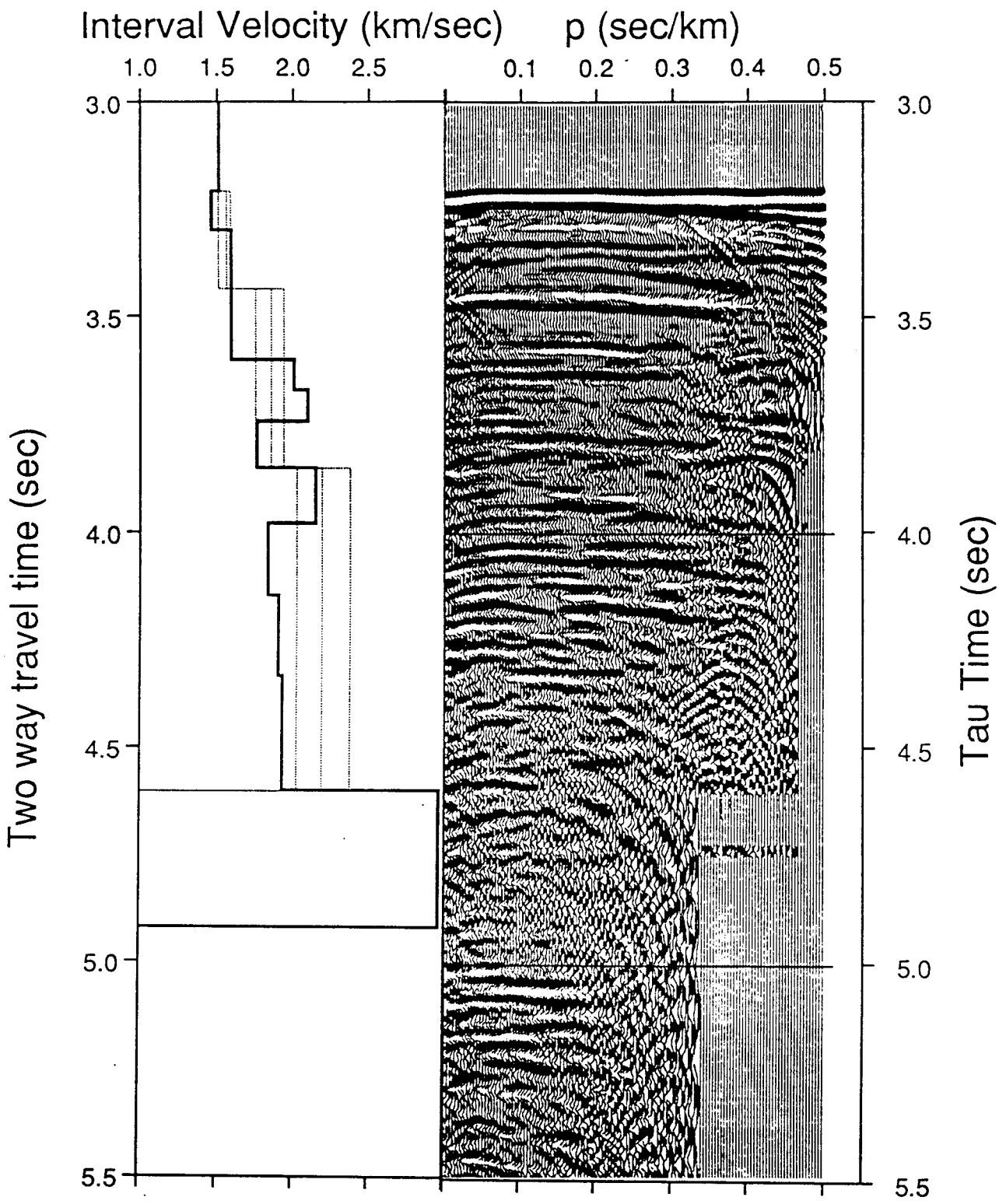
Interval Velocity (km/sec)
p (sec/km)
1.0
1.5
2.0
2.5
0.1
0.2
0.3
0.4
0.5
3.0
3.5
4.0
4.5
5.0
5.5
Two way travel time (sec)
Tau Time (sec)

## CDP 3302

| T0 | Interval Velocity | Lower Velocity Bound | Upper Velocity Bound |
|---|---|---|---|
| sec | km/sec | km/sec | km/sec |
| 3.190 | 1.507 | 1.502 | 1.512 |
| 3.409 | 1.498 | 1.451 | 1.590 |
| 3.826 | 1.883 | 1.800 | 1.980 |
| 4.593 | 2.181 | 1.960 | 2.295 |

| T0 | Interval Velocity |
|---|---|
| sec | km/sec |
| 3.188 | 1.508 |
| 3.280 | 1.570 |
| 3.409 | 1.609 |
| 3.583 | 1.635 |
| 3.639 | 1.895 |
| 3.739 | 1.938 |
| 3.825 | 1.684 |
| 3.975 | 1.993 |
| 4.121 | 1.698 |
| 4.314 | 1.971 |
| 4.593 | 2.213 |
| 4.698 | 2.226 |
| 4.891 | 2.437 |

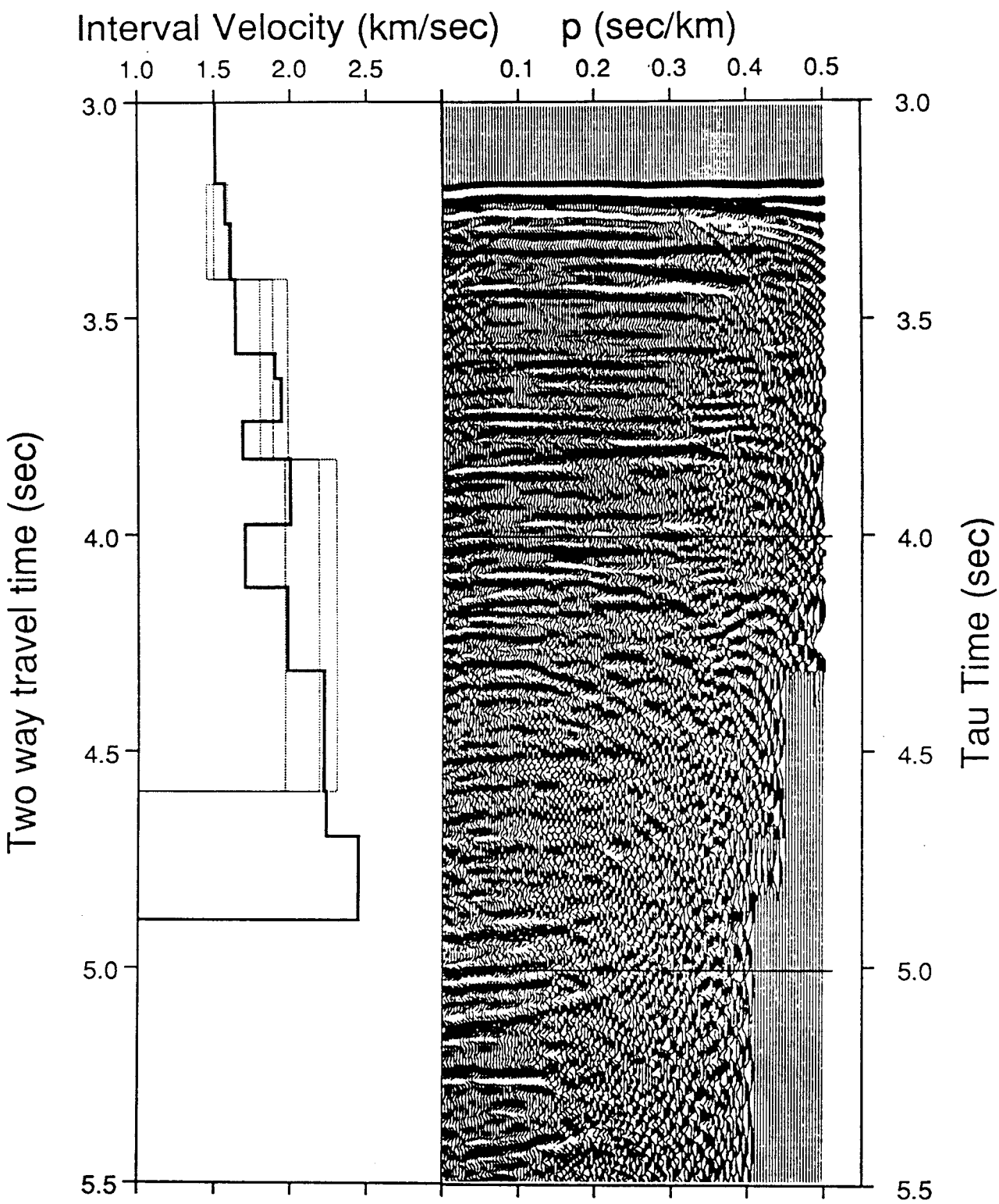
Interval Velocity (km/sec)
1.0
1.5
2.0
2.5
p (sec/km)
0.1
0.2
0.3
0.4
0.5
3.0
3.5
4.0
4.5
5.0
5.5
Two way travel time (sec)
Tau Time (sec)

## CDP 3402

| T0 sec | Interval Velocity km/sec | Lower Velocity Bound km/sec | Upper Velocity Bound km/sec |
|---|---|---|---|
| 3.167 | 1.507 | 1.502 | 1.512 |
| 3.363 | 1.503 | 1.480 | 1.519 |
| 3.819 | 1.891 | 1.810 | 2.037 |
| 4.560 | 2.163 | 2.087 | 2.319 |

| T0 sec | Interval Velocity km/sec |
|---|---|
| 3.166 | 1.506 |
| 3.244 | 1.504 |
| 3.365 | 1.513 |
| 3.549 | 1.588 |
| 3.611 | 1.784 |
| 3.721 | 1.886 |
| 3.821 | 2.068 |
| 3.914 | 1.878 |
| 4.108 | 1.954 |
| 4.292 | 2.190 |
| 4.562 | 2.129 |
| 4.664 | 2.184 |
| 4.853 | 3.074 |

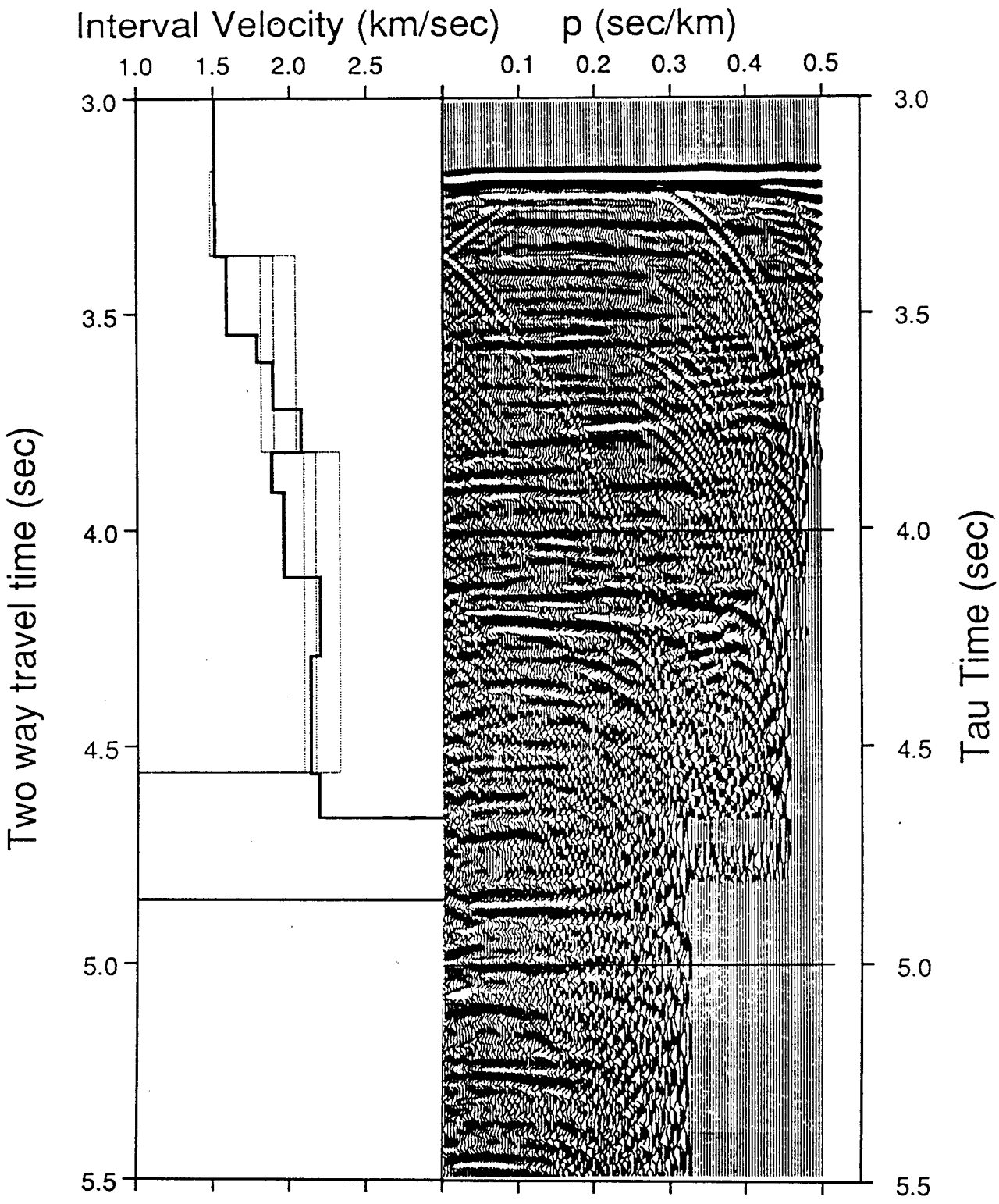
Interval Velocity (km/sec)
p (sec/km)
1.0
1.5
2.0
2.5
0.1
0.2
0.3
0.4
0.5
3.0
3.5
4.0
4.5
5.0
5.5
Two way travel time (sec)
Tau Time (sec)

## CDP 3502

| T0 sec | Interval Velocity km/sec | Lower Velocity Bound km/sec | Upper Velocity Bound km/sec |
|---|---|---|---|
| 3.147 | 1.507 | 1.502 | 1.512 |
| 3.340 | 1.512 | 1.485 | 1.542 |
| 3.803 | 1.842 | 1.785 | 1.936 |
| 4.542 | 2.149 | 2.070 | 2.360 |

| T0 sec | Interval Velocity km/sec |
|---|---|
| 3.143 | 1.505 |
| 3.340 | 1.489 |
| 3.500 | 1.624 |
| 3.599 | 2.012 |
| 3.666 | 1.699 |
| 3.802 | 1.819 |
| 3.930 | 1.694 |
| 4.072 | 1.683 |
| 4.267 | 2.362 |
| 4.552 | 2.382 |
| 4.652 | 3.011 |
| 4.832 | 3.011 |

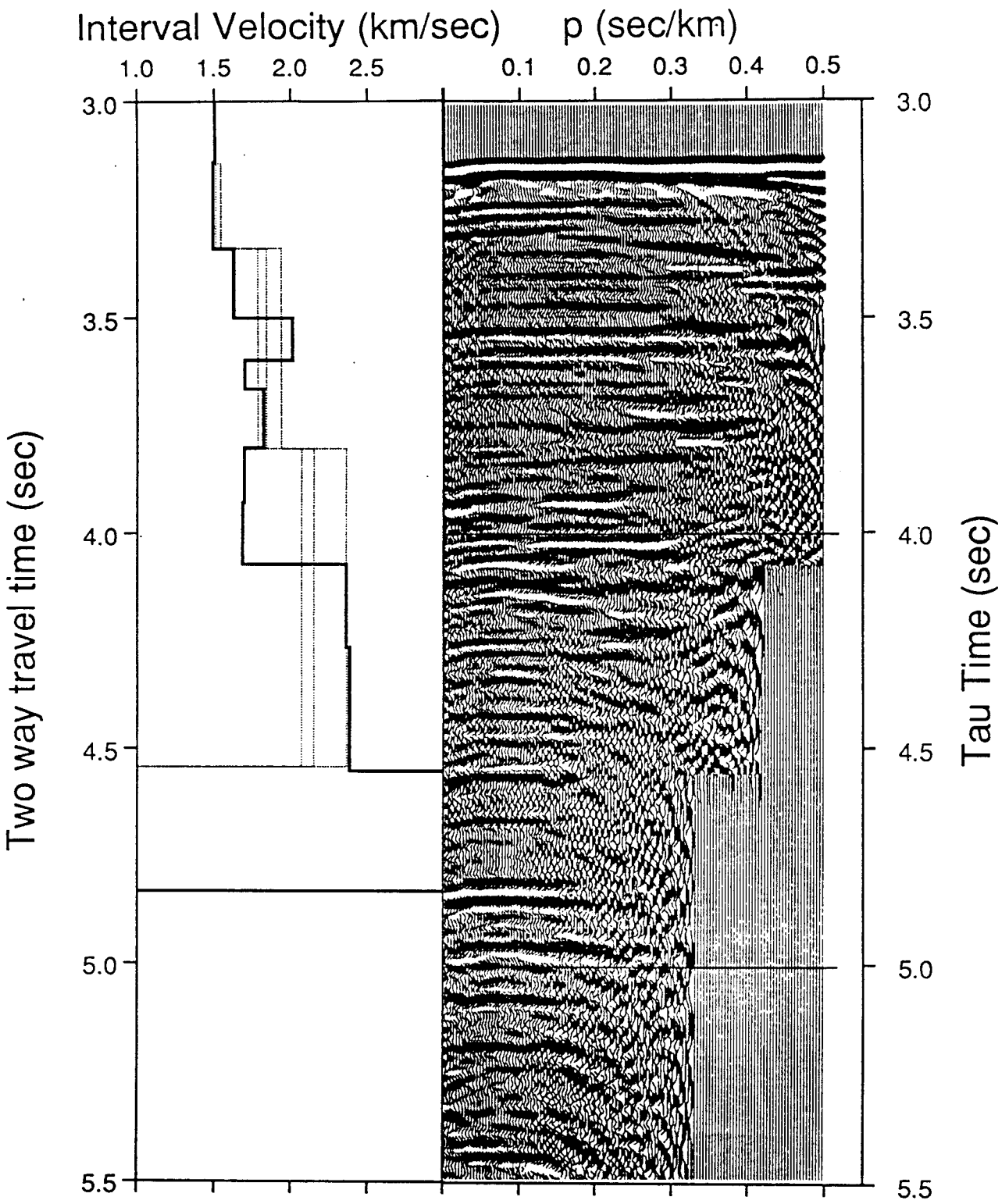
Interval Velocity (km/sec)
p (sec/km)
1.0
1.5
2.0
2.5
0.1
0.2
0.3
0.4
0.5
3.0
3.5
4.0
4.5
5.0
5.5
Two way travel time (sec)
Tau Time (sec)

## CDP 3602

| T0 sec | Interval Velocity km/sec | Lower Velocity Bound km/sec | Upper Velocity Bound km/sec |
|---|---|---|---|
| 3.119 | 1.507 | 1.502 | 1.512 |
| 3.295 | 1.569 | 1.468 | 1.630 |
| 3.756 | 1.861 | 1.740 | 1.946 |
| 4.460 | 2.190 | 1.993 | 2.410 |

| T0 sec | Interval Velocity km/sec |
|---|---|
| 3.118 | 1.506 |
| 3.295 | 1.501 |
| 3.440 | 1.651 |
| 3.550 | 1.753 |
| 3.628 | 1.871 |
| 3.754 | 1.894 |
| 3.911 | 1.800 |
| 4.039 | 2.008 |
| 4.226 | 2.062 |
| 4.459 | 2.011 |
| 4.570 | 2.153 |
| 4.771 | 2.777 |

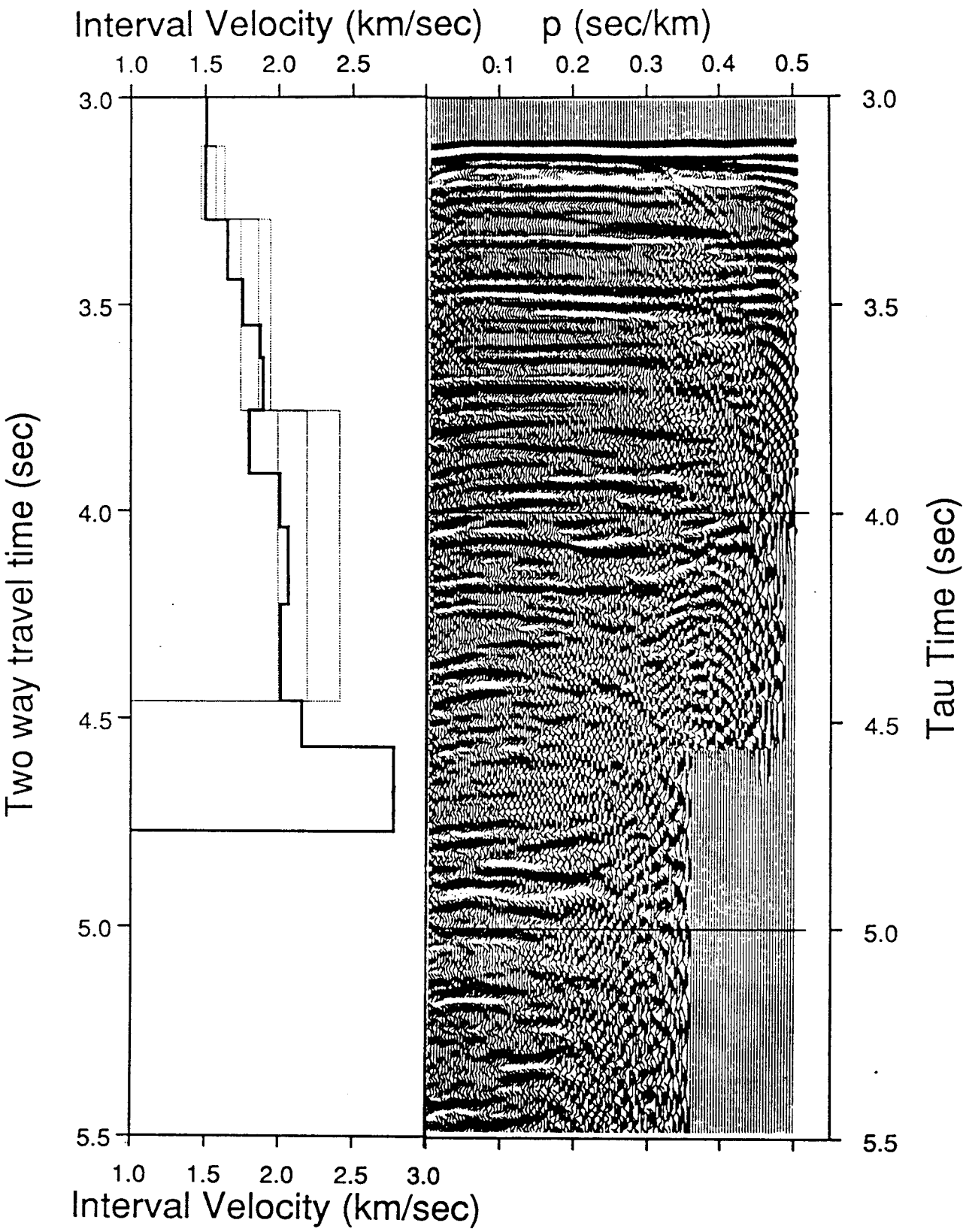
Interval Velocity (km/sec)
p (sec/km)
1.0
1.5
2.0
2.5
0.1
0.2
0.3
0.4
0.5
3.0
3.5
4.0
4.5
5.0
5.5
Two way travel time (sec)
Tau Time (sec)
Interval Velocity (km/sec)

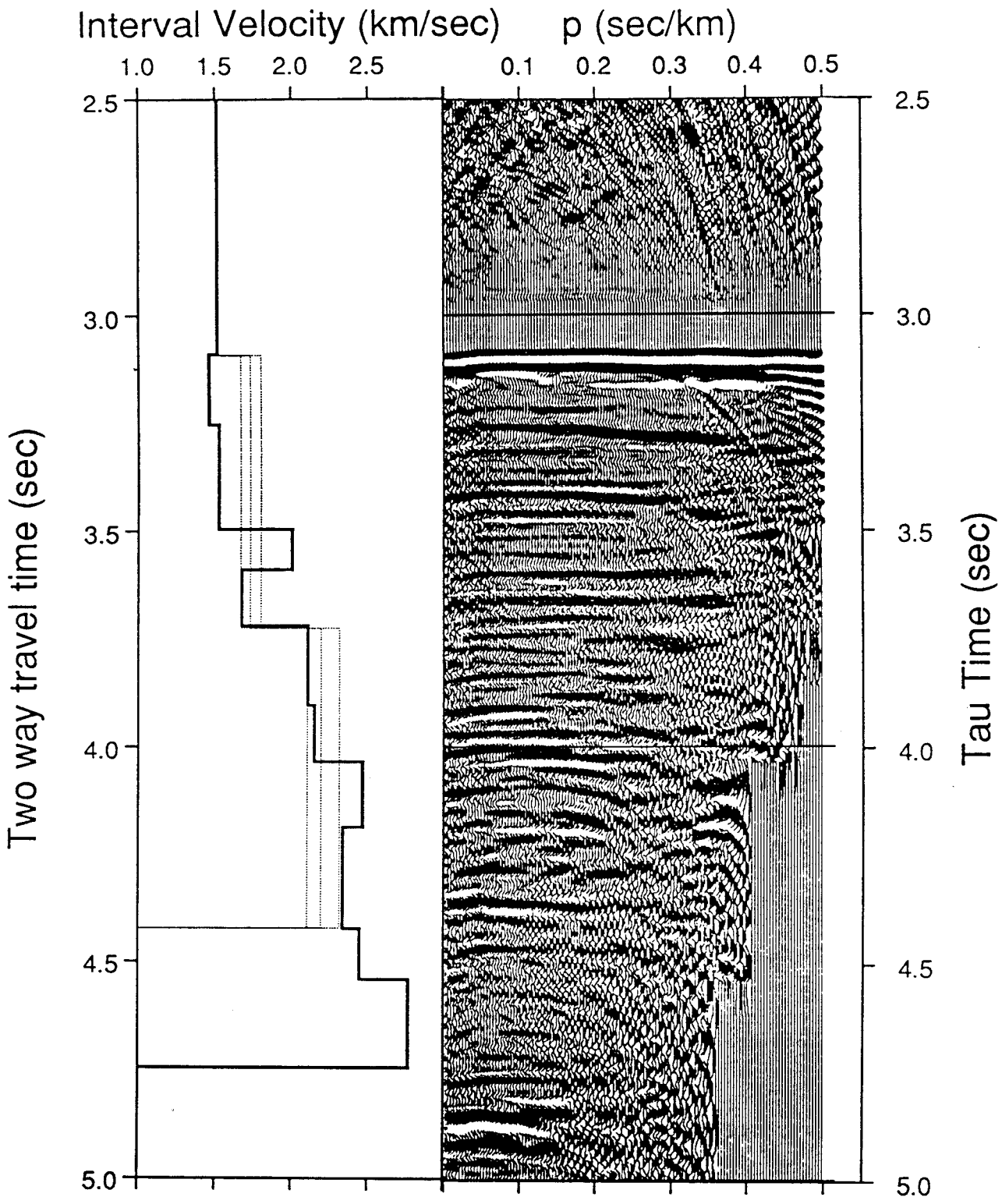
Interval Velocity (km/sec)
p (sec/km)
1.0
1.5
2.0
2.5
0.1
0.2
0.3
0.4
0.5
2.5
3.0
3.5
4.0
4.5
5.0
Two way travel time (sec)
Tau Time (sec)

## CDP 3802

| T0 sec | Interval Velocity km/sec | Lower Velocity Bound km/sec | Upper Velocity Bound km/sec |
|---|---|---|---|
| 3.066 | 1.507 | 1.502 | 1.512 |
| 3.700 | 1.772 | 1.652 | 1.836 |
| 4.370 | 2.189 | 2.072 | 2.340 |

| T0 sec | Interval Velocity km/sec |
|---|---|
| 3.060 | 1.513 |
| 3.190 | 1.523 |
| 3.363 | 1.523 |
| 3.461 | 1.482 |
| 3.560 | 2.119 |
| 3.697 | 2.020 |
| 3.889 | 2.137 |
| 3.995 | 1.699 |
| 4.152 | 1.908 |
| 4.369 | 2.839 |
| 4.500 | 2.839 |
| 4.700 | 2.372 |

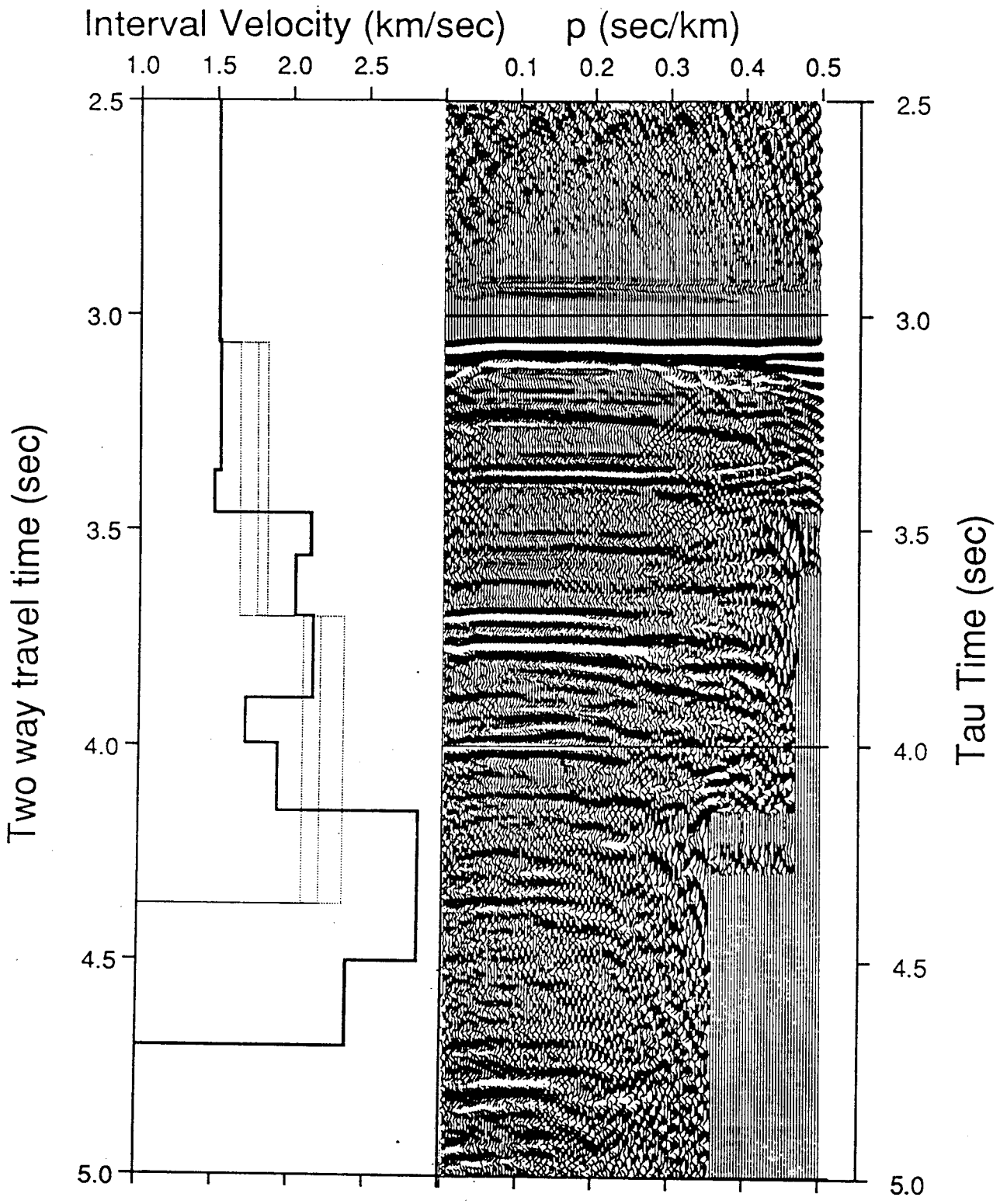
Interval Velocity (km/sec)
1.0
1.5
2.0
2.5
p (sec/km)
0.1
0.2
0.3
0.4
0.5
2.5
3.0
3.5
4.0
4.5
5.0
Two way travel time (sec)
Tau Time (sec)

## CDP 3902

| T0 sec | Interval Velocity km/sec | Lower Velocity Bound km/sec | Upper Velocity Bound km/sec |
|---|---|---|---|
| 3.030 | 1.507 | 1.502 | 1.512 |
| 3.641 | 1.770 | 1.740 | 1.806 |
| 4.465 | 2.122 | 2.015 | 2.273 |

| T0 sec | Interval Velocity km/sec |
|---|---|
| 3.025 | 1.504 |
| 3.101 | 1.750 |
| 3.310 | 1.750 |
| 3.428 | 1.661 |
| 3.529 | 1.890 |
| 3.645 | 1.801 |
| 3.893 | 1.861 |
| 3.976 | 2.078 |
| 4.127 | 2.169 |
| 4.334 | 2.415 |
| 4.469 | 2.415 |
| 4.680 | 2.415 |

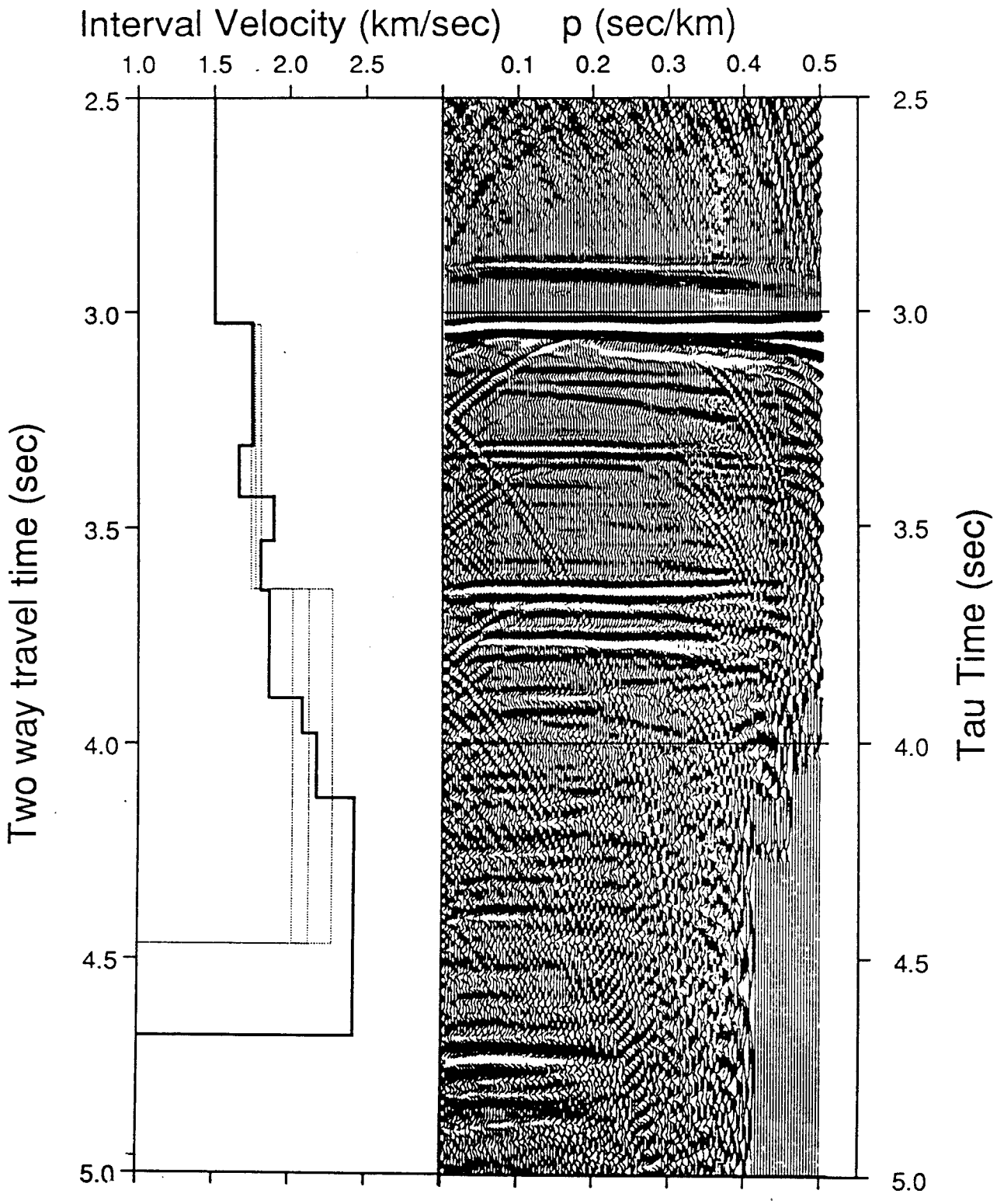
Interval Velocity (km/sec)
p (sec/km)
1.0
1.5
2.0
2.5
0.1
0.2
0.3
0.4
0.5
2.5
3.0
3.5
4.0
4.5
5.0
Two way travel time (sec)
Tau Time (sec)

## CDP 4002

| T0 sec | Interval Velocity km/sec | Lower Velocity Bound km/sec | Upper Velocity Bound km/sec |
|---|---|---|---|
| 2.985 | 1.507 | 1.502 | 1.512 |
| 3.602 | 1.755 | 1.720 | 1.800 |
| 4.264 | 2.182 | 2.027 | 2.308 |

| T0 sec | Interval Velocity km/sec |
|---|---|
| 2.978 | 1.509 |
| 3.257 | 1.542 |
| 3.362 | 1.874 |
| 3.462 | 1.746 |
| 3.602 | 1.892 |
| 3.857 | 1.996 |
| 3.946 | 1.832 |
| 4.060 | 1.905 |
| 4.263 | 2.279 |
| 4.401 | 2.152 |
| 4.623 | 3.094 |

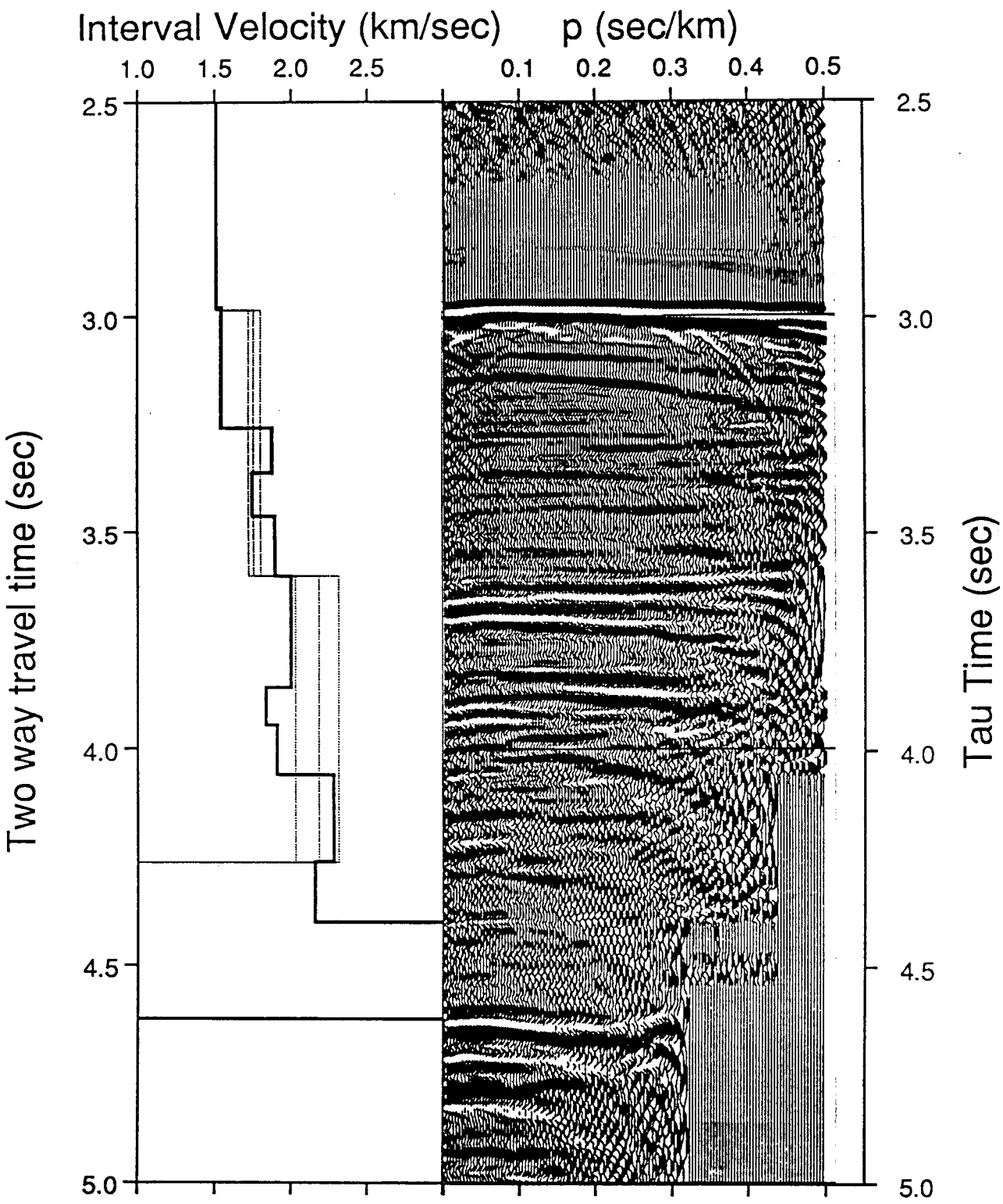
Interval Velocity (km/sec)
p (sec/km)
1.0
1.5
2.0
2.5
0.1
0.2
0.3
0.4
0.5
2.5
3.0
3.5
4.0
4.5
5.0
Two way travel time (sec)
Tau Time (sec)

CDP 4102

| T0 sec | Interval Velocity km/sec | Lower Velocity Bound km/sec | Upper Velocity Bound km/sec |
|---|---|---|---|
| 2.921 | 1.507 | 1.502 | 1.512 |
| 3.568 | 1.772 | 1.760 | 1.820 |
| 4.221 | 2.248 | 1.992 | 2.355 |

| T0 sec | Interval Velocity km/sec |
|---|---|
| 2.923 | 1.501 |
| 3.165 | 1.565 |
| 3.300 | 1.565 |
| 3.437 | 2.156 |
| 3.565 | 1.664 |
| 3.816 | 1.662 |
| 3.906 | 2.248 |
| 4.029 | 2.405 |
| 4.220 | 2.552 |
| 4.322 | 2.552 |
| 4.500 | 2.589 |

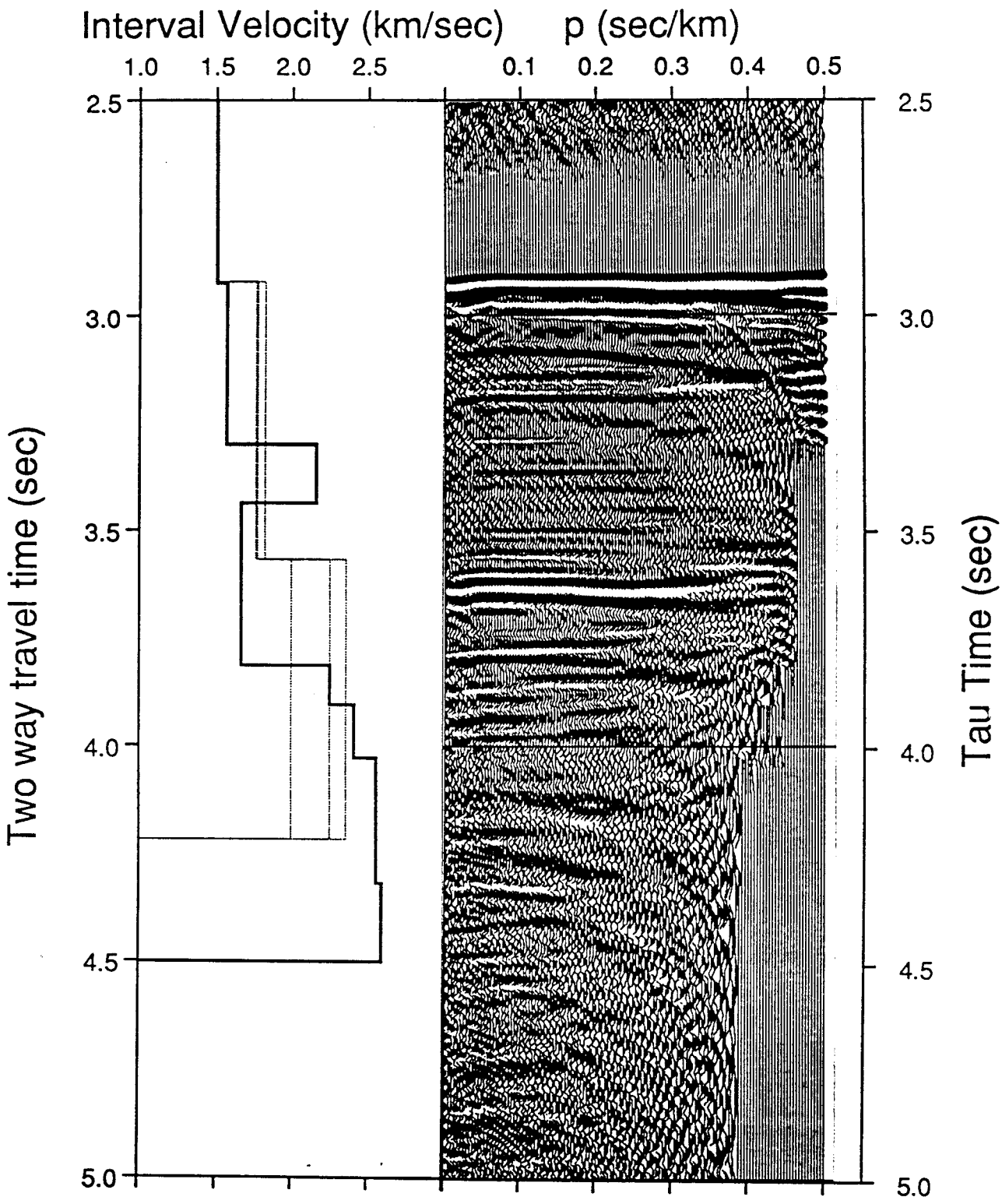
Interval Velocity (km/sec)
1.0
1.5
2.0
2.5
p (sec/km)
0.1
0.2
0.3
0.4
0.5
2.5
3.0
3.5
4.0
4.5
5.0
Two way travel time (sec)
Tau Time (sec)

## CDP 4202

| T0 sec | Interval Velocity km/sec | Lower Velocity Bound km/sec | Upper Velocity Bound km/sec |
|---|---|---|---|
| 2.849 | 1.507 | 1.502 | 1.512 |
| 3.519 | 1.730 | 1.710 | 1.760 |
| 4.183 | 2.091 | 1.980 | 2.227 |

| T0 sec | Interval Velocity km/sec |
|---|---|
| 2.849 | 1.507 |
| 3.088 | 1.501 |
| 3.243 | 1.725 |
| 3.369 | 1.962 |
| 3.515 | 1.919 |
| 3.752 | 1.830 |
| 3.861 | 2.098 |
| 4.003 | 2.212 |
| 4.183 | 2.226 |
| 4.302 | 2.311 |
| 4.559 | 3.294 |

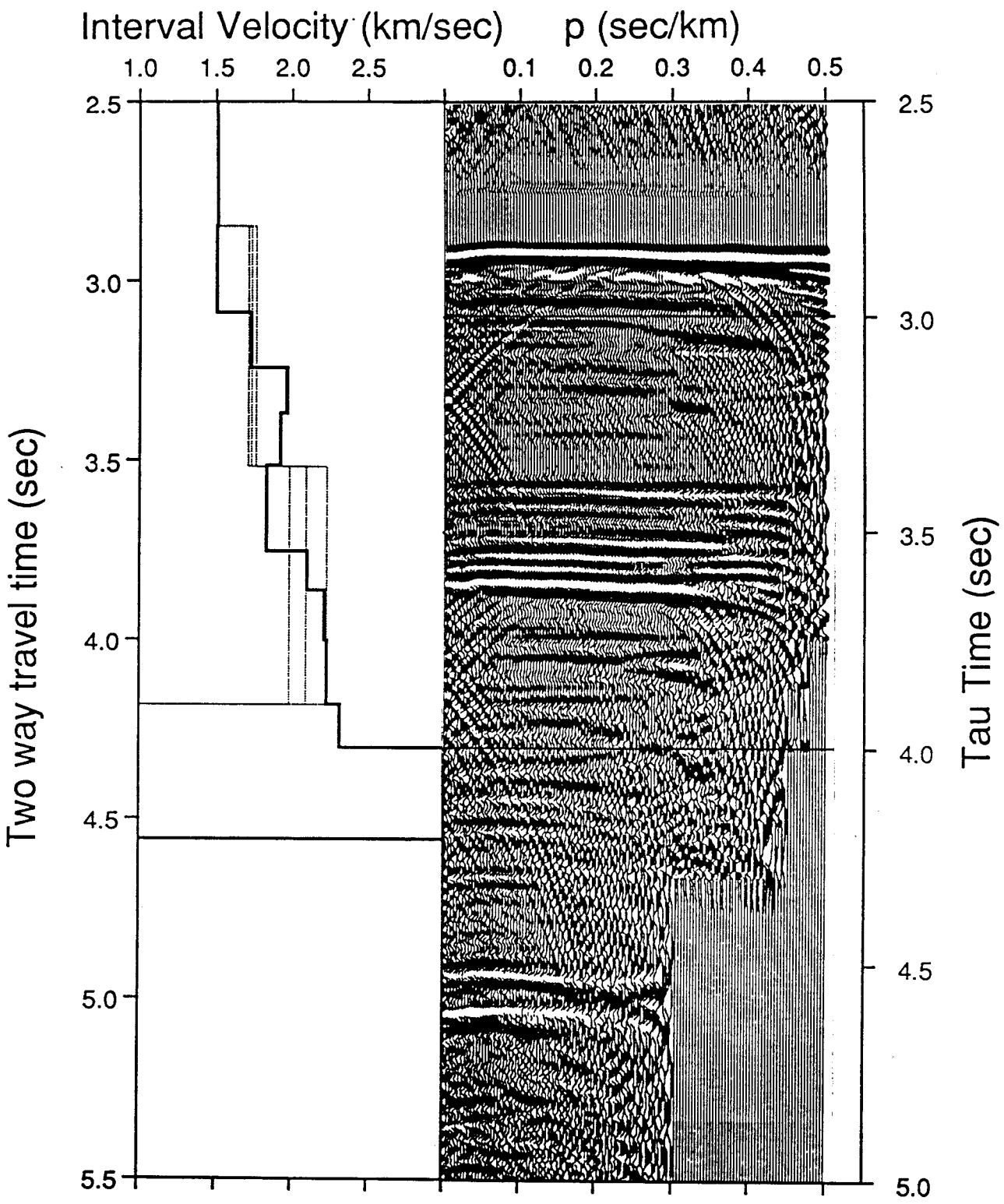
Interval Velocity (km/sec)
1.0
1.5
2.0
2.5
p (sec/km)
0.1
0.2
0.3
0.4
0.5
2.5
3.0
3.5
4.0
4.5
5.0
5.5
Two way travel time (sec)
Tau Time (sec)

## CDP 4302

| T0 sec | Interval Velocity km/sec | Lower Velocity Bound km/sec | Upper Velocity Bound km/sec |
|---|---|---|---|
| 2.768 | 1.507 | 1.502 | 1.512 |
| 3.498 | 1.769 | 1.755 | 1.841 |
| 4.140 | 2.180 | 2.040 | 2.310 |

| T0 sec | Interval Velocity km/sec |
|---|---|
| 2.769 | 1.505 |
| 3.024 | 1.593 |
| 3.199 | 1.593 |
| 3.339 | 1.879 |
| 3.499 | 2.060 |
| 3.716 | 1.888 |
| 3.806 | 1.950 |
| 3.951 | 1.895 |
| 4.139 | 2.379 |
| 4.262 | 2.343 |
| 4.570 | 3.118 |

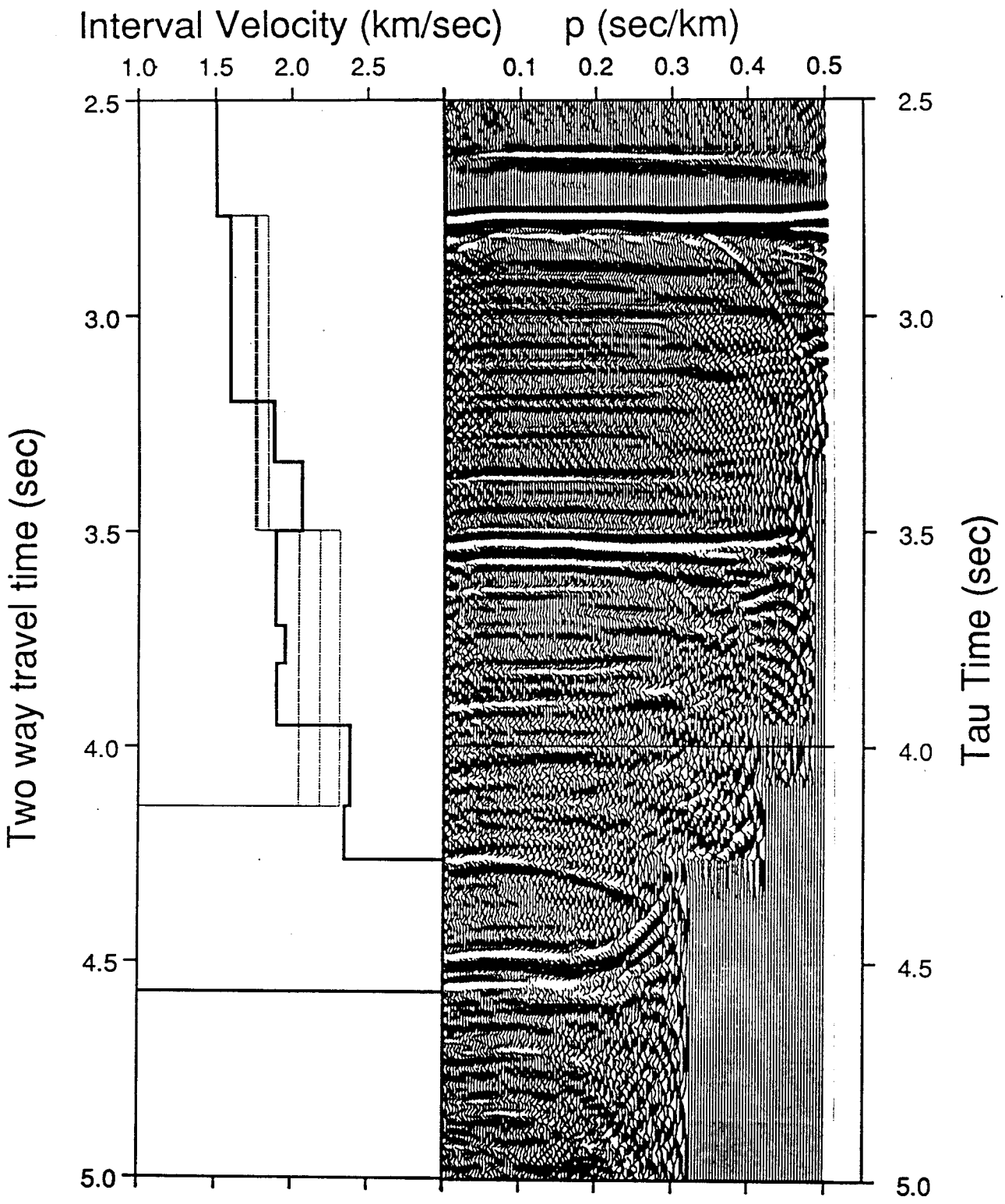
Interval Velocity (km/sec)
p (sec/km)
1.0
1.5
2.0
2.5
0.1
0.2
0.3
0.4
0.5
2.5
3.0
3.5
4.0
4.5
5.0
Two way travel time (sec)
Tau Time (sec)

## CDP 4402

| T0 | Interval Velocity | Lower Velocity Bound | Upper Velocity Bound |
|---|---|---|---|
| sec | km/sec | km/sec | km/sec |
| 2.661 | 1.507 | 1.502 | 1.512 |
| 3.455 | 1.837 | 1.803 | 1.855 |
| 4.092 | 2.214 | 2.093 | 2.419 |

| T0 | Interval Velocity |
|---|---|
| sec | km/sec |
| 2.658 | 1.513 |
| 2.933 | 1.483 |
| 3.120 | 1.841 |
| 3.278 | 1.776 |
| 3.453 | 2.119 |
| 3.626 | 1.773 |
| 3.741 | 1.704 |
| 3.896 | 2.574 |
| 4.085 | 2.651 |
| 4.195 | 3.049 |
| 4.425 | 3.154 |

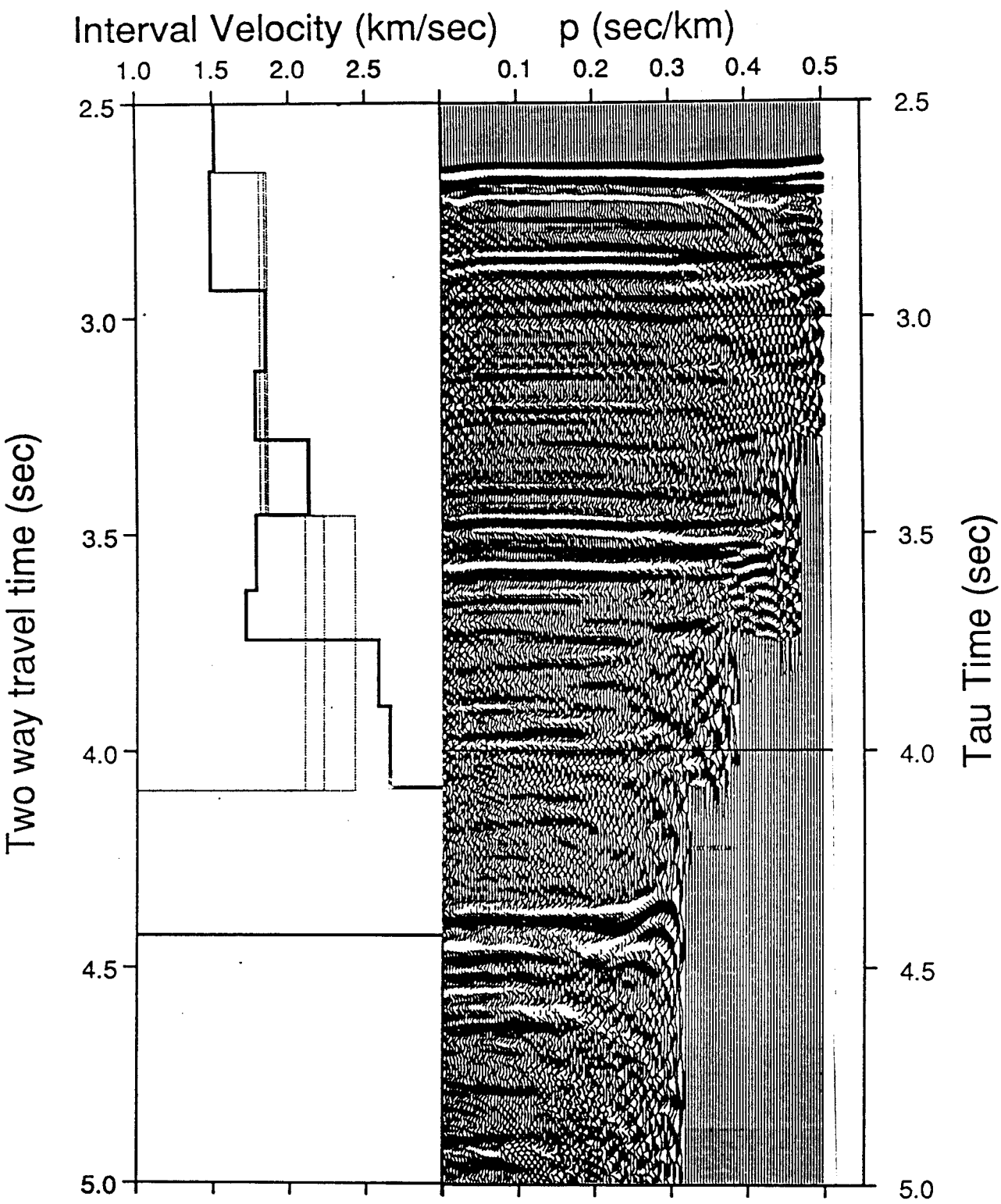
Interval Velocity (km/sec)
p (sec/km)
1.0
1.5
2.0
2.5
0.1
0.2
0.3
0.4
0.5
2.5
3.0
3.5
4.0
4.5
5.0
Two way travel time (sec)
Tau Time (sec)

## CDP 4502

| T0 | Interval Velocity | Lower Velocity Bound | Upper Velocity Bound |
|---|---|---|---|
| sec | km/sec | km/sec | km/sec |
| 2.535 | 1.507 | 1.502 | 1.512 |
| 3.404 | 1.797 | 1.750 | 1.870 |
| 4.002 | 2.413 | 2.350 | 2.523 |

| T0 | Interval Velocity |
|---|---|
| sec | km/sec |
| 2.538 | 1.518 |
| 2.840 | 1.600 |
| 3.027 | 1.861 |
| 3.202 | 1.954 |
| 3.398 | 1.881 |
| 3.549 | 2.092 |
| 3.655 | 2.127 |
| 3.807 | 2.325 |
| 4.009 | 2.294 |
| 4.123 | 2.901 |
| 4.340 | 3.380 |

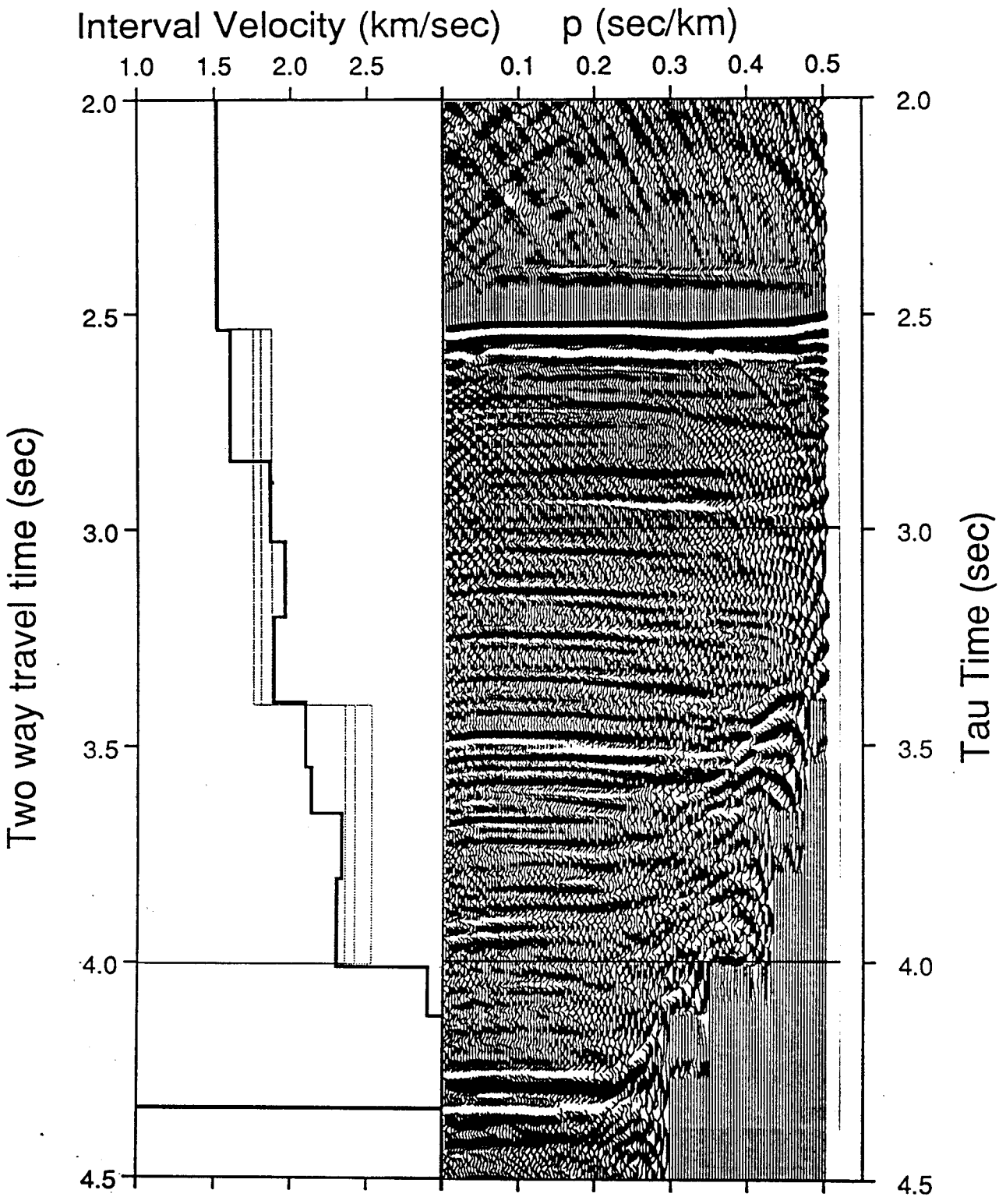
Interval Velocity (km/sec)
1.0
1.5
2.0
2.5
p (sec/km)
0.1
0.2
0.3
0.4
0.5
2.0
2.5
3.0
3.5
4.0
4.5
Two way travel time (sec)
Tau Time (sec)

## CDP 4602

| T0 | Interval Velocity | Lower Velocity Bound | Upper Velocity Bound |
|---|---|---|---|
| sec | km/sec | km/sec | km/sec |
| 2.392 | 1.507 | 1.502 | 1.512 |
| 3.340 | 1.830 | 1.785 | 1.897 |
| 3.885 | 2.486 | 2.288 | 2.540 |

| T0 | Interval Velocity |
|---|---|
| sec | km/sec |
| 2.393 | 1.516 |
| 2.739 | 1.712 |
| 2.928 | 1.531 |
| 3.127 | 1.986 |
| 3.340 | 1.853 |
| 3.459 | 2.104 |
| 3.548 | 2.186 |
| 3.701 | 2.369 |
| 3.889 | 2.704 |
| 4.008 | 2.813 |
| 4.195 | 3.087 |

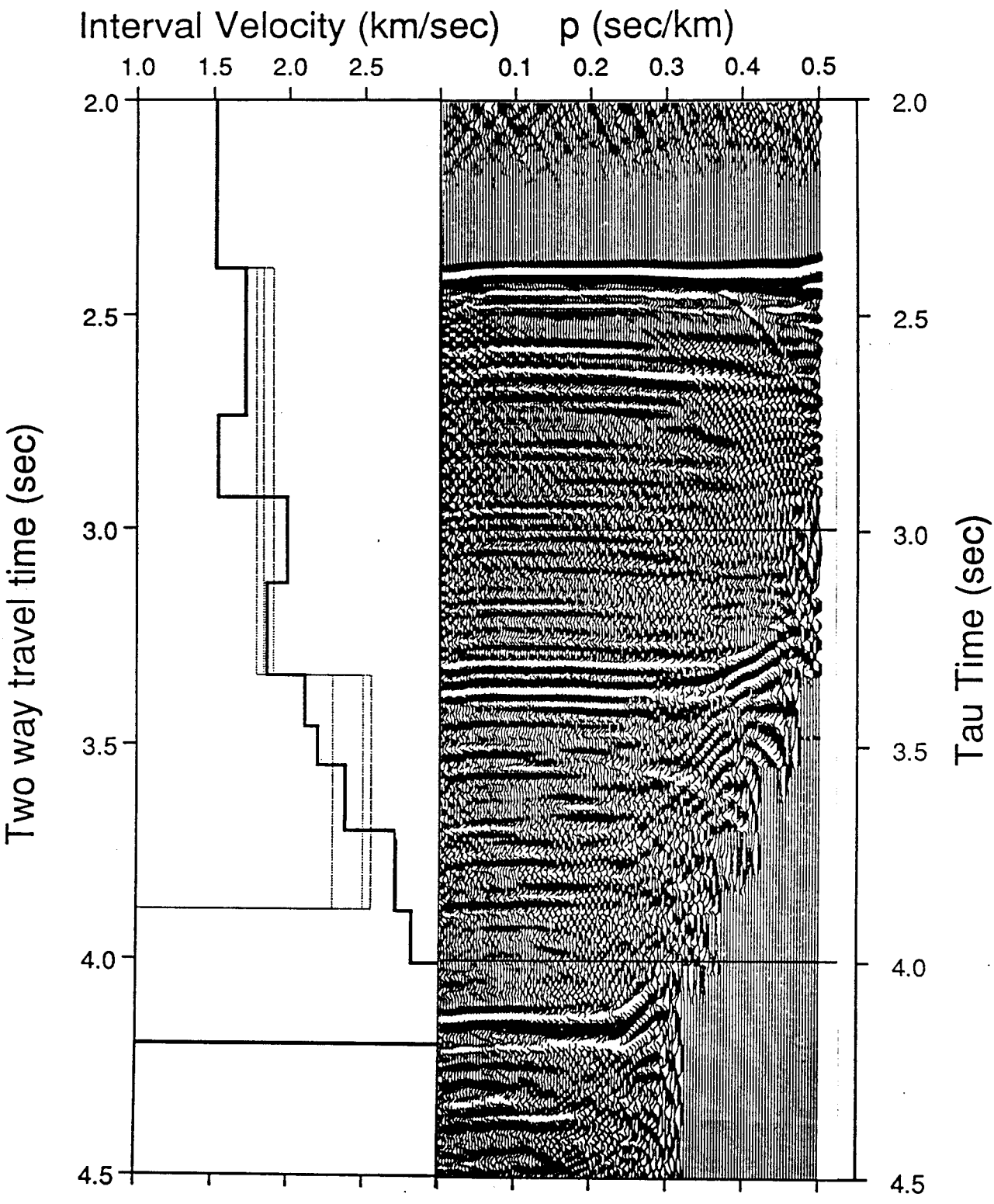
Interval Velocity (km/sec)
p (sec/km)
1.0
1.5
2.0
2.5
0.1
0.2
0.3
0.4
0.5
2.0
2.5
3.0
3.5
4.0
4.5
Two way travel time (sec)
Tau Time (sec)

## CDP 4702

| T0 | Interval Velocity | Lower Velocity Bound | Upper Velocity Bound |
|---|---|---|---|
| sec | km/sec | km/sec | km/sec |
| 2.247 | 1.507 | 1.502 | 1.512 |
| 3.238 | 1.785 | 1.750 | 1.870 |
| 3.780 | 2.457 | 2.350 | 2.590 |

| T0 | Interval Velocity |
|---|---|
| sec | km/sec |
| 2.243 | 1.512 |
| 2.621 | 1.535 |
| 2.834 | 1.963 |
| 3.039 | 1.852 |
| 3.233 | 2.013 |
| 3.367 | 2.452 |
| 3.437 | 2.748 |
| 3.621 | 2.807 |
| 3.773 | 2.592 |
| 3.881 | 2.592 |
| 4.003 | 2.592 |

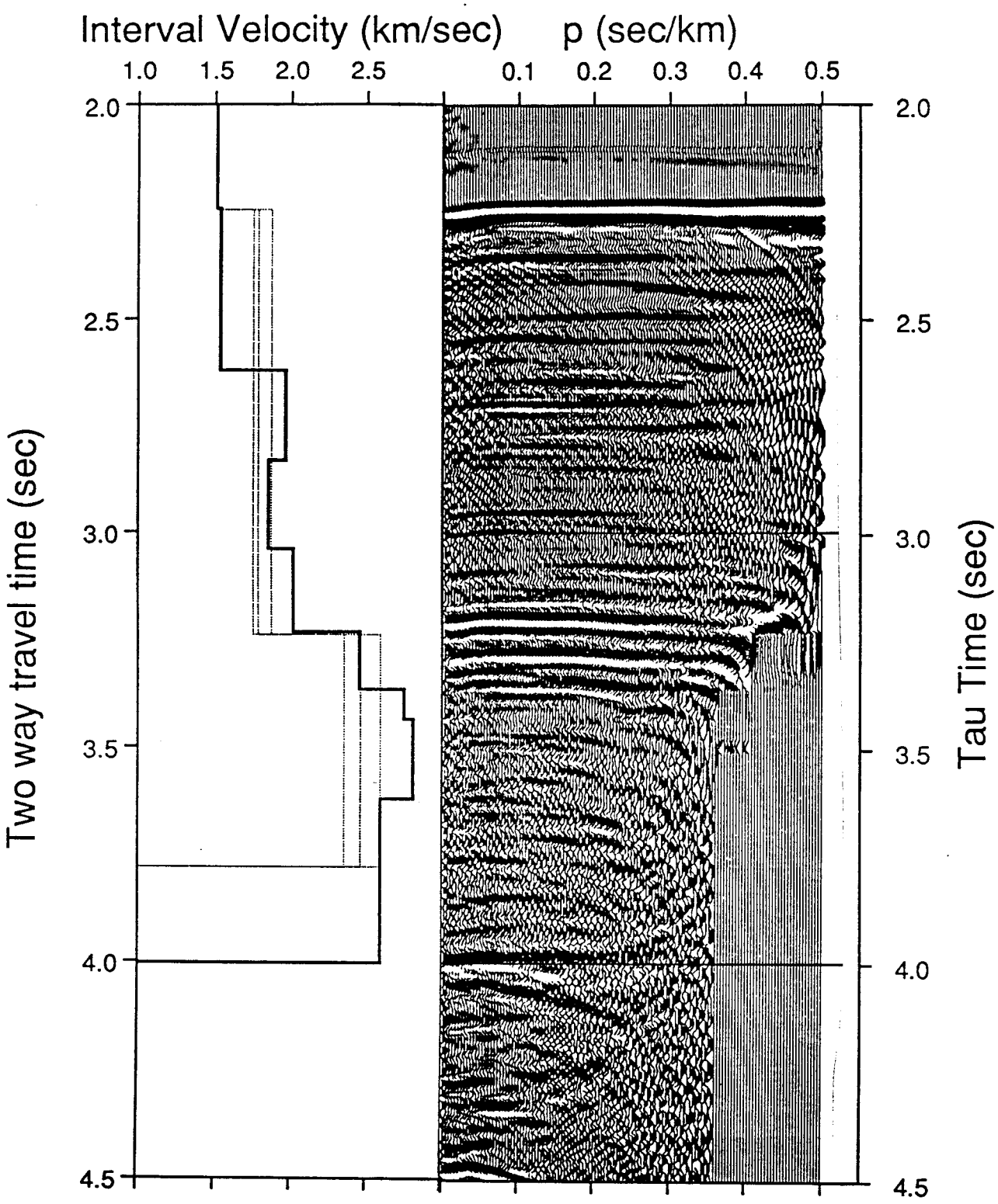
Interval Velocity (km/sec)
p (sec/km)
1.0
1.5
2.0
2.5
0.1
0.2
0.3
0.4
0.5
2.0
2.5
3.0
3.5
4.0
4.5
Two way travel time (sec)
Tau Time (sec)

## CDP 4802

| T0 | Interval Velocity | Lower Velocity Bound | Upper Velocity Bound |
|---|---|---|---|
| sec | km/sec | km/sec | km/sec |
| 2.104 | 1.507 | 1.502 | 1.512 |
| 3.153 | 1.829 | 1.795 | 1.887 |
| 3.655 | 2.577 | 2.340 | 2.675 |

| T0 | Interval Velocity |
|---|---|
| sec | km/sec |
| 2.100 | 1.518 |
| 2.555 | 1.618 |
| 2.719 | 1.618 |
| 2.931 | 1.921 |
| 3.153 | 2.186 |
| 3.254 | 1.839 |
| 3.360 | 1.839 |
| 3.520 | 2.690 |
| 3.651 | 2.690 |
| 3.735 | 3.063 |
| 3.810 | 3.063 |

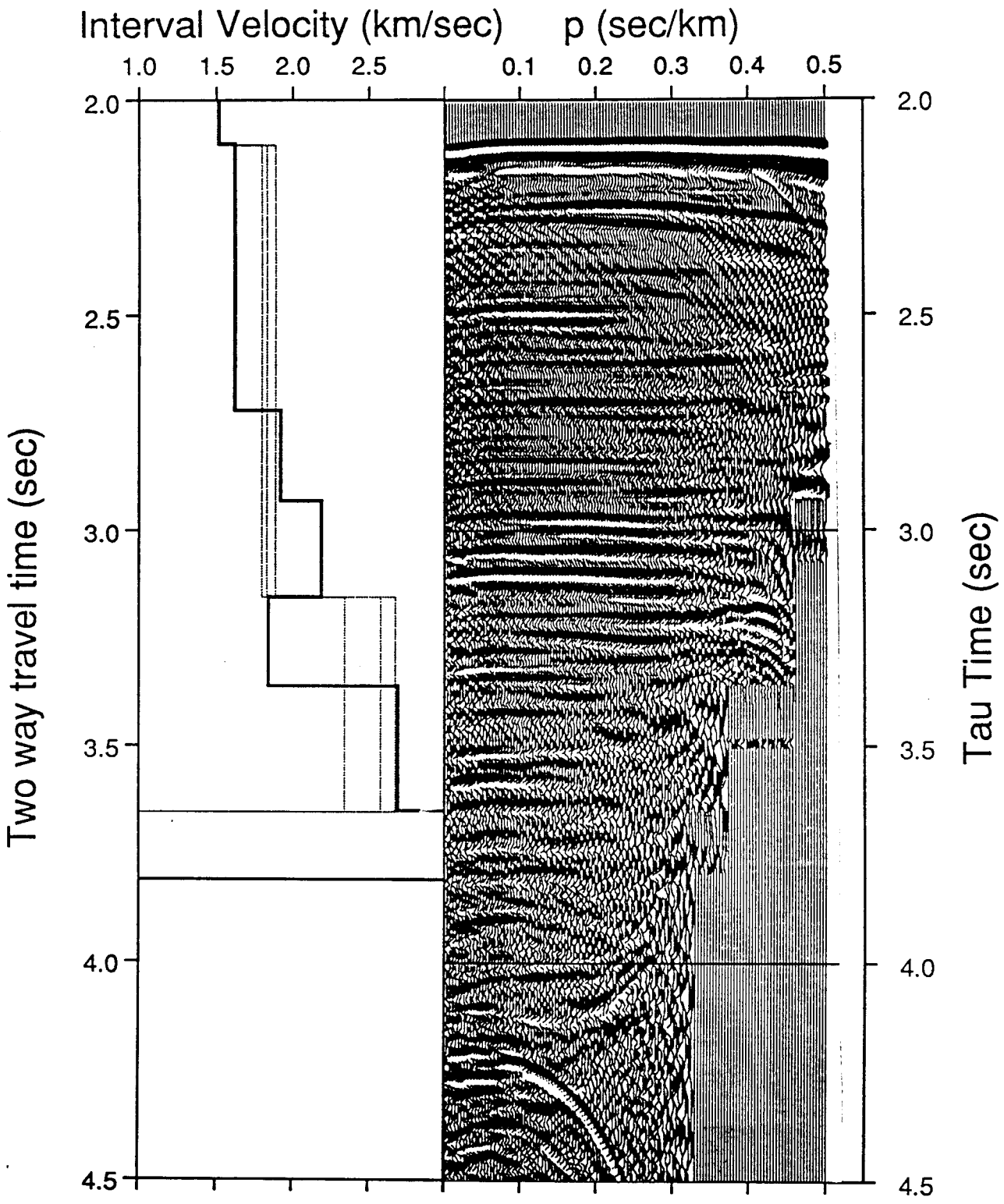
Interval Velocity (km/sec)
p (sec/km)
1.0
1.5
2.0
2.5
0.1
0.2
0.3
0.4
0.5
2.0
2.5
3.0
3.5
4.0
4.5
Two way travel time (sec)
Tau Time (sec)

## CDP 4902

| T0 | Interval Velocity | Lower Velocity Bound | Upper Velocity Bound |
|---|---|---|---|
| sec | km/sec | km/sec | km/sec |
| 1.987 | 1.507 | 1.502 | 1.512 |
| 3.050 | 1.791 | 1.772 | 1.850 |
| 3.539 | 2.715 | 2.616 | 2.815 |

| T0 | Interval Velocity |
|---|---|
| sec | km/sec |
| 1.989 | 1.506 |
| 2.442 | 1.731 |
| 2.609 | 1.611 |
| 2.829 | 1.863 |
| 3.049 | 2.011 |
| 3.140 | 2.159 |
| 3.236 | 2.428 |
| 3.373 | 2.401 |
| 3.534 | 2.908 |
| 3.680 | 2.908 |

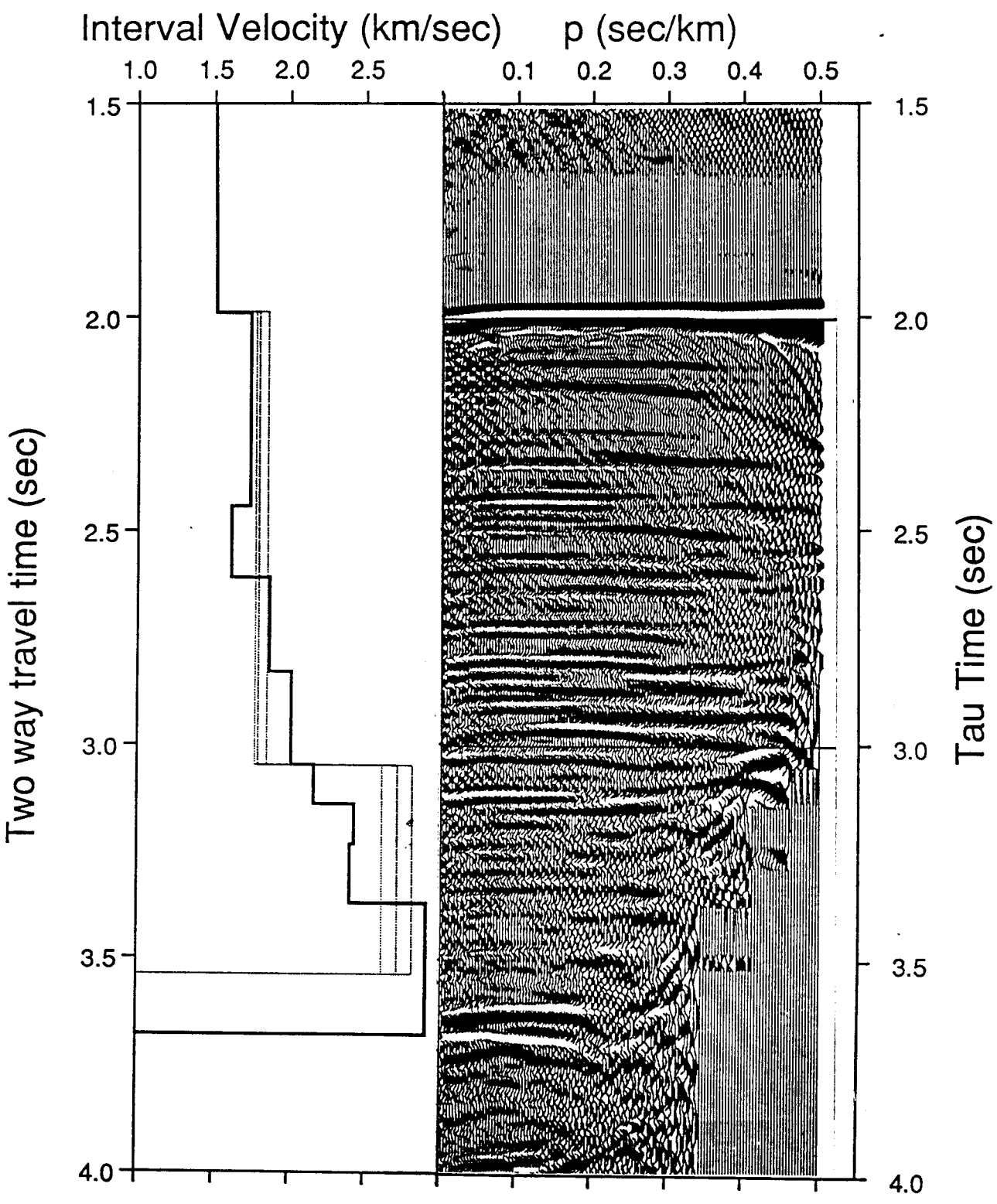
Interval Velocity (km/sec)
1.0
1.5
2.0
2.5
p (sec/km)
0.1
0.2
0.3
0.4
0.5
Two way travel time (sec)
Tau Time (sec)
1.5
2.0
2.5
3.0
3.5
4.0

## CDP 5002

| T0 | Interval Velocity | Lower Velocity Bound | Upper Velocity Bound |
|---|---|---|---|
| sec | km/sec | km/sec | km/sec |
| 1.887 | 1.507 | 1.502 | 1.512 |
| 2.881 | 1.806 | 1.790 | 1.864 |
| 3.436 | 2.613 | 2.550 | 2.685 |

| T0 | Interval Velocity |
|---|---|
| sec | km/sec |
| 1.890 | 1.507 |
| 2.325 | 1.664 |
| 2.473 | 1.872 |
| 2.686 | 1.860 |
| 2.880 | 1.812 |
| 3.060 | 2.174 |
| 3.120 | 2.715 |
| 3.248 | 2.747 |
| 3.434 | 2.918 |

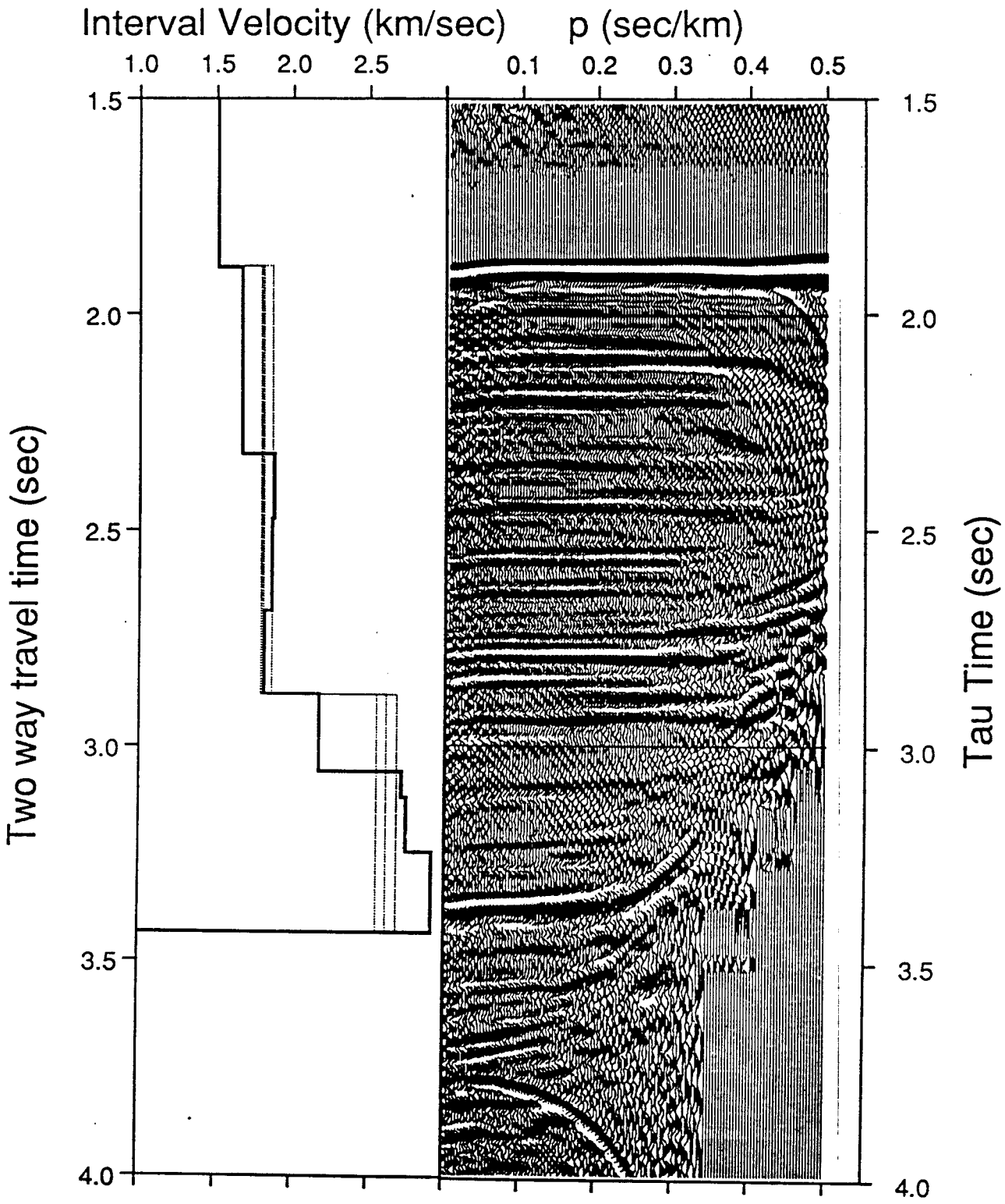
Interval Velocity (km/sec)
1.0
1.5
2.0
2.5
p (sec/km)
0.1
0.2
0.3
0.4
0.5
1.5
2.0
2.5
3.0
3.5
4.0
Two way travel time (sec)
Tau Time (sec)